ANKARA YILDIRIM BEYAZIT UNIVERSITY

GRADUATE SCHOOL OF NATURAL AND APPLIED SCIENCE

THE EFFECT OF WATER CEMENT RATIO AND CURING TEMPERATURE ON ALKALI AGGREGATE REACTION

M.Sc. Thesis by

Lina Mohammad ABED ALJAWAD

Department of Civil Engineering

JUNE, 2023

ANKARA

THE EFFECT OF WATER CEMENT RATIO AND CURING TEMPERATURE ON ALKALI AGGREGATE REACTION

A Thesis Submitted to

The Graduate School of Natural and Applied Sciences of

Ankara Yıldırım Beyazıt University

In Partial Fulfillment of the Requirements for the Degree of Master of Science in Civil Engineering, Department of Civil Engineering

By

Lina Mohammad ABED ALJAWAD

JUNE, 2023

ANKARA

M.Sc. THESIS EXAMINATION RESULT FORM

We have read the thesis entitled **"THE EFFECT OF WATER CEMENT RATIOS AND CURING TEMPERATURE ON ALKALI AGGREGATE REACTION"** completed by **LINA MOHMMAD ABED ALJAWAD** under the supervision of **PROF. DR. LUTFULLAH TURANLI** and we certify that in our opinion it is fully adequate, in scope and in quality, as a thesis for the degree of Master of Science.

Prof. Dr. Lutfullah TURANLI

Supervisor

Assoc. Prof. Dr. Afşin SARITAŞ

Jury Member

Asst. Prof. Dr. Fatih BEKTAŞ

Jury Member

Prof. Dr. Sadettin ORHAN

Director

Graduate School of Natural and Applied Sciences

ETHICAL DECLARATION

I hereby declare that this thesis was prepared in accordance with the Thesis Writing Manual of Graduate School of Natural and Applied Sciences in Yildirim Beyazit University.

- All data in this thesis are based from laboratory experimental test starting from method, procedure and results,
- All information are restricted to academic morals and ethics,
- All information that used as sources are cited and referenced,
- The cited data remains without changing.
- All of the preserved content and data in this experimental test are original,

and in any contrary case of above statements, I accept to renounce all my legal rights.

Date: **Signature:** **……..**

Name & Surname:…….

ACKNOWLEDGMENTS

I would like to extend my full thanks to my supervisor professor Dr. Lutfullah Turanli, and to my Co-Supervisor Assist. Dr. Alkan Hafçı, and special thanks for Assist. Research Dr. Duygu Demirtürk, for her limitless encouragement, advice, and supports throughout the study. Also, I would like to thank my parents for supporting me always. Finally, I would like to thank my beloved sister Dina Abdeljawad.

JUNE, 2023 **Lina Mohammad Abed Aljawad**

THE EFFECT OF WATER CEMENT RATIO AND CURING TEMPERATURE ON ALKALI AGGREGATE REACTION

ABSTRACT

The alkali-silica reaction (ASR) is a common chemical reaction in Portland cement concrete that results in the formation of an alkali gel that swells upon water intake and causes cracking of concrete. The extent of swelling depends on three factors: aggregate reactivity, temperature, and moisture. In this experimental study, the effect of two factors, temperature and water/cement ratio (w/c) on ASR was investigated. Two types of aggregates (A and B) were investigated using the RILEM AAR-2 method that is equivalent of ASTM C 1260. 54 mortar bars were cast and subdivided according to the w/c content in the mixture and the curing temperatures (40°C, 60°C, and 80°C). The expansion of the mortar bars was measured every three days up to 28 days. Moreover, scanning electron microscopy with energy dispersive X-ray spectroscope (SEM/EDX) was used to analyze the inner layers of the studied specimens and the reaction products, including the alkali gel. The results of the study showed that ASR had a destructive effect on the mortar bars when the temperature and w/c ratio increased. The expansion of the mortar bars had clear signs of internal cracking caused by ASR. The SEM imagery showed that the alkali gel covered a large area of the internal structure of the bars, especially for the bars exposed to high temperatures and high w/c ratios compared to those exposed to lower temperatures and w/c ratios. Based on the limited results of this study a recommended to utilize a maximum w/c ratio of 0.50 and a minimum curing temperature of 60 °C in testing.

Keywords: Alkali silica reaction, Accelerated mortar bar test, Scanning electron microscopy, Alkali-gel, Curing temperatures, Water cement ratio.

SU ÇİMENTO ORANI VE KÜR SICAKLIĞININ ALKALİ AGREGA REAKSİYONU ÜZERİNDEKİ ETKİSİ

ÖZ

Alkali-silika reaksiyonu (ASR), Portland çimento betonunda, su alımı üzerine şişen ve betonun çatlamasına neden olan bir alkali jel oluşumuyla sonuçlanan yaygın bir kimyasal reaksiyondur. Şişmenin boyutu üç faktöre bağlıdır: toplam reaktivite, sıcaklık ve nem. Bu deneysel çalışmada, sıcaklık ve su/çimento oranı (w/c) olmak üzere iki faktörün ASR üzerindeki etkisi araştırılmıştır. ASTM C 1260'a eşdeğer RILEM AAR-2 yöntemi kullanılarak iki tip agrega (A ve B) incelenmiştir. 54 çubuk harç dökülmüş ve karışımdaki w/c içeriğine ve kür sıcaklıklarına göre alt bölümlere ayrılmıştır (40°C, 60°C,ve 80°C). Harç çubuklarının genleşmesi 28 güne kadar her üç günde bir ölçülmüştür. Ayrıca, çalışılan numunelerin iç katmanlarını ve alkali jel dahil reaksiyon ürünlerini analiz etmek için enerji dağılımlı X-ışını spektroskoplu (SEM/EDX) taramalı elektron mikroskobu kullanılmış. Çalışmanın sonuçları, ASR'nin sıcaklık ve w/c oranı arttığında harç çubukları üzerinde tahrip edici bir etkiye sahip olduğunu göstermiştir. Harç çubuklarının genleşmesi, ASR'nin neden olduğu açık bir içsel çatlama göstergesidir. SEM görüntüleri, alkali jelin, özellikle yüksek sıcaklıklara ve yüksek w/c oranlarına maruz kalan çubuklar için, düşük sıcaklıklara ve w/c oranlarına maruz kalanlara kıyasla, çubukların iç yapısının geniş bir alanını kapladığı görülmüştür. Bu çalışmanın sınırlı sonuçlarına dayanarak, teste maksimum 0.50 w/c oranı ve minimum 60°C kürleme sıcaklığı kullanılması önerilmisti.

Anahtar Kelimeler: Alkali silika reaksiyonu, Hızlandırılmış harç çubuğu testi, Taramalı elektron mikroskobu, Alkali-jel, Kürleme sıcaklıkları, Su-çimento oranı.

CONTENTS

ABBREVIATIONS

AAR	Alkali Aggregate Reaction
ACR	Alkali Carbonate Reaction
ASR	Alkali Silica Reaction
Na_2O_{eq}	Alkali Equivalent
NaOH	Sodium Hydroxide
MBT	Mortar Bar Test
AMBT	Accelerated Mortar Bar Test
SEM	Scanning Electronic Microscopic.
EDX	Energy X-ray Spectrum
CPT	Concrete Prism Test
ACPT	Accelerated Concrete Prism Test

LIST OF TABLES

LIST OF FIGURES

CHAPTER 1

INTRODUCTION

1.1 General View of Alkali Silica Reaction

Concrete is a common material used in many structures such as tunnels, buildings, and bridges, due to its various advantages of reasonable cost, easy maintenance, and good durability. In spite of concrete advantages, concrete has low tensile strength and low ductility, which are the main concrete disadvantages. Concrete contains of ordinary Portland cement (OPC), which is works as a binder, with a mixture of coarse (gravel) and fine aggregates, in addition to the presence of water [1]. One of the prime features of concrete is high durability, which known as the capability of concrete to withstand the physical and chemical attacks. The most common physical attacks on concrete are corrosion, abrasion and erosion, while the best known chemical attacks are alkali aggregate reactions and sulfate attacks [2]. However, this experimental study is only focused on the impact of the chemical attacks, especially alkali silica reaction on the mortar paste.

Alkali aggregate reaction (AAR) first detected in 1930 by Thomas Santon [3]. And known as a chemical reaction between hydroxide ions and reactive silica. AAR is divided to alkali-silica reaction (ASR), and alkali-carbonate reaction (ACR), depending on the type of reactive silica. When the hydroxide ions reacts with certain types of rocks, then the reaction defined as alkali carbonate reaction (ACR). While the alkali silica reaction (ASR) or concrete cancer is a common occurrence happens in all of concrete structures, and define as a chemical interaction between alkali ions and siliceous aggregates, and produces an alkaline gel, which is the major cause of the reaction's growth [4].

The response of alkali-silica reaction appears on the surface of the concrete structures on the form of cracks. The severity of the (ASR) may be determined by the shape and the depth of the cracks that form, the most ordinary crack caused by ASR is map cracking or alligator cracking. Figure (1.1) represents a field image of map-cracking and its locations on concrete structure [5].

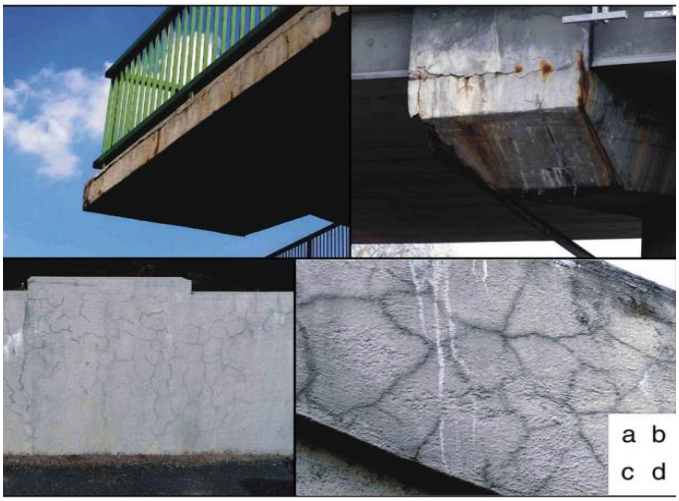

Figure 1.1 Map cracks in various places, where (a) shows cracks among the front, (b) head of the column destructed by the concrete spalling, (c) cracks all over the front side, (d) close view of the map cracking [5,6].

The reactivity of alkali silica reaction (ASR) depends on three main factors, which are sufficient amount of alkalis and silicate in the mixture, temperature, and relative humidity. ASR cannot be eliminated, but it can be reduced by controlling the factors responsible for the reaction [6]. For example, using cement with low alkali ingredients in regions contain of high alkali, will reduce the effect of ASR in long term. Since alkalis and silicate minerals are contributed in increasing the reactivity of alkali silica reaction, the source for each mineral must be determined. Most studies find that the source of alkalis came from cement [7].

The higher alkali ingredient in concrete the more continuous of the reaction [8]. While silica is generated from aggregates, the quantity of aggregate in the concrete mix is approximately about 60% to 75% from the total content, most of them are reactive aggregates, which contain of silicate mineral in their ingredient, so enough silica is needed to start the alkali silica reaction [9]. At this point, the type of aggregate plays a main part in ASR, because the source of silica came from aggregate, so the mineralogical properties of aggregate are so important [10]. In order to reduce the influence of ASR, aggregate with high amount of silica cannot be used in high silicate regions, because high amount of silica increases the reactivity of ASR. ASR formation is influenced by the previous factors. In this experimental study, the influence of altered curing temperatures, and various water/cement ratios on ASR formation were also investigated.

1.2 Formation of Alkali Silica Reaction

The formation of ASR begins when dissolved alkali ions in the pore solution reacts with siliceous ions, alkali gel is formed from this reaction. Moisture or water content accelerates the reaction rate, because the distention of the alkali gel depends on the ratio of presence water, while alkalis and silica supplies the continuity of the reaction [11]. The following equations shows the mechanism of ASR, and the swelling of the alkali gel in the presence of water [6-12].

$$Si\text{-}O\text{-}H + OH^- + Na^+ \rightarrow (Si\text{-}O\text{-}Na) + H_2O \quad \text{Eq (2.1)}$$

$$Si\text{-}O\text{-}Si + 2OH^- + 2\,Na^+ \rightarrow 2(Si\text{-}O\text{-}Na) + H_2O \quad \text{Eq (2.2)}$$

$$SiO_2 + 2NaOH + H_2O \rightarrow Na_2SiO_3.2H_2O \quad \text{Eq (2.3)}$$

1.2.1 Effect of Water Cement Ratio on the Behavior of Alkali Silica Reaction

Water content is one of the head factors effecting the reactivity of ASR. Water that exist in concrete is expressed by different forms, but one of the main forms is reacting water, this type of water form contributes in the formation of ASR, by transports the ionic species that involves in ASR [13]. Many studies confirmed the influence of high water presence on alkali silica reaction. A study revealed that when the amount of water content increased the reactivity of alkali silica reaction increased, because alkali-gel absorb water and expand [14]. The swelling of alkali gel due to high water absorption, caused cracks on concrete structure. Also, water content effects on cement hydration, and develop the growth rate of initial products [15-16].

1.2.2 Effect of Curing Temperatures on the Behavior of Alkali Silica Reaction

The effect of temperature in ASR was studied in three phases. First phase is the amount of alkali leaching, where high temperatures causes high leaching of alkalis, and thus continuity of alkali gel to form and swell [17]. Second phase is gel viscosity, previous studies confirmed that high temperatures reduce the viscosity of alkaline gel, where low viscosity allows easy expansion of the gel. Third phase is cement hydration and reaction products. High temperatures raised hydration rate of cement, in addition its

effects on the shape of hydration products. Also, high temperatures burns the layer of cement paste. Moreover, the opposite occurs at low temperatures [18-19]. After the factors that affecting on the alkali silica reaction have been briefly discussed, the following subtitles present the goal of this experimental study, and thesis contents.

1.3 The Goal of the Experimental Study

The key goal of this experimental study was to investigate on the potential reactivity of two types of natural aggregates, aggregate (A) and aggregate (B). Then, the study focuses on the effect of three altered of curing temperatures, namely 40 °C, 60 °C and 80 °C, with three various amounts of w/c ratios 0.4, 0.5 and 0.6. Furthermore, the study aims to explain how various amounts of water cement ratios effects on the behavior of alkali silica reaction, where the recommended water cement ratio in ASTM C 1260 is 0.47 [20]. But this study focused on a lower and higher ratio compared with the recommended ratio in the standard. Also, the study aims to inspect the mechanism of ASR, and hydration products under the influence of various curing temperatures and w/c ratios. In order to achieve the previous goals, the study proposed to use accelerated mortar bar test (AMBT). Then, scanning electron microscopic and x-ray spectrum analysis (SEM/EDX) was used to comprehend the reaction products.

1.4 Thesis Content

This thesis encompasses five chapters as follow:

Chapter 1 (Introduction):

This section includes an introduction to this study, study goal, and explains what the goal of performing the laboratory tests.

Chapter 2 (Literature Review):

In this section a summarization of the previous studies has been written to explain the concept of alkali silica reaction and how it’s formed, with the history of ASR, mechanism of ASR, and factors that influence on this reaction. Also, an explanation of the results that obtained from mortar bar test, and scanning electron microscopy with x-ray spectrum analysis (SEM/EDX).

Chapter 3 (Experimental Procedure):

The chapter explains the experimental procedure, starting with materials used in this test and their properties, the mixing procedure and casting of the mortar bars, the

preparation of sodium hydroxide, and the distribution of the groups tested. Also, test methodology was explained.

Chapter 4 (Results and Discussion):

This section contains of two sections, where first section illustrates the results of length change (expansion) of tested groups, with microscopic images of the specimens, and the second section discuss these results.

Chapter 5 (Conclusion):

This chapter is connected to the title of the thesis, with providing strong evidence of how the several of curing temperatures and water cement contents are effect directly on ASR, depending on the results.

CHAPTER 2

LITERATURE REVIEW

This chapter contains previous studies of alkali silica reaction (ASR). Where the first parts of this chapter clarify the mechanism of ASR, and explain in details the factors that increase the reactivity of ASR. The last parts of this chapter describe test methods for detecting the effects of ASR.

2.1 Overview of Alkali Silica Reaction

Concrete is one of the best commonly used materials of constructions such as, dams, bridges, tunnels, and buildings because it is low cost, low maintenance, very durable and easy to form. In addition, concrete is very resistant to external influences such as high temperatures, humidity and chemical attacks, etc. Despite the benefits, concrete has two major hindrances compared to other binding materials, tensile strength of concrete is quite low, with low ductile. As it known that the production of concrete includes of ordinary Portland cement (OPC) as a binder, coarse (gravel) and fine aggregates, water aimed at hydration with organic admixtures to regulate the workability and flow properties [21]. Therefore, it is inevitable that the constituents that make up the concrete will have an influence on the properties of concrete [22].

A crucial factor in concrete's success as a construction material is its high performance in service, particularly its durability. Concrete durability is the capability to resist the chemical and physical attacks that cause destruction [23]. The chemical and physical attacks affect durability of concrete. Physical attacks include corrosion, abrasion, and erosion, while chemical attacks include sulfate attack and alkali aggregate reaction [2]. Moreover, preceding studies are focused on the influence of chemical attacks, especially the effect of alkali-silica reaction on concrete structure.

The reaction between alkali hydroxide in concrete with certain types of aggregates is called alkali aggregate reaction (AAR), and divides to alkali-silica reaction (ASR), and alkali-carbonate reaction (ACR) [3]. Alkali silica reaction (ASR) defined as a case of deterioration caused by a chemical reaction between alkali oxides (Na2O, K2O) and reactive silica (SiO2) [19]. In 1930, the concept of AAR first detected by Thomas

Santon [24]. In the year of 1940, Thomas Stanton identified the deterioration of concrete as a result of a reaction occurred between alkalis and siliceous aggregates [25].

In 1943, Santon adopts an experimental method to focus on the parameters that effects on alkali-silica reaction [26]. However, the reactivity of ASR depends on three main factors, namely, sufficient amount of alkali and silica, relative humidity, and temperature. Also, the swelling of alkali gel depends on these factors. When one of these factors increased the alkali-gel expands and make a pressure on the concrete inner structure, causing a formation of cracks. Most of the cracks considered as non-deleterious, the common cracks due to ASR is map cracking [27]. Figure 2.1 shows the types of cracks that forms from the occurrence of ASR. The first type (A) is map-cracking, and this type of cracking appears as a random crack throughout the structure, with ability of the alkali-gel to leach from the cracks. The second type is pop-out cracking (B), which usually occurs when the reactive aggregate exposed to expansion, causing detach between the concrete and reactive aggregate [28].

Figure 2.1 Crack produced by ASR, where (A) is map-cracking , and (B) pop-out cracking [28].

According to previous studies, there are other parameters that effects on the reactivity of alkali- silica reaction. Santos et al. (2020) mentioned that aggregate type, and aggregate texture affect the reactivity of ASR [29]. While Silva et al. (2013) stated that coarse aggregates maximize the reactivity of alkali silica reaction, especially if the aggregate contains high amount of silica [30]. All the above parameters are involved

on alkali-silica reaction formation. However, the following section describes ASR formation in details.

2.2 Formation of Alkali Silica Reaction

In general, alkali-silica reaction occurs when the hydroxyl ions (OH^-), potassium ions (K^+) and sodium ions (Na^+) reacts with reactive silica (SiO2). The reaction produces a product called the alkali gel. As shown in Figure (2.2), the alkali gel expands with the moisture and temperature present, causing a pressure in the concrete inner structure, where the damage of alkali-silica reaction usually expressed by the induced of expansion. However, sufficient amount of alkalis and silica ensures the renewability of ASR [28].

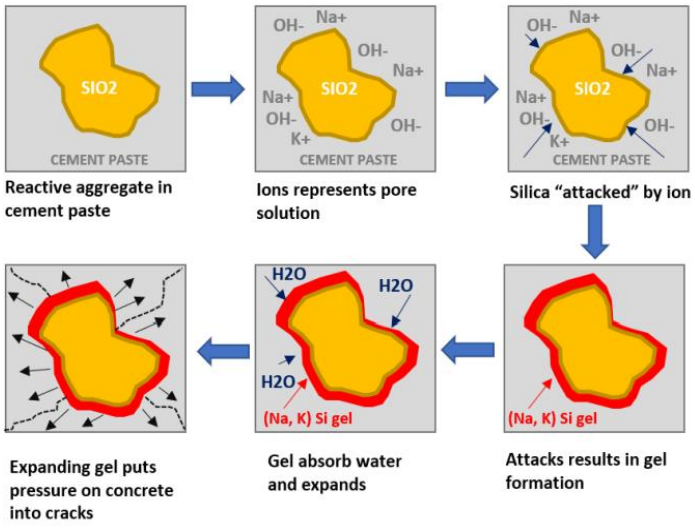

Figure 2.2 Diagram of ASR mechanism [28].

The mechanism of alkali-silica reaction can be expressed by equations. Table (2.1) contains equations that illustrate the formation of alkali-silica reaction. Normally, reaction starts when reactive silicate in aggregates reacts with water to form ortho-silica $Si(OH)_4$. Then the alkalis attacks ortho-silica acid through ions exchange, the substitution of alkalis by calcium ion is calling alkali recycling, the recycling of alkalis due to high reactivity of ASR leads to dissolution of portlandite, and forming calcium ions and hydroxyl ions [31].

Table 2.1 Mechanism of alkali silica reaction by equations [31].

Reaction phases	Chemical equation	Equation number
Re-polymerization of silica	$(SiO_2) + 2\ H_2O \rightarrow Si(OH)_{4(aq)}$	Equation (1)
Ion exchange	$Na^+ + Si(OH)_4 \rightarrow (OH)_3\ SiO\ Na + H^+$	Equation (2)
Recycling of alkalis	$2+((OH)_3\ SiO\ Na)_{(aq)} + Ca^{+2} \rightarrow ((OH)_3$ $SiO\text{-}Ca\text{-}\ OSi(OH)_3 + 2\ Na^+$	Equation (3)
Dissolution of portlandite	$Ca\ (OH)_2 \xrightarrow{\Delta} Ca^{+2} + 2OH^-$	Equation (4)

Previous studies illustrates the effect of alkali-silica reaction on cement, especially on the phases of cement hydration. Initially, hydration of cement proceeds in five phases, namely, mixing, dormancy, acceleration, speed reduction, and densification. The first three phases are so important in the formation of hydration products and cement strength [32].

In the first phase, where cement and water are mixed together, ettringite and calcium hydrate (CH) are formed first. The second phase is the coating phase for the layer formed in the first phase, which reduces the access of water into the inner layer. Calcium hydrate (CH) also begins to grow in this phase and formed in various shapes such as, hooded fractures, plates and myriad shapes. In the third phase, calcium hydrate gives strength to cement, and calcium silicate hydrate (C-S-H) is polymerized into spherical masses. Outer products (OP) and C-S-H gel are also hardened and form layers mixed with silicon, these layers produce a network of C-S-H gel [33].

Thus, when alkali silica reaction occurs, the reaction accelerates the process of hydration in cement, leading to strength loss of C-S-H, which allows the alkali solution to penetrate and destroy the inner layers. In addition, excessive formation of ettringite appears as an outcome of alkali-silica reaction, fibrous (C-S-H gel) [34]. Calcium silicate hydrate (C-S-H) is the base constituent formed during cement hydration, and expressed by ratio of calcium to silicon (Ca/Si) [35]. Where the various amounts of Ca/Si contributes in appearing of different minerals as shown below [36].

Table 2.2 The resulted minerals of the various Ca/Si ratios [36].

Range of Ca:Si	Mineral	Chemical formula
0.83-1.25	Tobermorite	$Ca_5Si_6O_{16}(OH)_2.7H_2O$
1.50-2.25	Jennite	$Ca_9Si_6O_{18}(OH)_6.8H_2O$

The elements that produced ASR products are abundant, and divided into major and minor products, where the major products includes silica, sodium, potassium and calcium, and the minor products includes iron, magnesium and aluminum [37].

Several studies conducted the result of ASR formation on cement hydration. Karakurt & Topçu (2011) confirmed that alkali-silica reaction increases the hydration ratio of cement. Moreover, they described the outer products that made during the rapid hydration of the cement to be delitescent materials, with high ability to diffuse and settle in the inner pores [38]. Zhang (2018) described the formation of alkali silica reaction as quick crystallization of hydration products. For example, through the initial hours of cement hydration, crystallization of initial products had foils shape, then after one day it changed to fibers [39].

The crystallization of products depends on the duration of hydration and sufficient space. For instance the crystallization of C-S-H changed to needle shape in sufficient space, while it changed to spherical or grainy shape in restrained space [30].

The space in microstructure of cement paste are represented in air voids and cracks. Also, air voids and cracks in the microstructure is considered as wide space of ettringite to form in, and it’s not significate in expansion. For example, once ASR occurs, the ettringite leaves its original place in cement paste and re-crystallized in air voids, this migration called secondary ettringite formation, and it’s not causing expansion [40]. However, Katayama (2010), revealed that most of hydration products, such as brucite, ettringite, and alkali gel are mainly exists in cracks, paste interface and air voids [41].

The alkali gel is considered as one of mainly products of ASR and contains from alkalis and silica. Where most of the alkali content came from cement, and source of silica content came from aggregates. The ratio of Ca/Si determined the texture of alkali gel. Davies & Oberholster (1988) investigated the texture of amorphous alkaline gel in day

14 and day 21, and handling temperatures of 23°C and 80°C. The study revealed three types of amorphous gel, based on the amount of Ca/Si. Where the texture of the gel was spongy when the ratio of Ca/Si is (0.82-1.2), massive gel at (0.55-0.61), and rosette shape at (0.18-0.41) as shown in tables below [42].

Table 2.3 EDX analysis of spongy and massive gel by Davies & Oberholster [42].

Chemical compounds percentage	**Massive gel**		**Spongy gel**	
	Un-washed	washed (96 hour)	washed (96 hour)	washed (8hour)
SiO_2	49.4	61.9	18.5	56.6
Al_2O_3	---	6.2	---	---
CaO	28.2	31.9	20.8	43.4
K_2O	---	---	4.1	---
Na_2O	22.5	---	56.6	---
Ca/Si	00.61	00.55	1.20	0.82

Table 2.4 EDX analysis of massive gel and rosette phase by Davies & Oberholster [42].

Chemical compounds percentage	**Massive gel** (immersed in NaOH solution)			**Rosette phase** (immersed in NaOH solution)		
	Unwashed	2 hour	84 hour	Unwashed	2 hour	84 hour
SiO_2	61.7	64.6	60.8	71.7	73.6	71.0
Al_2O_3	3.1	---	1.6	0.7	---	---
CaO	16.3	20.4	37.6	12.4	17.8	26.5
K_2O	17.7	14.1	---	14.8	8.6	1.7
Na_2O	1.2	0.9	---	0.4	---	0.8
Ca/Si	00.28	00.33	00.66	00.18	00.26	00.40

In addition, the nature and origin of the aggregates shows a significant part in the formation of alkali gel. However, the following subtitle explains how the origin, kind, and quantity of silica minerals in aggregates effect on ASR.

2.3 Effect of Aggregates on Alkali Silica Reaction

Aggregates are one of the main components of concrete, and it account about 60% up to 70% of the total volume of concrete [43]. Previous study show that the origin aggregate, the texture of aggregate, the formation, and the mineralogical constituents of the aggregates, especially silica, have an effect on the reaction with alkaline silica. First, aggregates are classified based on weight and size. According to weight aggregates are classified to normal-weight aggregates, light-weight aggregates, and heavy-weight aggregates. While according to size, aggregates are classified as coarse and fine aggregate [44].

The most usage in concrete mixture is normal weight aggregate, and it's divided into natural aggregate and artificial aggregate. The source of natural aggregate came from bed rocks. The classification of rocks depends on how it's formed, mainly there are three types of rocks. First type is igneous rocks, and it's formed from fast cooling of magma or lava. Second type is sedimentary rocks, and it's formed beneath seabed and raised up. Third type is metamorphic rocks, this type of rocks is formed due to excessive high pressure and heat [45].

Most aggregates that came from igneous rocks shows well-performance in concrete, because they have high toughness, hardening and dense. Additionally, igneous rocks are widely spread and exist on earth crust. The texture of igneous rocks are related to the rock formation, either rapid cooling or slow cooling. Igneous rocks are divided according to the mineralogical component in their ingredient, felsic igneous rocks are rich in silica with high amount of sodium, potassium and aluminum, such as tridymite. Mafic igneous rocks contains of high proportion of magnesium and iron with silica inside. While ultra-mafic igneous rocks contain of more magnesium than mafic igneous rock. Sedimentary rocks are made from main minerals inside such as; quartz (Si), potassium feldspar and muscovite, and they merged in sedimentary rocks through clay minerals, dolomite, gypsum, calcite and halite. Also, limestone is derived from carbonate sedimentary rock, rich in calcium and composed of calcite and aragonite [46].

Most of the aggregates that derived from igneous rocks are rich in silica, and easily reacts with alkali dissolved ions in cement, the reaction between alkaline pore solutions with minerals of silica such as: opal and quartz that are mostly obtained in

aggregates, is called alkali-silica interaction. The proportion of silica in the aggregate contributes on increasing or decreasing the intensity of alkali-silica reaction. Also, the silica content in aggregates must be limited to reduce the negative effect of alkali-silica reaction [10]. American Concrete Institute-ACI 201, determine the most reactive silicate minerals, with their chemical composition and physical parameters, the arrangement of minerals atoms reveals the physical nature of the silica as amorphous or crystalline. However, most of amorphous silicate minerals such as: opal are rich in silica, and the origin of these minerals came from volcanic rocks [47].

Table 2.5 ACI 201 classifications of deleterious silicate minerals [47].

Reactive substance	**Chemical-formula**	**Physical-parameter**
Opal or potch	($SiO_2.nH_2O$)	Amorphous- Unshaped
Calcedony	(SiO_2)	Micro-crystalline /Crypto-crystalline
Quartz	(SiO_2)	a)Micro-crystalline/Crypto-crystalline b) Crystal-like
Cristobalite- quartz	(SiO_2)	Crystalline
Tridymite-quartz	(SiO_2)	Crystal-like
Rhyolitic, dacitic, andesitic	(SiO_2), with amounts of AL_2O_3	Glassy
Crypto-crystalline devitrification products	FeO_{22} , alkaline earth, and alkalis	Material similar to the matrix of volcanic rocks or fragments in tuffs

The researchers found that not all of the deleterious silicate minerals can react in alkaline solutions. For example: opal and quartz, both consist of the same chemical composition (SiO_2), but quartz is non-deleterious when reacts with alkalis, because of the stable organization of quartz atoms, which leading to low ability of this mineral to dissolve and reacts with alkalis. While opal is highly dissolve and reacts with alkalis because opal atoms are un-systematic [6].

Ahmad et al. (2018) determined siliceous aggregate in three minerals, namely, quartzite, granite and granitic gneiss [48]. The amount of silica presents in concrete

mixture is expressed by aggregate reactivity, if the reactivity of aggregates increases, then the durability of the concrete decreases, also ASR effects the durability of concrete, and leads to destructive crack on concrete structure [15]. Referring to Zivronaite & Pranckeviciene (2017), the reactivity of aggregates was tested through using Lithuanian aggregates, were the amount of reactive rocks inside as followed: sand contents was set between 4.0% until 4.6%, while 1.5% until 2.4% was exist in gravel. However, a sign of crack was appeared on concrete surface. The crack type classified as pop-out cracking, mention that this type of cracking caused because of the poor quality of concrete and poor bonding between particles [49].

According to Czapik (2020), three different aggregates were tested to ensure reactivity of some types of aggregate, namely, rhyolite, granite rhyodacite, and sedimentary carbonate rocks. The study revealed to formation of glass matrix is formed in rhyolite and rhyodacite due to rapid cooling, these kind of aggregates are categorized as reactive aggregates, because of the ability of glassy matrix to dissolved in environments that contain alkalis [50]. Also, the reactivity of aggregates are increased by aggregate size. Aggregate size particles effect on harm evolution into two methods; the extent of cracks on aggregates at different sizes, and the reaction between expanding (reactive) and non-expanding aggregates (non-reactive) in a densely packed structure. In addition, different size classes of expanding aggregates maximize the expansion average of ASR [51].

Also, the origin of aggregates takes a significant influence on the reactivity of alkali-silica reaction. The alkali gel that produced during ASR is influenced by the minerals present in the aggregate. For example, if the aggregate consists of limestone which is derived from the minerals of calcite and aragonite, the gel forms as small rounded grains over the aggregate particles [52]. It’s important to mention that the minerals of calcite and aragonite are also contributes on increasing the amount of alkalis, as they are found in cement production. For example, crushed limestone is used as an important additive in cement production and contains a high percentage of alkalis [53]. However, the contribution of alkalis in the process of alkali silica reaction is discussed deeply below.

2.4 Effect of Alkalis on Alkali Silica Reaction

Alkali-silica reaction is a renewable reaction that depends on the aggregate reactivity, a sufficient amount of water, and high temperature [54]. The previous section discussed the effects of silica content on the alkali silica reaction. This section deals with the effect of alkalis on alkali-silica reaction. ASR is increased by alkalis, and the ratio of alkalinity is expressed by PH value, the acidic materials are below seven, and the alkali materials are above seven, since alkali silica reaction increased through alkalis, then the soluble alkali increases the amount of PH value, the normal value of PH in cement is ranged between 12 to 13.8, but the soluble alkali such as: Na^+, K^+ , and OH^- will increase the PH value above the normal range, which means that the rate of ASR will be increase. The neutral charge balance between the ions depends on good crystallization of silica in concrete structure, while poor crystallization leads to difference in charges and accelerate ions movement, and the danger of this stage provides harmful cracking of concrete structure [55]. Since alkali sources are wide and abroad, alkali sources must be determined. However, most studies indicate that the prime source of alkalis came from ordinary Portland cement, cementitious materials and partly from the external environment [7]. The quantity of alkali contents in cement is represented by alkali equivalent (Na_2O_{eq}), and this ratio determines the cement alkalinity. Cement classified as low alkali, When the amount of alkalis is less than 0.6 %, and vice versa [56].

Portland cement generally gained alkalis from the manufacturing or clinker process. Also, cement consists of four main components that are responsible of cement strength, and on the initial products during its hydration. Portland cement consists of four constituents, namely, tri-calcium-silicate (C_3S), di-calcium-silicate (C_2S), tri-calcium-aluminate (C_3A), and tetra- calcium-aluminate ferrite (C_4AF). C_3S (alite) and C_2S (belite) are responsible for the strength of the cement, and account of 75% of the total weight of cement. Also, the chemical formula of alite is (Ca_3SiO_5), and for belite is (Ca_2SiO_4). However, the chemical reaction between C_3S and C_2S is forming calcium silicate hydrate (C-S-H), which is the primary bond and product of Portland cement hydration. C_3S is responsible of initial hardening and early strength. During cement production, C_3A releases high heat effects on the initial hydration of the cement, so gypsum or calcium sulfate dehydrate is added to reduce the effect of C_3A. When water

is added to C_3A and gypsum, ettringite has formed, but when water is added to C_3A without gypsum, calcium aluminate hydrate has formed [57,58]. Many studies revealed that the amount of alkali contents effects on the stability of hydration products. Liu et al. (2013) investigate the effect of high alkali presence on the initial products of cement hydration, especially ettringite and C-S-H gel. The study detect that the high alkali content leads to the instability of ettringite [59]. While Leemann et al. (2020) mention that alkalis increased the reactivity of alkali-silica reaction, because the pore solution in concrete contains dissolved alkalis such as, sodium, potassium and calcium ions, which combine with dissolved silica, causing to subsequent formation of alkali-silica products [60]. Kim et al. (2019) investigated the effect of alkali-silica reaction on the hydration of Portland cement. Where a diagram was prepared in the study to illustrate this effect (see below). The figure shows that during ASR the pores are filled with dissolved alkalis, and the initial cracks occurs (a), while the width and length of these cracks increased (e). Also, the alite and belite stages forms crystal stages, that contains of low amounts of silica, magnesium, sodium, and potassium [61].

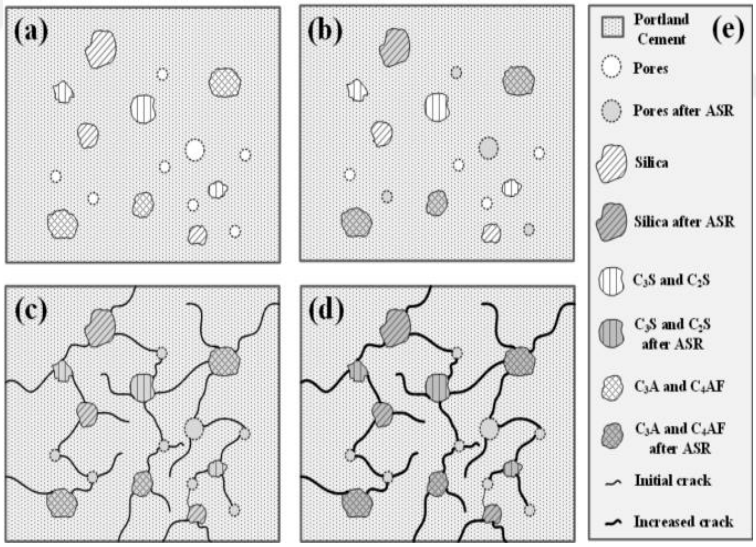

Figure 2.3 Shows formation of Cement hydration during alkali silica reaction [61].

Smaoui et al. (2005) mentioned that high alkali content has effect on the hardened cement- paste of concrete, and mortar by causing premature hydration of the hardened cement-paste, bleeding of concrete, drying and shrinkage [62]. Not only the alkalis are effects on the reactivity of ASR, but water also contributes in increasing the reactivity of ASR. The following section discussed the influence of water ratio on ASR.

2.5 Effect of Moisturizing on Alkali Silica Reaction

Water is essential component of concrete and forms the cement-paste through the process of hydration. Moreover, the addition of water in cement had changed the phase of hydration form AF_m phase to AF_t phase [63]. The moisturizing forms in concrete are presented in many forms, such as capillary pore water, adsorbed water, water in the interlayer, and chemically bound water [64]. Capillary water is absorbing water that adheres to voids and is displayed when the voids are higher than 50mm, while small voids less than 50mm hold excessive water in hydration or free water. The interlayer-water is present within the C-S-H layer and cannot evaporate. The chemically bound water is involved in chemical processes that take place in the concrete or mortar, such as ASR and sulfate-attack. This type of water is called reactive water, and its reduced durability and strength of the concrete. Therefore, water transports the ionic forms that contributes in alkali silica reaction, while the reacting water remained in the amorphous gel [12]. The formation of cement paste acts as an adhesive that holds the aggregates together, fills the voids, and facilitates workability, while less water in the cement- paste effects on the workability of the concrete [65]. Water cement ratio (w/c) known as the ratio of the weight of water to the weight of cement in the mixture content. The quality and strength of the concrete depends on the level of this ratio. Additionally, the concrete expansion can be effected by w/c ratio [66].

The quantity of water/cement ratio controls on capillary porosity. Also, when the ratio of water/cement increases the capillary pores is increased, and that leads to increase the reactivity of ASR, because one of the main factors that effects on alkali-silica reaction is water [67]. Previous study investigates on the relationship between porosity and water/cement contents. Ravindrarajah & Whitson (2011) confirms on a good correlation between porosity and water/cement content. As presented in figure below, when the amount of w/c ratio increased, the initial porosity also increased [68].

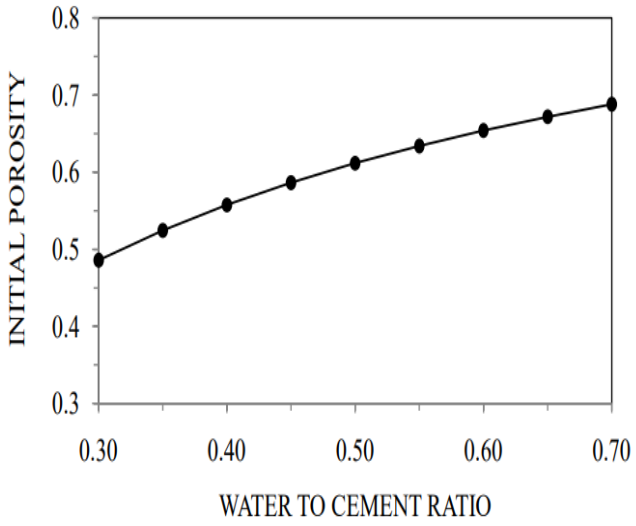

Figure 2.4 Shows correlation between water cement ratio and concrete porosity [68].

Previous studies investigates the effect of water/cement ratios in two parts. First part is the effect of water/cement ratio on cement hydration products. Where Knapen & Gemert (2008) found that the proportion rate of hydration, the growth rate of C-S-H, are rely on the amount of water/cement content in the mixture [69]. Agbo et al. (2013) mentioned that most of initial products, namely, calcium silicate ($2CaO{\cdot}SiO_2$), calcium-hydroxide $Ca(OH)_2$, and calcium- aluminate ($CaAl_2O_4$), are found as insoluble initial products. The high amount of water cement content is enough to raise the spacing among cement grains, through covering the spaces with water, causing weak bonds in structure [70].

Vladimir (2009), revealed that the hydration products are organized homogeneously in the inside structure when the amount of water/cement content is relatively low, the reason of that related to dense C-S-H layer that formed because of low w/c content, where the crystallization of products particles are very smooth and fine [71].

Zhang et al (2018) found that the curing conditions effects on the shape of hydration products. As shown below, curing at high relative humidity causes the water to evaporate, and as a result of that the fiber forms in a shape of clusters with short rods. While the fibers forms in a bundles with long rods, when it's cured in chemical solutions [39].

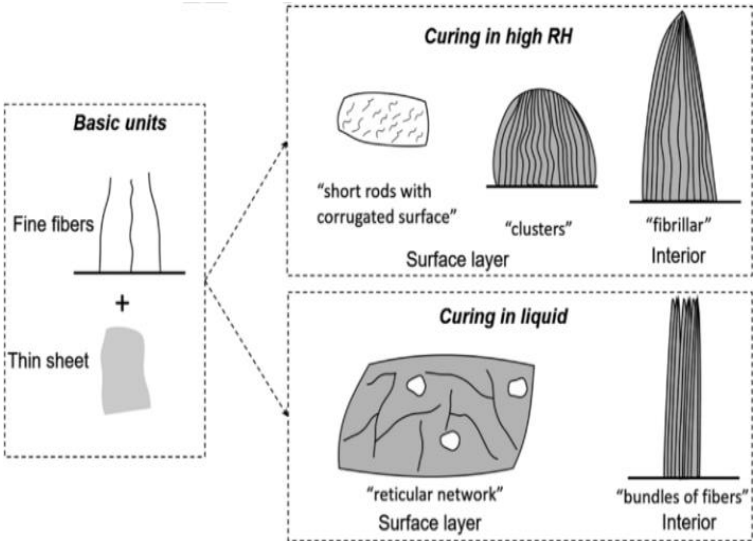

Figure 2.5 The impact of curing conditions on fibers shapes [39].

The influence of water/cement ratio and relative humidity has a great impact on alkali silica reaction reactivity. However, Poyet et al. (2006), study the impact of relative humidity on alkali- silica reaction, through measuring the mass variations loss in samples. The study found that the mass variation was ranged between 2.5% at 59 % RH, and an increase of 2.4 % at 100 % RH. The average mass of the 82% RH specimens remains stable during the test, which means that the initial relative humidity in the inner voids of the specimens was 82 %. The higher the percentage value of relative humidity, the higher reactivity of ASR [35].

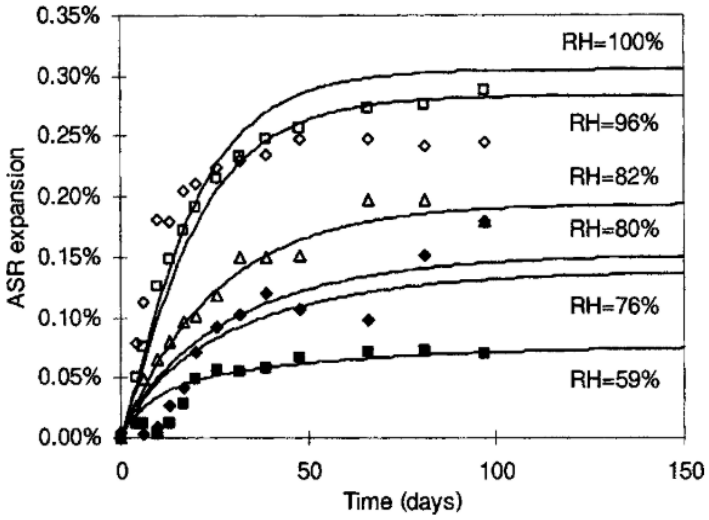

Figure 2.6 The impact of relative humidity (RH) in % on expansion of ASR [35].

Second part is the impact of alkali-silica reaction on reactive aggregates. However, reactive aggregates described as aggregates that chemically active when mixed with other products, and it's developed and expands. Reactive aggregates are divided into two types according to the amount of siliceous content in their minerals as; fast reactive aggregate, and slow reactive aggregate [72]. Munir et al. (2018) detect the properties of reactive aggregate on alkali-silica reaction, the study revealed that reactive aggregate absorbs water according to moisture state. Laboratory humidification is necessary for understanding the ASR mechanism, so increasing the humidification content during the test increases the absorption rate, which accelerates the rate of alkali-silica reaction, with the swelling of alkali gel, and that leads to form a deleterious crack. Also, the deformation caused by ASR seems to be long-lasting and cumulative when water is provided [73].

Water and temperature are essential for increasing the reactivity of alkali-silica reaction. The next section discuss the influence of altered temperatures on alkali-silica reaction.

2.6 The Effect of Temperature Variations on Alkali Silica Reaction

The effect of temperature variations on ASR reactivity were discussed in this part. The amount of silica and alkali plays a basic role in concrete durability, because dissolved alkalis in pore solution reacts with silica and produce a chemical reaction with deleterious effects on concrete called alkali-silica reaction (ASR) or ``concrete cancer``, and alkali-gel formed from this reaction [3]. The reaction depends on three main factors, which are temperature, humidity, and the amount of alkali and silica in the mixture, temperature and humidity considered as external factors caused by the environment. The temperature has a wide impact on the effects of ASR on concrete or mortar. Previous studies indicate a direct relationship between temperature, expansion, and final expansion [74].

Kawabata et al. (2019) mentioned that the leaching of alkali content increases with temperature, leads to a decrease in alkali ions inside the pore solution of mortar, thus explains the lower values final expansions [75].

Saouma & Perotti (2006) studied the effect of temperature variations on the reactivity of alkali aggregate reaction (ARR). As displayed in Figure 2.8, the experimental study relied on a comparison between a laboratory specimens at 38 °C, with an in situ dam

specimen at an average temperature of 7°C. The study showed that higher temperature increases the reactivity of alkali-silica reaction. Also, the study discovered that there's no correlation between high temperatures and final expansions [76].

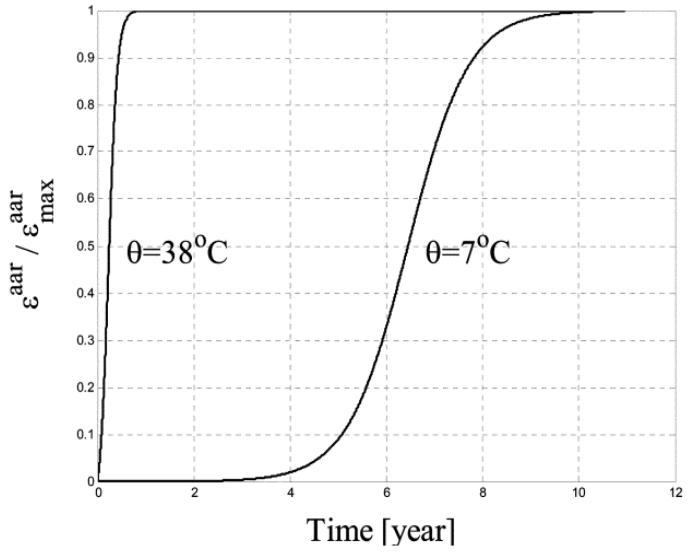

Figure 2.7 Shows the influence of temperature variations on (AAR) [76].

Yang et al. (2021) confirmed that there are three stages of expansion mechanism and damages, the stages are: elastic expansion, aggregate failure, and cracking of the cement paste. When the temperature increases, the amount of alkali content released and distributed through the cracks. Amount of alkalis on the face of mortar bars increased, and that explained why the stickiness of the alkali-gel losses at high temperatures, and less damage occurs in early stages of the expansion, because of the amount of alkali silica gel is restricted in low temperatures. The following figure describe these stages within 38 days [77].

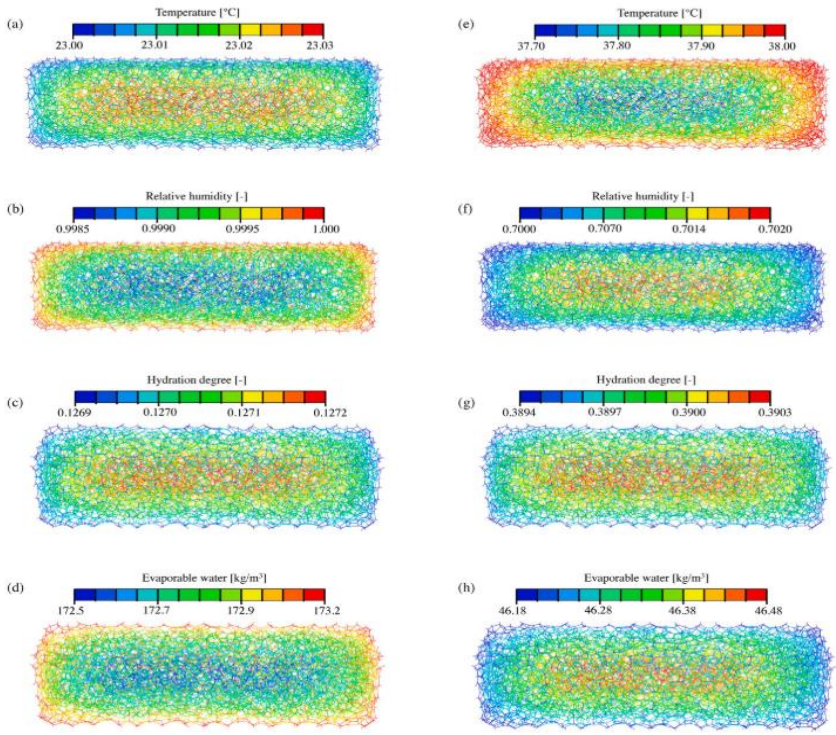

Figure 2.8 The phases hydration of the samples, where figure from a to d are related to the hydration within 4 days , and figure from e to h are related to hydration within 38 days [77].

Kawabata et al. (2022) mention that the capability of alkali gel to expand is decreased in high temperatures, which means that the expansion in late stage at low temperatures is higher, and the expansion due to long term is higher [78]. Crovace et al. (2021) stated that the viscosity of alkali-gel is higher in low temperatures, opposite than higher temperatures, and that explains why the expansion increased when the temperature increased [79].

The high leaching of alkalis due to high temperature, causes a porous and reticular on the surface of concrete or mortar microstructure, also made the distribution of hydration products such as ettringite tends to be heterogeneous [62].

The impact of high temperatures on the microstructure of concrete and mortar appears through hydration rate of cement and hydration products. Zhang et al. (2018) declared that the hydration products will raise during the first hours and days from the ASR, and distribution of hydration products will be gelatinous. While in low temperatures the distribution of hydration products is uniform and crystalline [39].

Kunther et al. (2015) studied the growth rate of ettringite in low temperature by the effect of ASR, the study revealed that the growth of ettringite crystals is slow and well

distributed, and the cracks caused by expansion was micro-cracks [40]. While the fast growth of ettringite, under high temperature, especially above 70°C, leads to precocious deterioration of the microstructure of concrete or mortar, and this case is called delayed ettringite formation (DEF) [80].

Ma et al. (2017) mentioned that delayed ettringite formation cannot be evaded in some cases, and the influence of (DEF) formed a destructive effect on the concrete structures. (DEF) was also discovered to occur at temperatures lower than 70°C, and that related to other factors, such as the amount of alkalis in the cement, finesse of cement, aggregate particles, and percentage of moisturizing [81]. Jime'nez et al. (2010) state that high temperature causes evaporation of C-S-H gel and shrinkage of the cement-paste, resulting in blasting of the materials. However, the pressure generated by the water evaporation due to the high temperature leads to the destruction of the pore walls, reduction of the cement strength and development of massive cracks. In addition, high temperatures leads to the dissolution of portlandite to calcium oxide (CaO) and water, and the resulting (CaO) is a very hygroscopic component whose volume exposed to increase when its re-hydrate. Also, the huge pressure that is created further decreases the compressive strength and can cause collapse [82].

The effect of temperature variations was detected through experimental studies. Sinno et al. (2021) observed the behavior of alkali silica reaction under several of curing temperatures and found that the aggregates increased the presence of alkali ions inside pore solution at high temperatures. Also, the cracks appear on the surface of cement-paste when the temperature was above 40°C, and the distribution of the cracks was uneven [83].

Experimental tests are used to define the effect of alkali-silica reaction on concrete or mortar. The tests are based on controlling the main factors that effect on ASR, such as; temperature, humidity, amount of silica and alkali, and other factors [84].

The following section defines the tests that used to determine the effect of alkali-silica reaction.

2.7 Test Methods Used to Determine Alkali Silica Reaction

As well as knowing the mechanism of alkali-silica reaction (ASR) in concrete, there is also a need of several test methods to detect this reaction. The most popular tests used to determine the reactivity of ASR on natural aggregates are accelerated mortar

bar test (AMBT), and concrete prism test (CPT). Both measures the expansion caused by alkali-silica reaction, relying on whether the aggregate contains reactive silica or not, and the amount of reactive silica determines whether the reaction is deleterious reaction or not, but accelerated mortar bar test is preferred because it can be done in a short time [85]. Also, scanning electron microscopic with energy dispersive x-ray spectroscope (SEM/EDX) was used to detect on alkali-silica reaction products.

2.7.1 Mortar Bar Method (MBT)

The mortar bar test used to measure the potential-reactivity of aggregates by measuring the linear elongation of mortar bars due to the reaction of ASR. Also, ASTM C 1260, and ASTM C 1293, are used as a base standard for determine the potential-reactivity of aggregate. By referring to ASTM C 1260, some instructions must be followed during the test, first the alkali content of cement is negligible, because the specimens are originally immersed inside sodium hydroxide solution (alkali solution), also the curing temperature of the soaked solution is between 80.0 C ± 2.0°, Then, it is important to mention that for the sample three intermediate measurements must be taken within 14 days, and the relative humidity should not be less than 50 %, and room temperature should not be less than 20 °C [20].

Owsiak (2017) explains mortar bar test as a process used to specify the potential deleterious cement aggregate, through immersing mortar bars in $NaOH_{(aq)}$solution at 80 °C within 16 days. The test was used quartz sand with opal, which known as reactive aggregates, to control on the elongation of bars due to ASR, where the maximum expansion value gives an indication of worst causes that the aggregate exposed [86]. The expansion of mortar bars depends on the nature of aggregate, and on the amount of reactive silica. Expansion limits are determined according to international conference in (1993) as follow: when the maximum expansion for the mortar bar test is less 0.1% or 0.15% after 14 days of test duration, then the behavior of aggregate is innocuous or non-deleterious, but if the expansion value is higher than 0.2 % or 0.25 %, then the aggregates are deleterious [87]. The differences between mortar bar test, and accelerated mortar bar test was discussed in the section below.

2.7.2 Accelerated Mortar Bar Test (AMBT)

Accelerated mortar bar test methodology or RILEM AAR-2, is a method used to distinguish between expanding and non-expanding aggregates, by immersing the

specimens of mortar bars inside sodium hydroxide solution, and measure the expansion of the specimens. The test also used ASTM C 1260 as a standard. However, test methodology depends on a specific standard of mortar bars, which are 3 specimens with a size of 25 x 25 mm, and length of 250 to 300 mm should be prepared, while the curing temperature is about 80°C. The draft of British standard method DD 249:1999, and the National Council of Cement and Building Materials in India has stated that [88]. Compared to the mortar bar test, this test gives higher expansion, because the alkali-content and the surface area of the specimens are higher. In addition, the effect of alkali silicon reaction is not noticeable in the AMBT when the aggregate is innocuous. Also, the expansion values are non-considered if the expansion exceeds 0.2 %, because the aggregates are classified as highly deleterious. It's important to note that AMBT is not appropriate for all types of aggregate, for example, it cannot measure the reactivity of glass aggregates within 14 days [89]. The accelerated mortar bar method is unable for chert aggregate, because the test method is used to determine the pessimum behavior, but it can't be sure that the pessimum proportion showed by the test corresponds with that exhibited by a comparable method [90]. To achieve best results, Trottie et al. (2021) recommends that the coarse aggregates should be uniformly crushed by crushing device, to achieve high consistency between aggregates and cement paste. The absorption rate must be consistent with the standard water content in the mixture, because decreasing or increasing the water content effects on the rate of alkali-silica reaction. [91]. Gress et al. (2015) compared between ASTM C 1260 and modified ASTM C 1260, through using modefing ASTM C 1260 on larger sample size and less amount of alkali solution. The compasrion was rely on the expansion rate of these two samples, where the early rate of expansion was quickly accelerated in the specimens with holes and cut sides, 21 days after, the expansion with holes was higher than solid specimens, and the specimens with holes achieved around one third of the expansion in 21 days. Also, the sample with high alkali amounts was not appear early expansion as the others [92]. In general, rapid expansion of mortar bars means that there is good correlation with aggregate performance in concrete, but if the expansion does not exceed 0.1 %, then ASR is slow and the effect of this process takes several years to appear, which means that it is not deleterious and normal [93].

2.7.3 Scanning Electron Microscopy with Energy Dispersive X-Ray Spectroscope (SEM/EDX)

The (SEM /EDX) test method is used to detect the formation of alkali silica gel (ASG), in addition to analysis the mineralogical composition of the gel. The X-ray function allows analysis of product crystallizations that are difficult to identify with optical microscopy [5]. The principle of scanning microscopy is to expose the specimen to a beam of electrons. The electrons penetrate the microstructure and provide information about the range of the damage formed by the expansion of mortar bars. Two methods are used to make the sample for scanning microscopy: first method is dry potting, in which a section is removed from the sample and the sample is dried with temperature of 65°C for 24 hours, to ensure water evaporation. Then the sample is placed in a pot covered of epoxy resin, with the top of the sample exposed to laboratory air. After using a vacuum, the epoxy resin sample is stored at a temperature less than 65°C, then sample is ready for slicing and polishing. The second method is wet potting, in which alcohol is used to fill the pores, and then low viscosity epoxy resin is used and cured [94]. In order to understand the crystallization mechanism of mortar or concrete paste after exposing to curing conditions, scanning electron microscopy (SEM) and backscattered electron microscopy is used for this purpose. Pospisil et al. (2017) state that the cracks that appeared on scanning image (SEM/EDX) gives an indication of the intensity of ASR. When the cracks are close to cement paste, then the expansion that caused from ASR is non deleterious, and the amount of amorphous gel is low, with high amount of calcium ions inside. While, the cracks that appeared close to the surface of aggregate particles, reflects high magnitude of amorphous gel with low amount of calcium ions inside, this case was appeared only when the expansion that caused from ASR was deleterious [95]. Shin et al. (2015) describe the cracks caused by ASR as their location and how they are related to each other. Also, the products of alkali gel appear in the SEM images by colors, where white a color in the images shows un-hydrated cement paste, and hydrated cement paste is exist in light gray areas. The dark areas represent the aggregate particles, and the grains of un-hydrated cement are shown as dark gray areas [96].

Voltolini et al. (2011) found by means of (SEM /EDX) that when the sample extends more than 0.1%, the dark edge covers the silicon aggregate, while the micro-cracks are

filled with alkali gel and extend through cement paste to aggregate particles. In addition, the study revealed three types of voids, the first type formed during mixture and casting, and it has bubble shape which increased by increasing the amount of water in the mixture. The second void formed by aggregate dissolutions, where the alkali gel fill the voids then dry, this process caused a spongy shape of these voids, and the volume of these voids increase by increasing the reactivity of ASR. The third type is cracks due to the expansion of ASR, which is usually filled with alkali gel. The following figure showed the shape of these types [97].

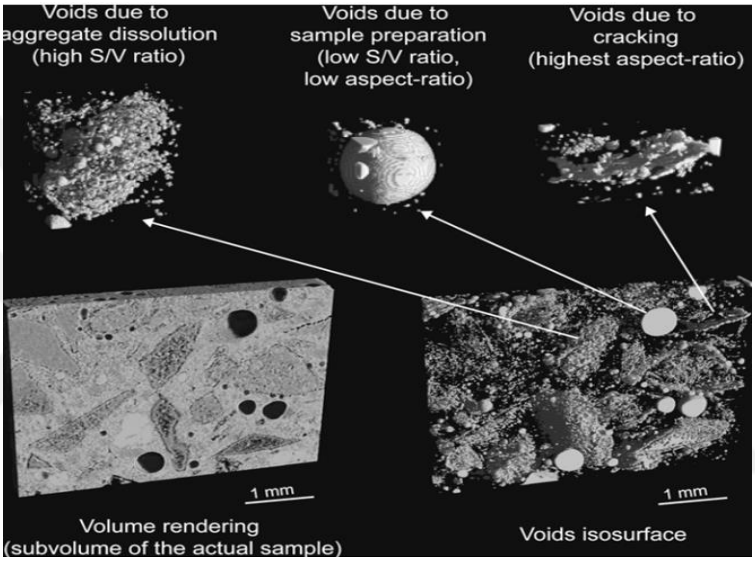

Figure 2.9 Shows type of voids due to alkali silica reaction [97].

Thaulow et al. (1996) found that the gel produced contained high and variable amounts of silica and lower and varying amounts of calcium [98]. Also, the gel occurs in cracks and has a higher calcium content, and it passes through the hardened cement paste than inside the aggregate [99].

2.8 Other Test Methods

Many studies and research have been done since Thomas Stanton discovered ASR to determine the deleterious behavior of reaction, the shape of the fractures produced by this reaction, and techniques to mitigate its effects [86]. In the previous section, some testing methods were presented, such as mortar bar test method (MBT), accelerated mortar bar test method, and scanning electron microscopy (SEM). These tests have advantages and limitations. For example, (AMBT) is the suitable test method to measure the potential-reactivity of aggregates in 14 days, but (AMBT) is not suitable

for all types of aggregates, such as lightweight aggregates and chert aggregate. Also, the amount of alkali content in MBT and AMBT are not considered [100,101].

However, other test methods are used to investigate the effect of alkali-silica reaction, not only for mortar, but for concrete, such as, concrete prism test, and Autoclave test method.

2.8.1 Concrete Prism Test (CPT)

This test is one of the common and reliable test for measuring the reactivity of ASR. The prisms are made with dimensions of (75 × 75 × 285) mm, and the value of water/cement ratio is set between 0.42 to 0.45 in the mixture, the weight of cement is 420kg/m^3. Test reference is ASTM C1293. The amount of alkali in this test is 1.25 Na2Oeq, and the prisms are immersed in sodium hydroxide. The curing temperature of concrete prisms is 38°C.

The main disadvantage of this test is that it takes a long time to get the final results 52 week at most, perhaps more than a year, and this is because the alkali quantity and curing temperature are low [102]. In order to measure the elongation of samples within 13 weeks rather than 52 weeks, the prism test for concrete was converted to an accelerated prism test by increasing the curing temperature up to 60°C, with using the same reference ASTM C1293 [103].

2.8.2 Autoclave Test Method

Fournier & Berube (1991) have developed a new method for measuring the expansion that occurred by the reactivity of alkali-silica reaction on mortar bars, the test is driven and modified form of ASTM C 227. The test methodology is to mix sodium hydroxide NaOH with water to increase the amount of alkali in the solution, since alkalis enhance the alkali-silica reaction. Then mortar bars are placed in autoclave device under a degree of 23°C, with high relative humidity, for two days. The autoclave test is suitable when the steam cut is 130°C [104].

Also, the test is modified to accelerated autoclave test method, this test method was used from various researchers in order to measure the reactivity of ASR in a short period, when it's referred to a short time means that it not exceeds one day, for concrete prism specimens the test duration is ranged between 4 to 24 hours, and called accelerated autoclave concrete prism test, while in mortar bars it is between 4 to 6 hours, and called accelerated autoclave mortar bar test. Also, the factor of temperature

is strongly appears in this test, because high temperature increases the reactivity of ASR, the curing temperature in this test is set between 111°C and 150°C [105].

The preparation of autoclave specimens are prepared by ASTM C 1293, for autoclave concrete prism test, or by ASTM C 1260, for autoclave accelerated mortar bar test. One day after casting, the original length of the specimens is determined, then they are placed in the autoclave for 4, 6 hours or one day and totally soaked in a NaOH solution, with a curing temperature usually of 130°C, and a pressure of 0.20 MPa. The principle of this test is to measure the expansion due to alkali silica reactivity under high pressure and temperature. However the specimens are cooled to an ambient temperature of 23°C, and the final length is measured over one hour [106].

CHAPTER 3

EXPERIMENTAL PROCEDURES

3.1 Introduction

This experimental study investigates the influence of alkali-silica reaction (ASR) on mortar bars, through assessing the potential reactivity of two types of aggregates, namely aggregate (A) and aggregate (B). The study adopts three altered curing temperatures 40°C, 60°C, and standard 80°C, with different proportions of water cement ratios 0.4, 0.5 and 0.6. The experimental study employed accelerated mortar bar test (AMBT), based on ASTM C1260 standard, which is used to discover the potential aggregate reactivity of unstable silica [20]. In addition to methodology and preparation of accelerated mortar bar test (AMBT), and scanning electron microscopy with energy dispersive x-ray spectroscope (SEM/EDX). In short, this chapter clarifies in order, the used materials, experimental specimen's classification, and equipment.

3.2 Materials

Mortar specimens were prepared using the following materials:

3.2.1 Cement

Ordinary Portland cement type I 42.5R (rapid hardening) with high early strength was used in the test. This type of cement gains strength quickly, and type (I) in ordinary Portland cement, indicate that the proportion of other materials in this cement does not exceed 5%, which mean that this type of cement is classified as pure Portland cement. While (42.5R) is the value of the initial strength [107].

Table 3.1 displays the chemical components of the usage cement, in addition to the amount of alkali content (Na_2O_{eq}), which was 0.85%. The cement classified as high alkali cement because the value Na_2O_{eq} was higher than 0.6%. Also, the cement contained of high proportion of potassium oxide (K_2O). Table 3.2 illustrates the physical properties and strength of the used cement.

Table 3.1 Properties of cement type I 42.5 R

Chemical properties of cement					
SO_3	MgO	K_2O	CL	Na_2O	Na_2O_{eq}
1.97	1.83	0.86	0.03	0.29	0.85

***Na2Oeq = Na2Oeq + 0.658 K2O** [108]**.**

Table 3.2 Physical properties and cement strength

Physical properties of the cement						
Blane fineness	Sp. W. gr/cm3	Fine % (32 micron)	Fine%(40 micron)	In. set.	Fin. Set.	Volume expansion
3598	3.12	12.4	6.7	196	248	1
Strength of cement						
Days				**TS EN 197-1**		
2	51-week 20 Dec – 26 Dec-2021		MPa	**Minute 20**	**25.5**	
7	50-week 13 Dec – 19 Dece-2021		MPa		**37.9**	
28	47-week 22 Nov– 28 Nov-2021		MPa	**42.5-62.5**	**48.2**	

3.2.2 Aggregate

Two different aggregates were used in this experimental study, and the test procedure was designed to distinguish between these two types. The aggregates were labeled as A and B. Table (3.3) illustrate the distribution of one kilogram of aggregates needed for the mix design. The sieve numbers are 10, 18, 20, 40, 50 and sieve100. Also, Table 3.4 represent the physical properties of tested aggregates.

Table 3.3 Distribution of returned weight

Sieve number	**Weight in gram**
10	178
18	250
20	63
40	272
50	32
100	1000

Table 3.4 Physical properties of aggregate

Bulk density	Aggregate (A)	Aggregate (B)
Saturated surface dry	2.59	2.64
Oven-dry	2.54	2.62
Water absorption (24 hour)	1.83	0.6

3.2.3 Sodium Hydroxide

Sodium hydroxide (NaOH) was presented as a solid material, but it was used in the test as a soluble solution. The solution consist of 40 g of NaOH dissolved in one liter of distilled water. Table (3.5) shows the specification of NaOH that used in the test.

Table 3.5 NaOH specification

Specification	Approximate values
Purity	98%
Sodium carbonate	0.5%
Sodium chloride	0.02%

3.3 Specimen Description

In this experimental study three main groups, namely, group one (G1), group two (G2), and group three (G3), were used to study the effect of ASR on mortar bars. However, the total number of bars cast was 54, divided of 18 bars for each main group, the major criterion of this division is the curing temperatures. While the minor criteria of the same group based on the amount of water/cement ratios, and aggregate types. Table 3.6 describes the characterizations of the main test groups, and Table 3.7, 3.8 and 3.9, illustrates in detail a description of group one, two, and three.

Table 3.6 Characterizations of test groups

Group number		**Group 1**			**Group 2**			**Group 3**		
Specifications	**Water/cement ratio**	0.4	0.5	0.6	0.4	0.5	0.6	0.4	0.5	0.6
	Curing temperature	40°C			60°C			80°C		
	Aggregate type	(A)		(B)	(A)		(B)	(A)		(B)

3.3.1 Group G1:

The curing temperature of the mortar specimens in this group was 40°C, and the group contained of 18 samples that were divided into three different sections, according to the water cement ratios. However, there were six mortar bars in each section of this group, divided equally in to aggregate (A) and aggregate (B). Also, all of six samples were casted with the same water/cement ratio and placed in the same soaking solution (1N NaOH). Table (3.7) clarified the distribution of the samples in the first group.

Table 3.7 Group one distributions

	Group description						
Group one	**Water/cement**	0.4	0.4	0.5	0.5	0.6	0.6
	Aggregate type	(A)	(B)	(A)	(B)	(A)	(B)
	Curing temperature	40°C	40°C	40°C	40°C	40°C	40°C
	Soaked solution	NaOH	NaOH	NaOH	NaOH	NaOH	NaOH

3.3.2 Group G2:

The curing temperature of this group was 60°C and contained of 18 mortar bars that were divided into three sections, and distributed according to the amount of water/cement ratios in the mixture. Where each sample had 6 bars, three of them made from aggregate (A), and aggregate (B). Also, all of the tested samples in this group was immersed in hydroxide solution. Table 3.8 shows group two distributions.

Table 3.8 Group Number 2 distributions

	Group description						
Group two	**Water/cement**	0.4	0.4	0.5	0.5	0.6	0.6
	Aggregate type	(A)	(B)	(A)	(B)	(A)	(B)
	Curing Temperature	60°C	60°C	60°C	60°C	60°C	60°C
	Soaked solution	NaOH	NaOH	NaOH	NaOH	NaOH	NaOH

3.3.3 Group G3:

In this group, there were eighteen samples, divided exactly according to the same classification system of group one and group two. These samples were divided into three different sections, each section had 6 samples, three of which was made from aggregate (A), and aggregate (B). The curing temperature in this group is 80℃. However, the following table show the distributions of this group.

Table 3.9 Group Number 3 distributions

Group three	Group description						
	Water/cement	0.4	0.4	0.5	0.5	0.6	0.6
	Aggregate type	(A)	(B)	(A)	(B)	(A)	(B)
	Curing temperature	80°C	80°C	80°C	80°C	80°C	80°C
	Soaked solution	NaOH	NaOH	NaOH	NaOH	NaOH	NaOH

3.4 Preparations of Test Equipment

The preparation of the equipment's before the test was necessary to achieve accurate results, avoid errors that cost money and time, because different variations will appear on the required ratios, if the preparation was neglected. However, five pieces of equipment were used in this experimental program, described in the following sections:

3.4.1 Oven Dry

The preparation was accomplished by operating the oven dry before one day of casting, to inspect the device ability to conserve heat without seepage, also to ensure that the oven has reached the required temperature.

Figure 3.1 Oven dry.

3.4.2 Molds

In this test, the required molds for casting six samples of mortar bars was three molds, with a dimension of 25*25*250 mm. Each mold was equipped with two identical pins to cast in mortar bars for taking expansion measurements. In this test, the molds were prepared before casting. At first the molds were fully cleaned by dry wipes , this step is important to ensure dust removal from the molds, then plastic sheets (See figure below), was used to cover the molds, which was used to reduce corrosion in molds, and to prevent the bars to broke when it's removed from molds. At last the edge of the molds from the inside and the place where the pins are placed in, was covered in oil for the same reasons above.

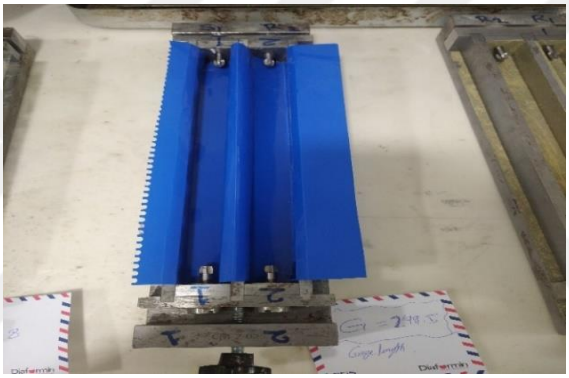

Figure 3.2 Mold covered with plastic sheet.

3.4.3 Mixer

According to ASTM C-305, the mixing process must be done in three revolutions: slow, medium and fast. The mixer that used in the laboratory had two revolutions: slow at 62 Rev/min and medium at a speed of 165 Rev/min. Based on the standard, the revolutions were accepted. Figure 3.3 showed the mechanical mixer.

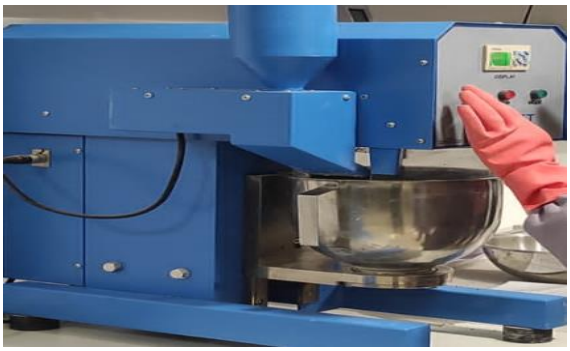

Figure 3.3 Mechanical mixer.

3.4.4 Plastic Containers

Rectangular containers were used to match the length of mortar bars, the placement of the bar samples in the containers required a distance between the edge of the container and the bar, as well as a distance from bar to bar. The plastic number is important for the quality of the container, plastic number 5 was used in this test because it is lightweight and resist heat. The containers can withstand temperatures up to 100ºC. Also, the lid of the container must be well closed to prevent evaporation. The following figure shows the organization of mortar bars inside the plastic container.

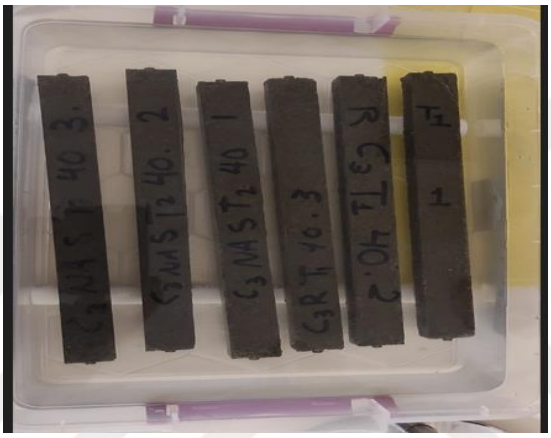

Figure 3.4 Plastic container.

3.4.5 Reading Device

Reading device was used to record length change (expansion) on mortar bars. Before measuring, the device must place in flat surface, then the reading rod is used to gain zero reading (0.00), before placed mortar bars in the device, as shown in figure below.

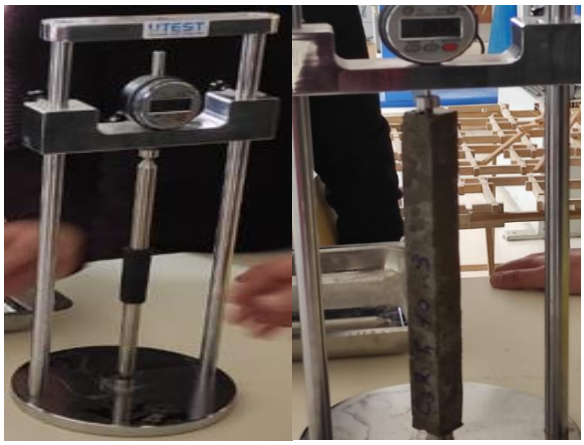

Figure 3.5 Calibration of reading device.

3.5 Experimental Tests

This experimental study used three test methods to achieve the final result, starting with the accelerated mortar bar test method (AMBT), and scanning microscopy with energy x-ray dispersive (SEM/EDX).

3.5.1 Accelerated Mortar Bar Test (AMBT)

The potential reactivity of tested aggregate was measured through using AMBT, with ASTM C 1260. In this test two kinds of aggregates were used aggregate (A), and aggregate (B). However, the test started with mixing process and casting, because increasing the quality of casting perform accurate results. This test used ASTM C 305 as a reference for mixing process, as follow:

1. The mixing materials were adding to the same bowl as described in ASTM C1260, the mixing materials was 440g of cement and 990g of aggregate, where the type of used aggregate depends on tested group.

2. The cement and aggregates were mixed in dry-state, the mix speed started with slow speed for 30 second, to ensure consistency between cement and aggregate particles with water.

3. While mixing, water was supplied according to the required water/cement ratio in tested group, after that the mixer speed changed to medium. Then the mixer was stand for 90 seconds, to mix all of mortar that collected in the bottom of mixer together.

4. The mixer housing was closed, and the mixing was in medium speed for 60 second. Figure (3.6) shows cement and aggregates that used of sample preparation.

Figure 3.6 Mixing process where (A) Cement and aggregate, (B) medium mixing speed.

After mixing, mortar was casted in the molds on two layers, within two minutes, where each layer was hammered around 15 to 30 times to remove air bubbles, then the surface of the molds was trimmed to get rid from excessive mortars (Figure 3.7). Few hours after casting, the surface of the molds covered in a moist sheet, to conserve inner humidity from fast evaporation (Figure 3.8), then the samples placed in room temperature at 24°C for one day. Then the mortar bars removed from the molds and immersed in water, the specimens were stored in the oven according to their group number, then after one day the initial length was measured by reading device.

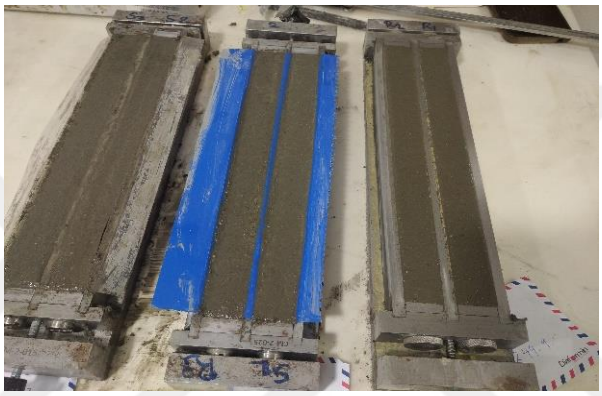

Figure 3.7 Fresh mortars in the molds.

Figure 3.8 The steps of mixing and casting of mortar bars.

After the initial length was taken, the samples must be immersed in alkaline solution for 28 days. In this experimental study, sodium hydroxide was used as a solution in which the samples were immersed for the required interval time of the experiment. The required amount of sodium hydroxide solution was constant of all samples, the concentration of 1N (equivalent to one mole of solute per liter of solution), sodium

hydroxide must be dissolved in distilled water. The test used 40 g of sodium hydroxide with 900 ml of distilled water, where water poured into a glass flask and mixed with 40 g of sodium hydroxide. Since sodium hydroxide has a corrosive effect on the skin and eyes, safety instructions must be followed.

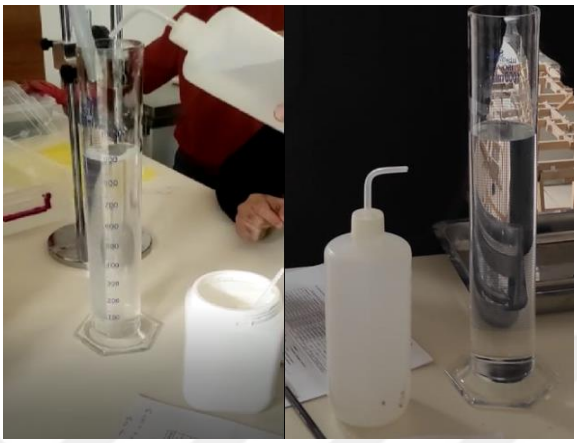

Figure 3.9 NaOH solution preparation.

After sodium hydroxide prepared, the mortar bars was fully immersed in, and placed in oven, the temperature of oven depends on group number as explained in section (3.3). However, the expansion of mortar length was measured every three days and recorded as presented in Figure (3.10).

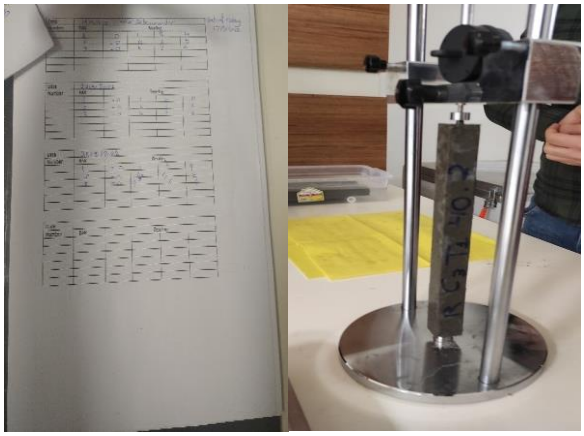

Figure 3.10 Expansion measurement.

3.5.2 Scanning Electronic Microscope with Energy Dispersive X-Ray Spectroscope (SEM/EDX)

The scanning electron microscopy with energy dispersive X-ray spectroscope (SEM/ EDX) method is considered as non-destructive test methods that can detect the effect

of alkali-silica reaction with the reaction products, especially alkaline gel, on the microstructure of concrete or mortar. Figure (3.10) shows (SEM/EDX) device, which has four detectors. The first detector is a secondary electron detector that produces topographic and morphological data as well as 3-D images. The second detector is the 5-segment backscatter electron detector, which provides atomic composition and Z-contrast information. These detectors provide a clear image of the alkaline gel, with different magnification levels, because the device has resolution of 1.20 (nm) to 3.00 (nm), with a magnification of 30× to 1,500,000×. Also, the voltage of the device is ranged from 0.5 to 30 (kV). However, the final detector is the EDS detector, which is used to identify the elemental constituents that produced from alkali silica reaction, with a graphical EDX mapping that clarifies the elemental concentrations and distributions throughout the sample.

Figure 3.11 Scanning electron microcopy device with Energy Dispersive X-Ray Spectroscope (SEM/EDX).

The specimens of mortar bars must be prepared before using (SEM/EDX), the methodology of test is explained below.

3.5.2.1 Test Methodology and Preparation

After 28 days of test duration, the specimens have reached the maximum expansion caused by alkali-silica reaction, the silica-gel has formed in the infrastructure of the mortar bars. In order to study the impact and the formation of alkali silica products on the mortar bars, scanning electron microscope with x-ray energy spectroscope was used to serve this purpose. The (SEM/EDX) was divided into two phases, namely, secondary electron image (SE) and backscattered electron imaging (BE). Samples must prepare before imaging to ensure high resolution for microscope images. Two

methods was followed to prepare samples for scanning image dry method and wet method, but in this experimental study, since the specimens are previously dried, dry method was followed, and no-epoxy was used. The mortar bars were taken from the sodium hydroxide solution because the bars were fully saturated in the solution and left for one day to dry, under the laboratory degree. Then the samples were placed in the oven for 24 hours, with a temperature of 65°C. However, oven temperature must not exceed 65°C, and the most important step in this method is to ensure evaporation of water content of the mortar samples by using oven drying, because water interferes with the polymerization and on the resolution of the SEM images, and that lads to reduce image accuracy [94]. To ensure high quality of mortars microscopy, preparation process is important, the mortar samples were taken from oven and placed in laboratory degree for 24 hours. After that samples was cut into slices, and classified according to its original groups, as shown in figures below. Each group contain of six bags made from aggregate (A) and (B). The classification of the plastic bags for each group was distributed according to curing temperature and water/cement ratio. The last step is dust removal, by using brush, the outer surface of the samples was brushed to remove fine obstacles before scanning. Then the specimens were taken to the central laboratory to start the (SEM/EDX). Before starting the tests, the SEM samples were prepared with the following LEICA ACE 200 Coating Device (Figure 3.12). It allows the surfaces of non-conductive samples to be made conductive. It can be automatically coated homogeneously with conductive metals or carbon.

Figure 3.12 LEICA ACE 200 coating device.

CHAPTER 4

RESULTS AND DISCUSSION

This chapter shows the results and discussion of the experimental study in three sections. The first section of this chapter shows the expansion curves of the tested mortar bars through 28 days, using the (AMBT) method with ASTM C 1260 to estimate the reactivity of the aggregates. In the second section, scanning electron microscopy and energy dispersive x-ray spectroscopy (SEM /EDX) was used to analyze the ASR products. In the third section, the results of (AMBT) and (SEM /EDX) were discussed.

4.1 Group Classifications and Expansion Results

In this experimental study, 54 mortar bars were cast and divided into three major groups according to curing temperatures and water/cement ratios, as shown in Table (4.1).

Table 4.1 Group classification according to curing temperature and w/c.

Group ID	Water/cement			Curing temperature
Group 1	0.4	0.5	0.6	40 ºC
Group 2	0.4	0.5	0.6	60 ºC
Group 3	0.4	0.5	0.6	80 ºC

The preparation and measurement of mortar bars in this study was accomplished by using (AMBT), the reactivity of tested aggregates was measured in the 14th day of the test period, and determined according to ASTM C 1260. Also, standard categorized aggregates as harmless or innocuous, if the expansion value was lower than 0.1%. While aggregates classified as potentially-reactive or harmful, if the expansion percentage was extended from 0.1% to 0.2%, but if the expansion value exceed the percentage limit of 0.2%, then the aggregates classified as highly reactive [20]. However, expansion percentage of mortar bars was calculated by this equation.

$$L = ((L_t - L_{rt}) - (L_0 - L_{R0})/250) * 100L \qquad \text{Eq (4.1)}$$

Where (L) is change in length and expressed in percent %, (L_0) is the initial comparator reading, and (L_{R0}) is initial reading of reference bar, L_t is at day, comparator reading. Groups divisions were discussed in chapter 3, section 3.3. The following subtitles shows the average expansion results of each group:

4.1.1 Expansion Results of Group 1

The following figures shows the expansion of eighteen bars made form aggregate (A) and aggregate (B) at altered amounts of water/cement ratios (0.4, 0.5, and 0.6), with constant curing temperature of 40ºC for all samples.

In the first section of this group, w/c was 0.4, with curing temperature of 40ºC, as shown in figure below.

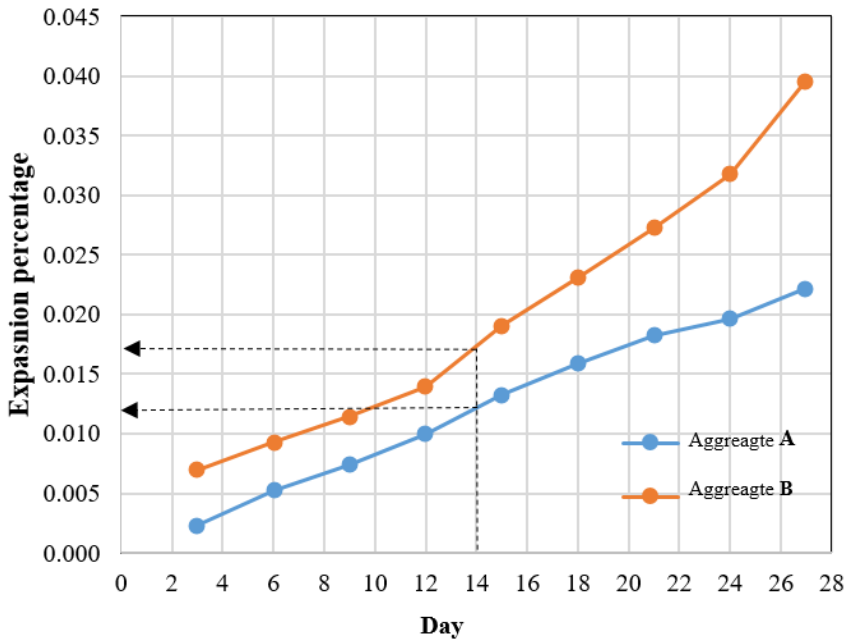

Figure 4.1 Expansion curves of tested aggregates at w/c: 0.4 and 40 ºC.

Figure (4.1) illustrates the average expansion curves of two types of aggregates within 28 days. As shown, the percentage expansion value of aggregate (A) at day 14 was 0.013%, while in aggregate (B) was 0.018%.

Figure (4.2) provides the expansion curves of both types of aggregates when water/cement ratio increased to 0.5, where the expansion percentage of aggregate (A) was 0.019%, and 0.015% for aggregate (B).

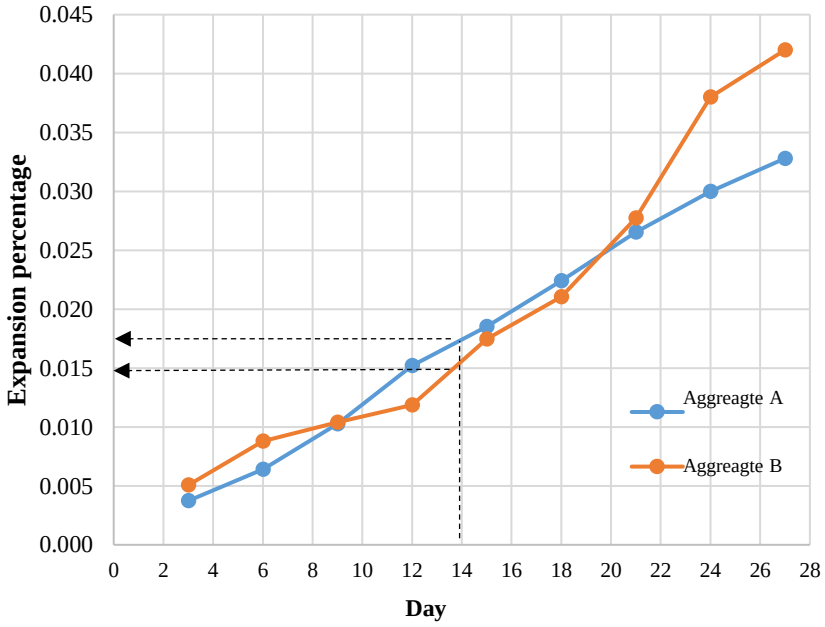

Figure 4.2 Expansion curves of tested aggregates at w/c: 0.5 and 40 ºC.

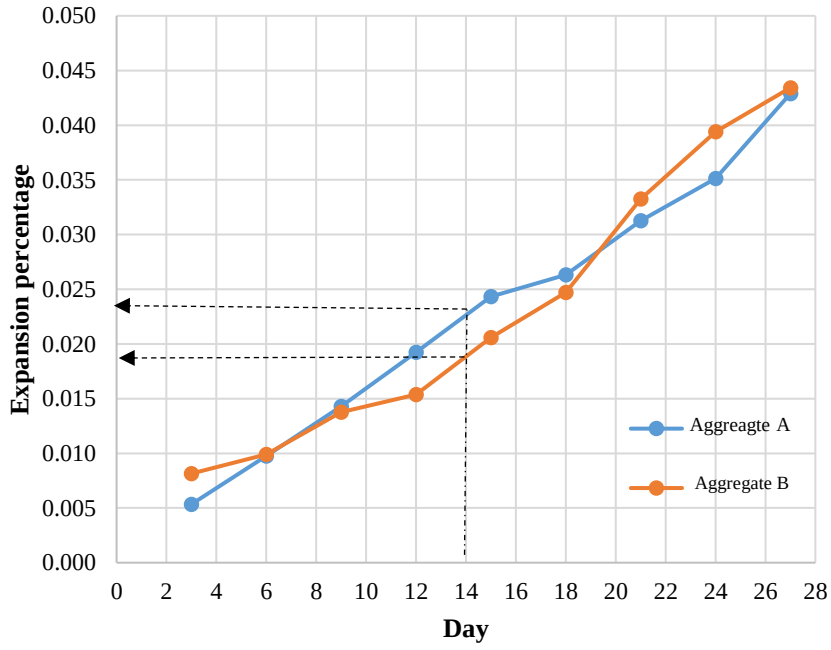

Figure 4.3 Expansion curves of tested aggregates at w/c: 0.6 and 40 ºC.

Figure (4.3) illustrates the performance of aggregate (A) and aggregate (B). Where the expansion percentage of aggregate (A) was 0.024%, and for aggregate (B) was 0.019%.

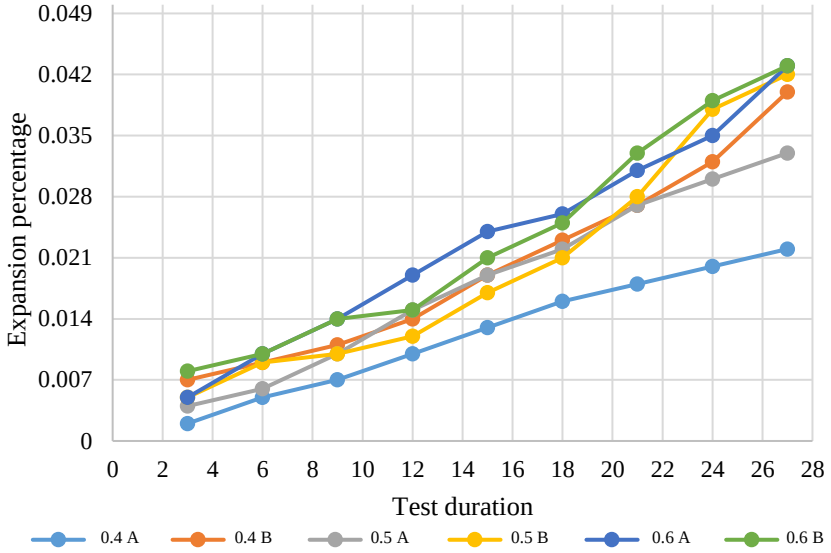

Figure 4.4 Comparison between tested aggregates at w/c: (0.4, 0.5 and 0.6) and 40 ºC.

Figure (4.4) shows the limited differentiations between tested aggregates in day 14 with the end of test duration, when water/cement ratio raised to 0.6, the reactivity of aggregate (A) in day 14 was higher than aggregate (B), then after day 14 the opposite has occurred.

4.1.2 Expansion Results of Group 2

This group illustrates the expansion results of two types of aggregates at a curing temperature of 60ºC, and different water cement ratios as follow: 0.4, 0.5 and 0.6, as appeared in figures below.

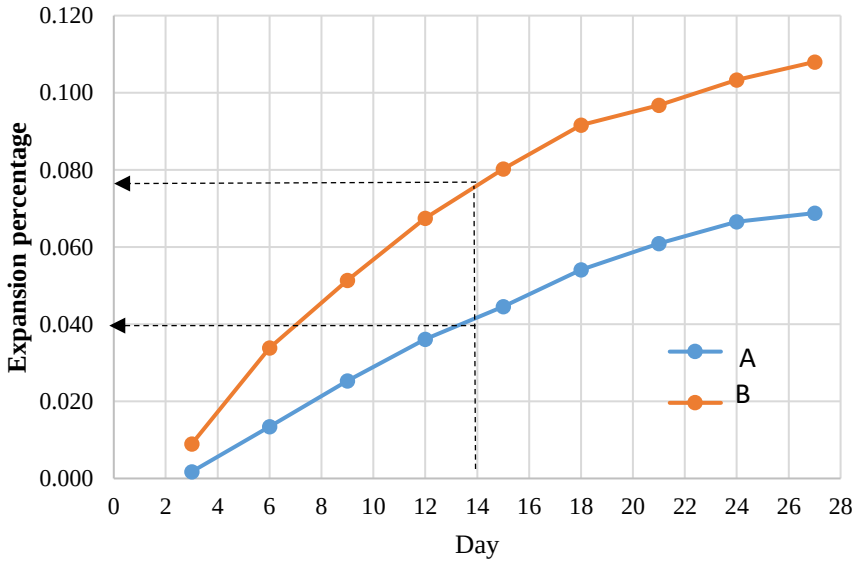

Figure 4.5 Expansion curves of tested aggregates at w/c: 0.4 and 60 ºC.

The previous figure (Figure 4.5) shows the expansion curves of tested aggregates at 0.4 w/c. Where the expansion percentage of aggregate (A) was 0.043%, and 0.078% to aggregate (B).

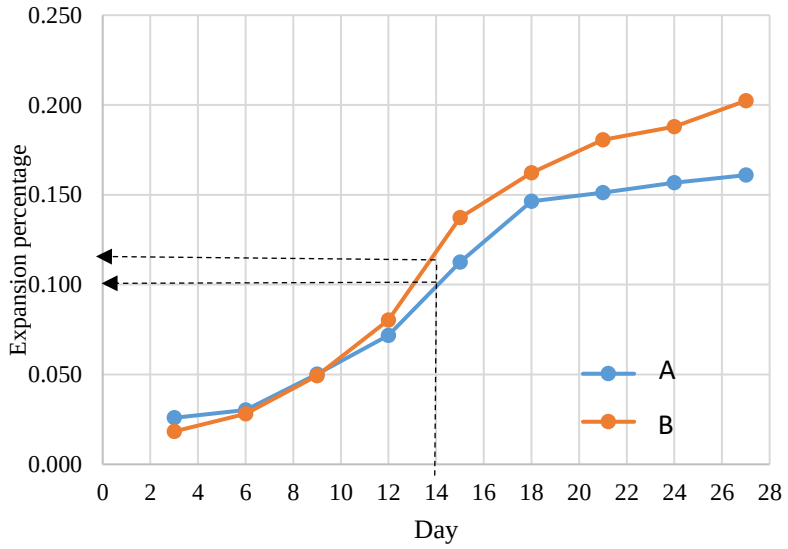

Figure 4.6 Expansion curves of tested aggregates at w/c: 0.5 and 60 ºC.

Figure (4.6) illustrates the reactivity of tested aggregates at w/c: 0.5. Where the expansion value of aggregate (A) in day 14 was 0.1%, and for aggregate (B) was 0.137%.

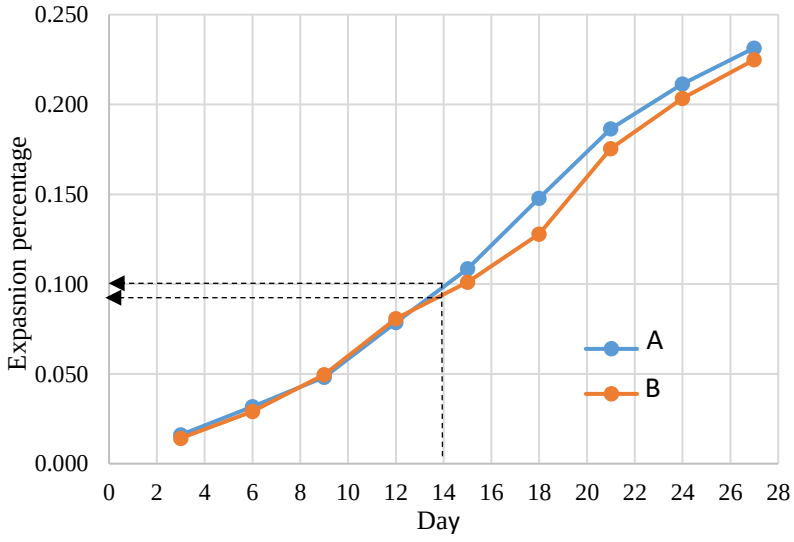

Figure 4.7 Expansion curves of tested aggregates at w/c: 0.6 and 60 ºC.

Figure (4.7) shows the expansion values of tested aggregates at 0.6 w/c, the expansion values of both types of aggregates were similar to each other and higher than 0.1%.

Figure (4.8) provides comparison between all of expansion curves of group 2, and temperature of 60ºC. As shown the reactivity of aggregates gradually increases as water/cement ratio increases. Also, the reactivity of both types of aggregates was deleterious at 0.5 and 0.6 w/c.

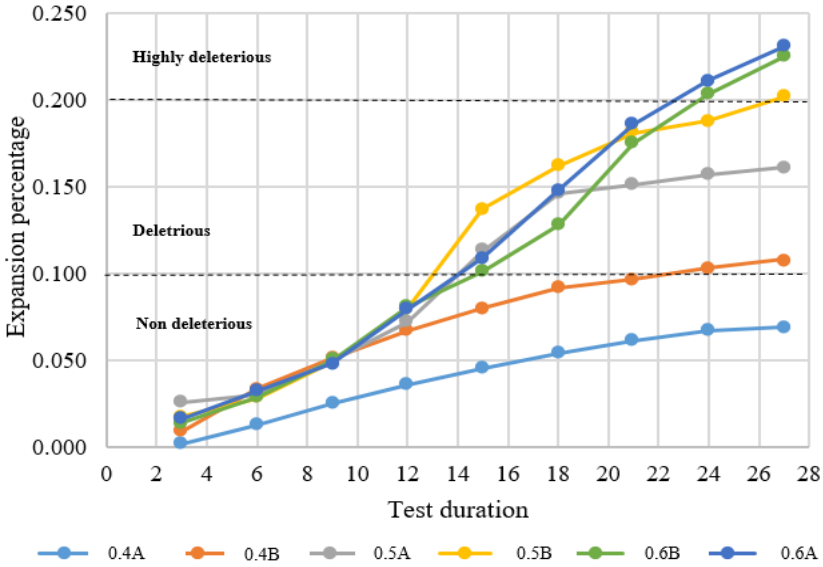

Figure 4.8 Comparison between tested aggregates at w/c: (0.4, 0.5 and 0.6) and 60 ºC.

4.1.3 Expansion Results of Group 3

In this group the expansions due to alkali silica reaction were measured, through increasing the curing temperature to 80ºC, and altered water/cement ratios (0.4, 0.5, and 0.6).

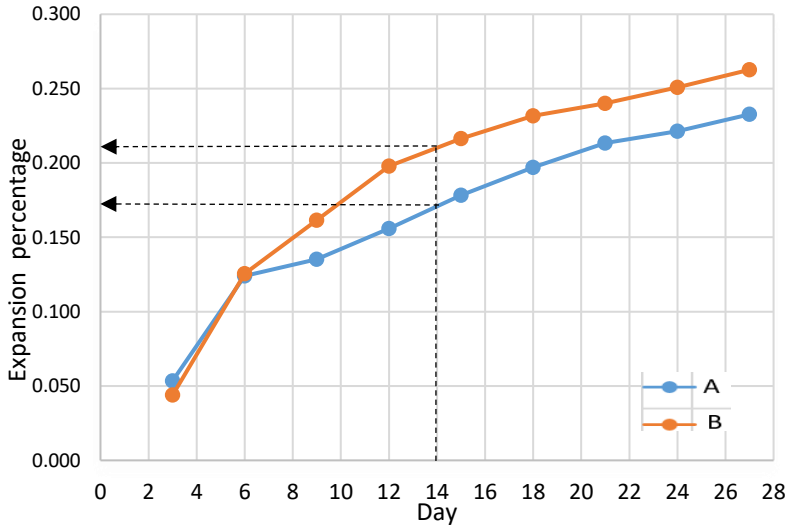

Figure 4.9 Expansion curves of tested aggregates at w/c: 0.4 and 80 ºC.

Figure (4.9), shows expansion of 6 mortar bars under a curing temperature of 80°C, and 0.4 water/cement ratio. The expansion percentage of aggregate (A) was 0.178%, while in aggregate (B), the expansion value was 0.219%.

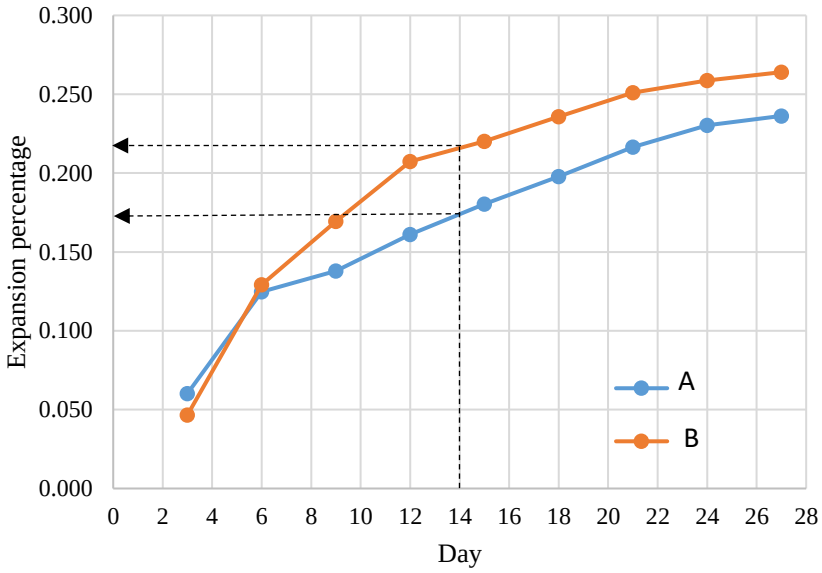

Figure 4.10 Expansion curves of tested aggregates at w/c: 0.5 and 80 ºC.

Figure (4.10) shows the reactivity of tested aggregates at 0.5 water/cement content. Where the expansion percentage of aggregate (A) was 0.180%, and 0.223% to aggregate (B). The reactivity of aggregate (B) was higher than aggregate (A).

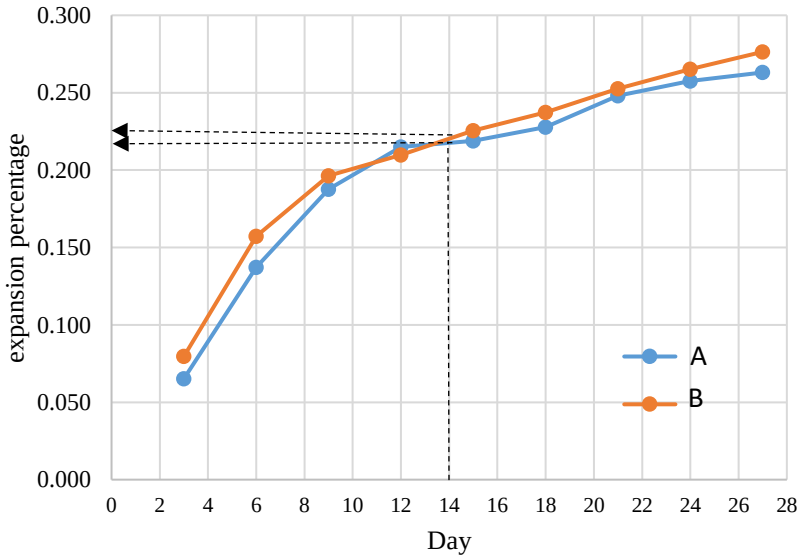

Figure 4.11 Expansion curves of tested aggregates at w/c: 0.6 and 80 ºC.

In Figure (4.11) the potential-reactivity of aggregate was measured by increasing the amount of water/cement ratio up to 0.6. Where the expansion percentage of aggregate (A) was 0.220%, and 0.226% to aggregate (B). Therefore, the reactivity of aggregate (B) was higher than aggregate (A).

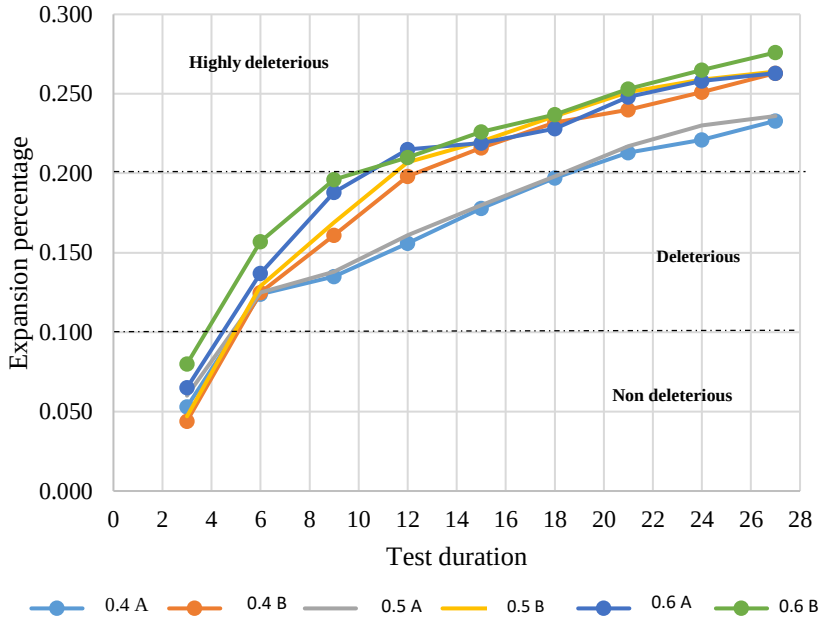

Figure 4.12 Comparison between tested aggregates at w/c: (0.4, 0.5 and 0.6) and 80 ºC.

The comparison of all expansion curves of group 3 at a temperature of 80ºC was shown in Figure (4.12), where most of the potential reactivity of tested aggregates was highly deleterious and exceeded 2%. However, for aggregate (A) at (0.4 and 0.5) w/c, the behavior of aggregates was deleterious, possibly because of temperature seepage from containers.

4.2 Evaluation of Scanning Electron Microscopy With Energy-Dispersive X-ray Spectrom (SEM/EDX) Results

The second part of this chapter, scanning electron microscopy and energy dispersive x-ray (SEM /EDX) was employed ASR microstructure, especially the alkali gel. The following (SEM) images show the alkali gel, crack distributions, and the other ASR products. X-ray was used to study chemistry of the ASR products. Figure (4.13) clarified the basic constituents of mortar specimens after ASR. Also, Figure (4.14) showed some of the main products produced as a result of the ASR.

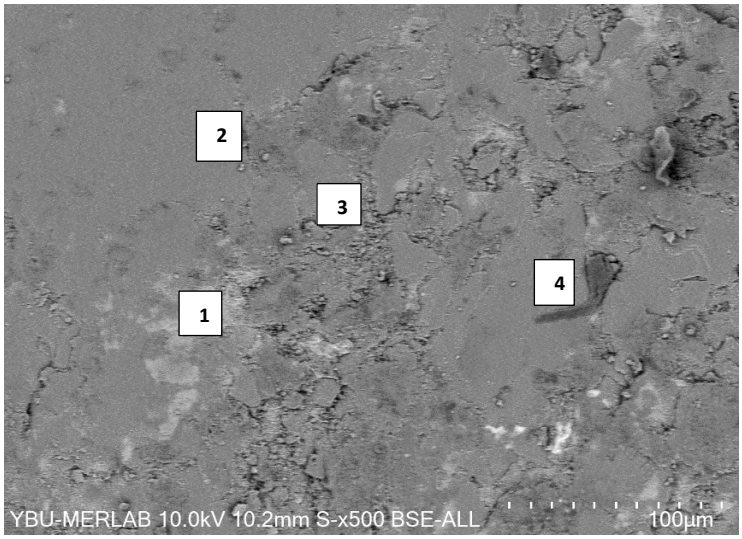

Figure 4.13 Shows the surface of cement mortar sample, where white zones shows un-hydrated cement paste (1), light-gray zones shows hydrated cement paste (2), dark-gray zones shows un-hydrated cement particles (3), dark zones shows aggregate particles (4).

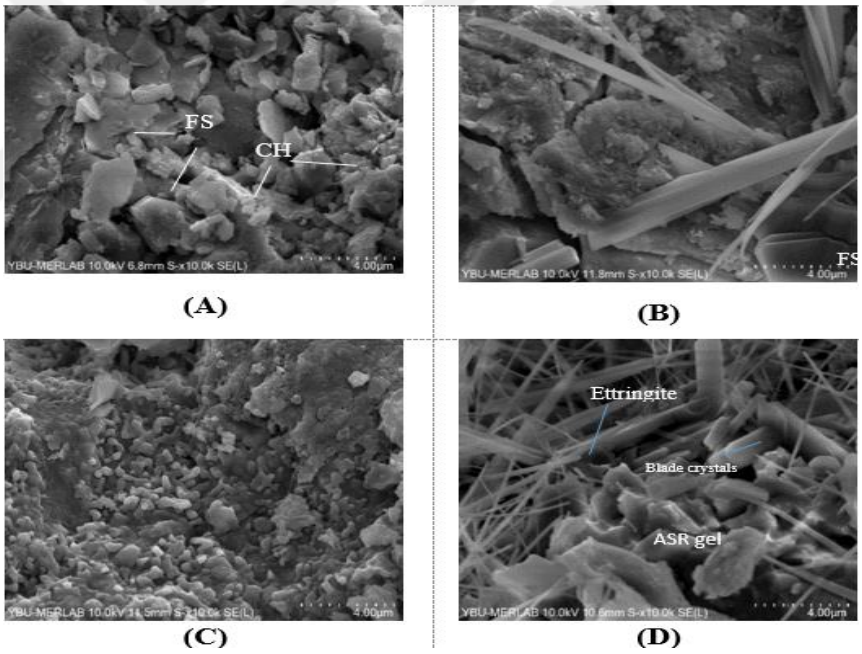

Figure 4.14 Alkali silica products, where (A) shows fridels salt (FS) and calcium hydrates (CH), columnar ettringite ((B), silicon dioxide or stishovite (C), rosette-shape of ASR gel and ettringite (D).

4.2.1 SEM/EDX-Results of Aggregate (A) at Different W/C Ratios and 40°C Curing Temperature

The following SEM images, showed the impact of ASR on mortar bars samples under a curing temperature of 40°C, and different amounts of water/cement ratios (0.4, 0.5 and 0.6). The specimens were made from aggregate (A). The specimens were

completely immersed in NaOH solution for 28 days before SEM imagining. Additionally, it was used EDX map spectra to show elemental ratios resulting from the ASR. Figures 4.15, and Figure 4.16 were presented at different resolutions, with SEM images of 100 (µm) resolution, showing the main features of the internal structure. While SEM images at 10 (µm) resolution clearly show the hydration products. The SEM images of the specimen prepared with aggregate (A), and 0.4 w/c ratio, as can be seen in Figure 4.15, where initial ettringite has formed.

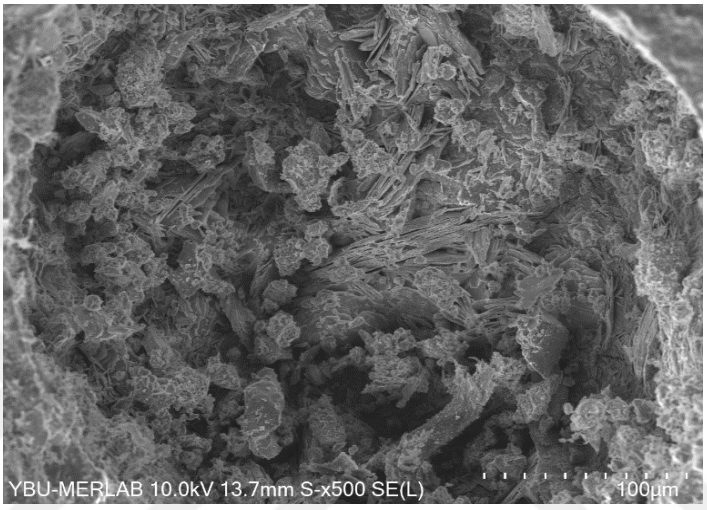

Figure 4.15 SEM image shows aggregate (A) at w/c: 0.4 with curing temperature of 40°C.

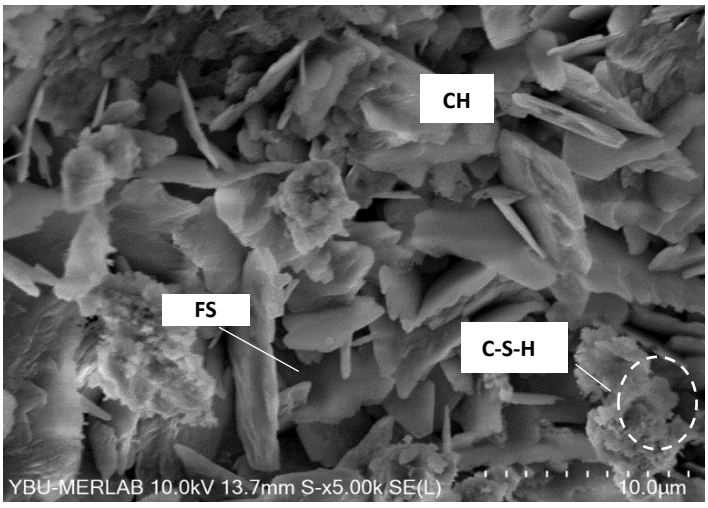

Figure 4.16 SEM image shows hydration products of aggregate (A) at w/c: 0.4 and 40°C.

Figure (4.16) provides the hydration products formed at w/c: 0.4, where there was an intense formation of calcium hydroxide (CH), Friedel salt (FS) and calcium-silicate-hydrate C-S-H. Also, the shape of hydration products at this phase was in the form of

foils, and they were homogenous. Figure (4.17) displays an SEM image of the sample that was created using aggregate (A) and w/c: 0.5. The image revealed the presence of numerous short needle-shaped ettringite formations on the cement paste's surface. Although micro-cracks can be seen throughout the cement paste, the cracks are narrow and short in length.

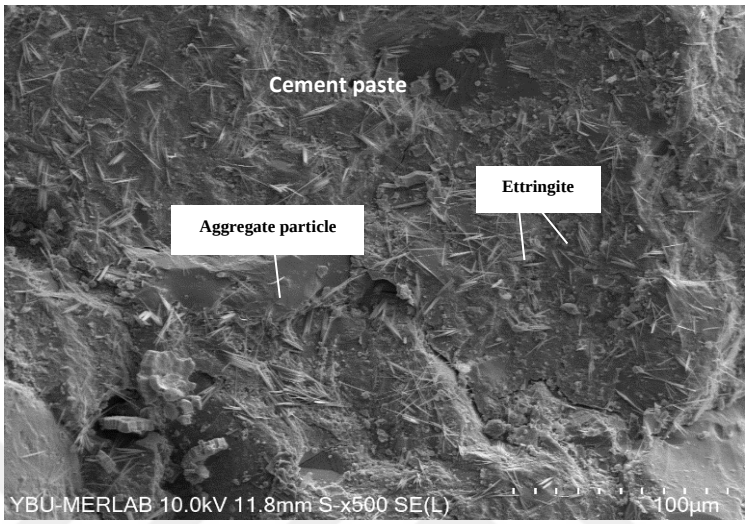

Figure 4.17 SEM image of aggregate (A) at w/c: 0.5 with a curing temperature of 40°C.

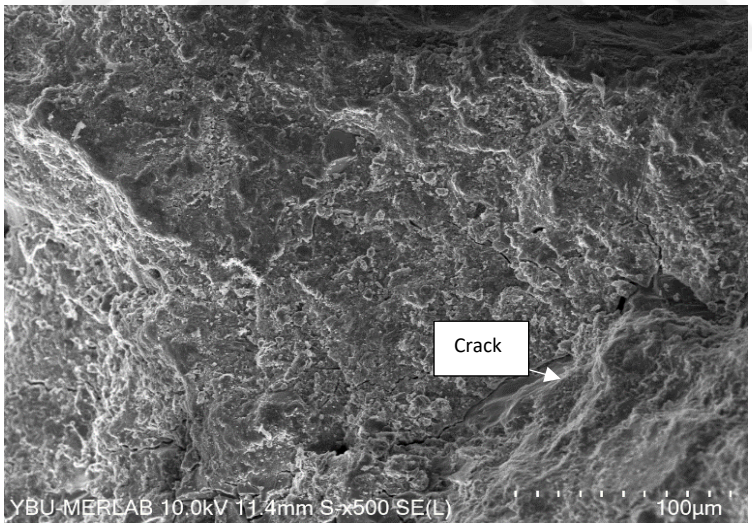

Figure 4.18 SEM image of aggregate (A) at w/c: 0.6 with curing temperature of 40°C.

Figure (4.18) illustrates a SEM image of a specimen prepared with aggregate (A) and a water/cement ratio of 0.6. The image shows a longitudinal micro-crack formed between the hardened cement pastes, aggregates and distributed into cement paste. The SEM images presented earlier showed the surface of mortar paste, its hydration products, cracks under the of influence various w/c ratios, and curing temperature of

40°C. The findings indicated that when w/c ratio was 0.4, no evidence of alkali-silica reaction was observed, and most of the hydration products were initial products such as friedel salt, calcium hydrate, and C-S-H. However, with an increase in the w/c ratio to 0.5 and 0.6, the formation of ettringite increased, and the C-S-H changed from foils to fibers (needle shape) with short rods. Furthermore, the EDX results provide an analysis of the chemical elements that resulted from the ASR under the influence of 40°C and different amounts of w/c ratios, i.e., 0.4, 0.5, and 0.6 for samples made from aggregate (A).

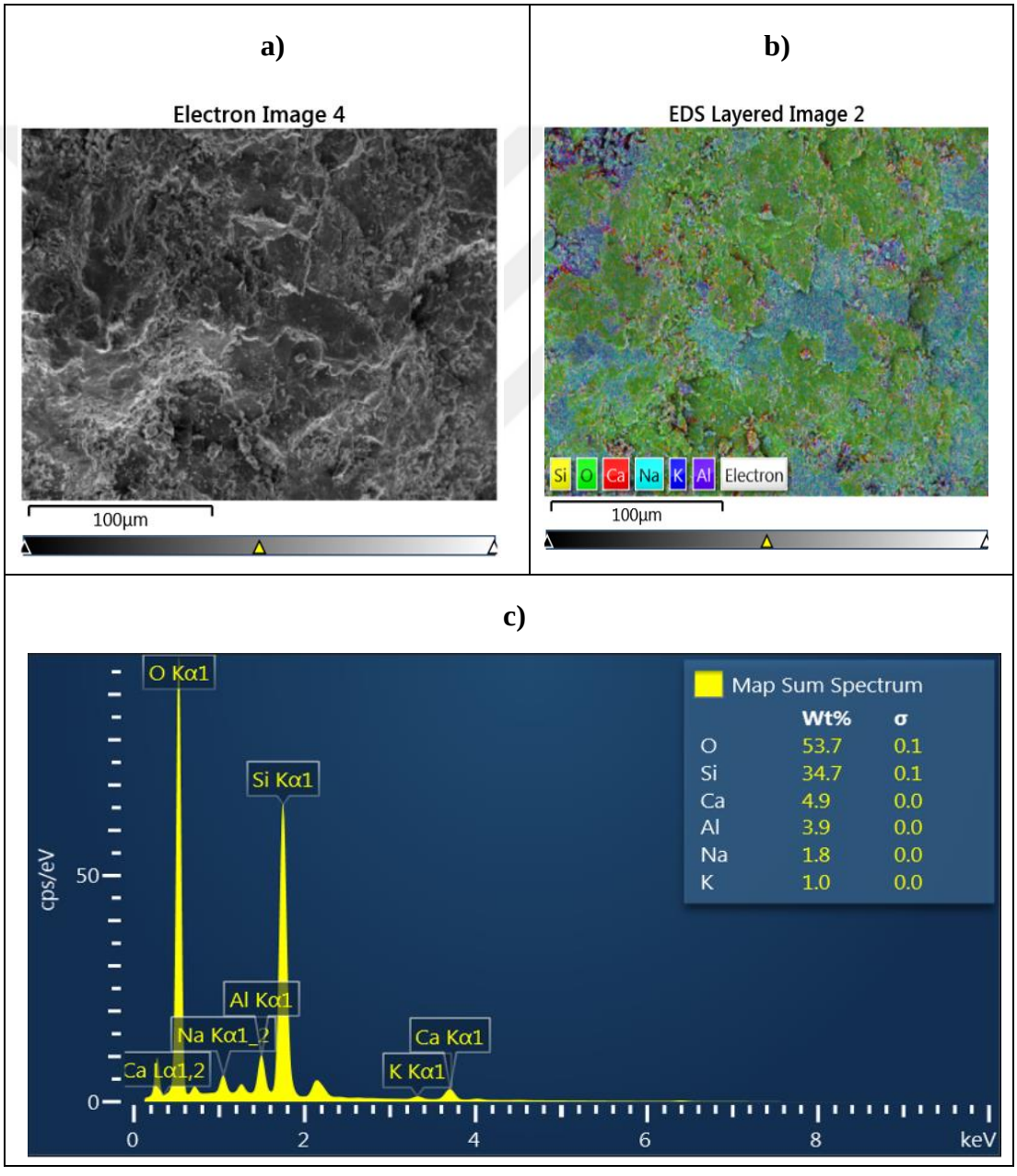

Figure 4.19 EDX-results, **a)** electron image, **b**) EDS layered image of combined elements, **c**) elemental ratios with Map sum spectrum of aggregate (A) at w/c: 0.4 and 40°C.

In Figure 4.19 a strong formation of silicate elements was observed over the inner surface of specimen at w/c: 0.4. While the results in Figure 4.20 indicate a high distribution of the calcium element inside air voids and on the face of the hardened mortar paste when water/cement ratio reaches 0.5.

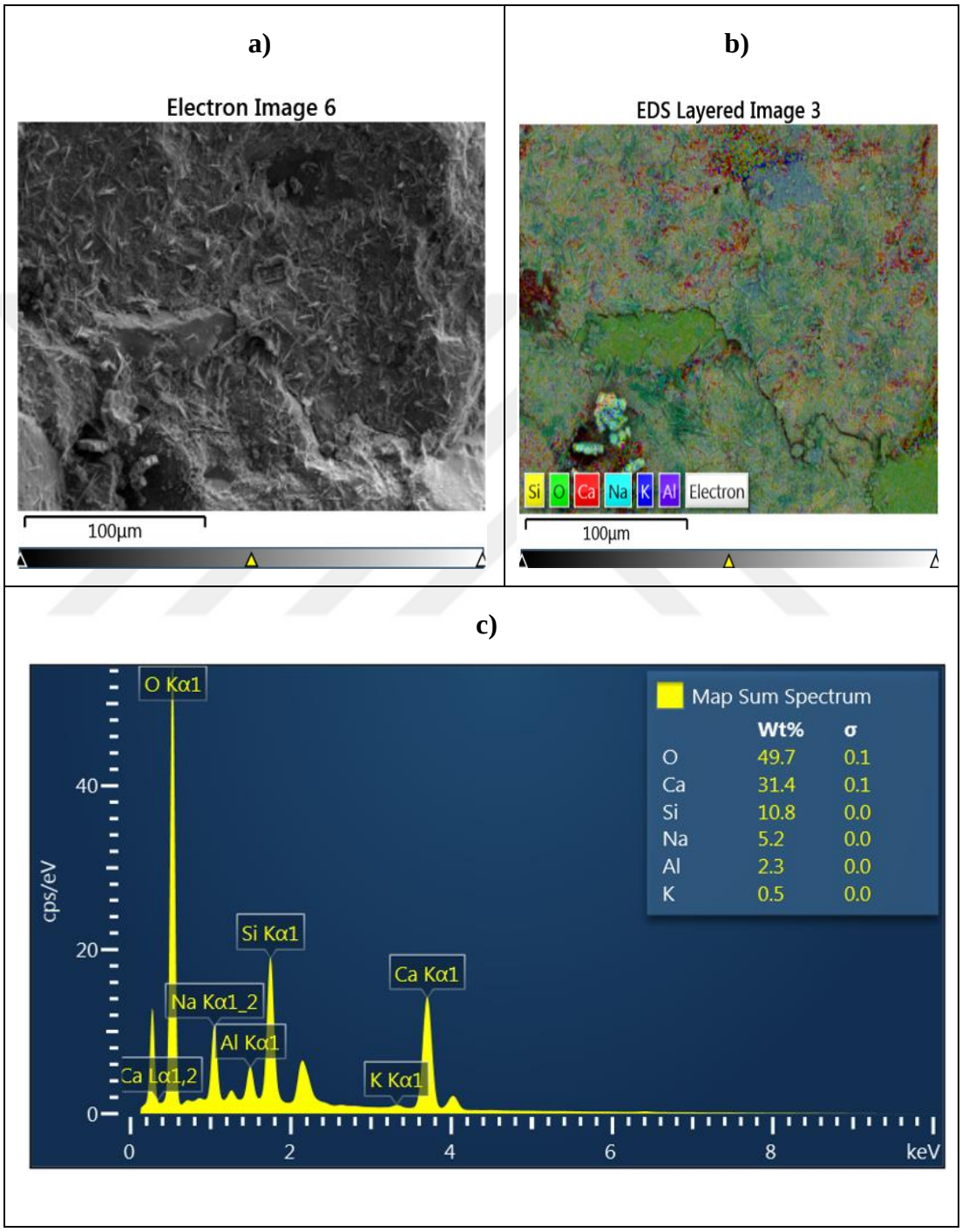

Figure 4.20 EDX results**, a)** electron image, **b)** EDS layered image of combined elements, **c)** elemental ratios with Map sum spectrum of aggregate (A) at w/c:0.5 and 40°C.

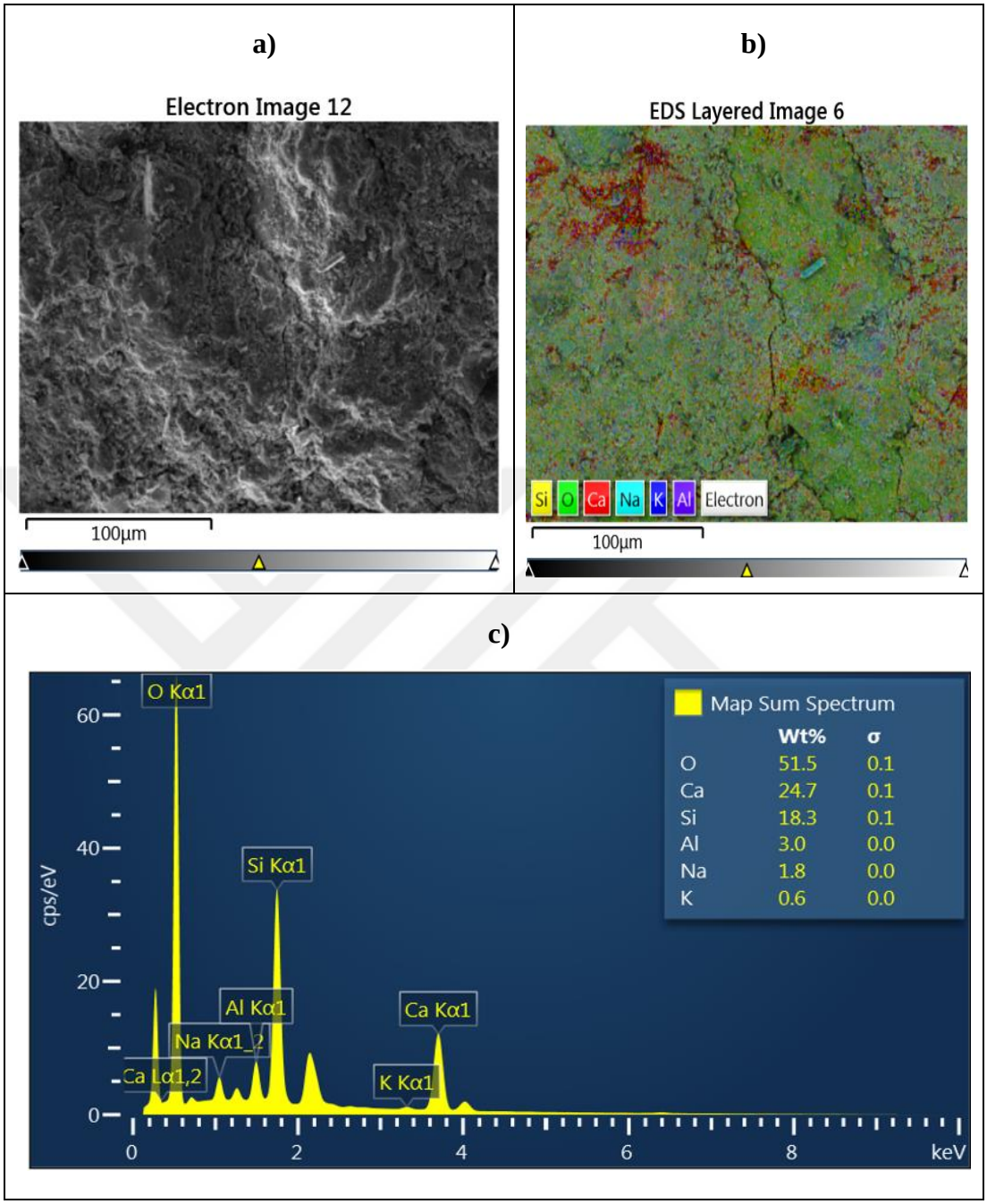

Figure 4.21 EDX results**, a)** electron image**, b)** EDS layered image of combined elements**, c)** elemental ratios with Map sum spectrum of aggregate (A) at w/c: 0.6 and 40°C.

In Figure 4.21, the formation of calcium was higher than that of silica, while the combination of sodium and potassium was lowest, as shown in section (c). However, the formation of calcium occurred mainly near the aggregate particles, at the edge of the cracks, and on the aggregate particles, as shown in section (b). In order to compare between all of above figures, Table (4.2) shows the elemental ratios due to ASR of the

samples which were made from aggregate (A) with different water/cement ratios at a curing temperature of 40°C.

Table 4.2 Elemental ratios of aggregate (A) with various amounts of w/c ratios at 40 ºC.

Water/cement	Ca/Si	(Na+K)/Si
0.4	0.14	0.08
0.5	2.91	0.52
0.6	1.35	0.13

Referring to Table 4.2 and previous EDX-results, the concentrations of the elements potassium and sodium were higher when at w/c: 0.4, while calcium element appeared more intensely when the water cement ratio was increased to 0.5 and 0.6. The ratio of Ca/Si indicated that the formation of silicate decreased when calcium increased. This explains why Ca/Si ratio was higher when w/c ratio were 0.5 and 0.6.

4.2.2 SEM/EDX-Results of Aggregates (B) at Different W/C Ratios and 40°C Curing Temperature

The following SEM images, showed the effect of ASR on the mortar bar samples, under a curing temperature of 40°C, and three different values of w/c ratios 0.4, 0.5 and 0.6. The mixture content of the specimens made from aggregates (B), where they completely immersed inside the solution of sodium hydroxide for 28 days. By the end of the test duration, SEM images were taken using EDX map spectra to analyze the chemical elements that resulted from ASR.

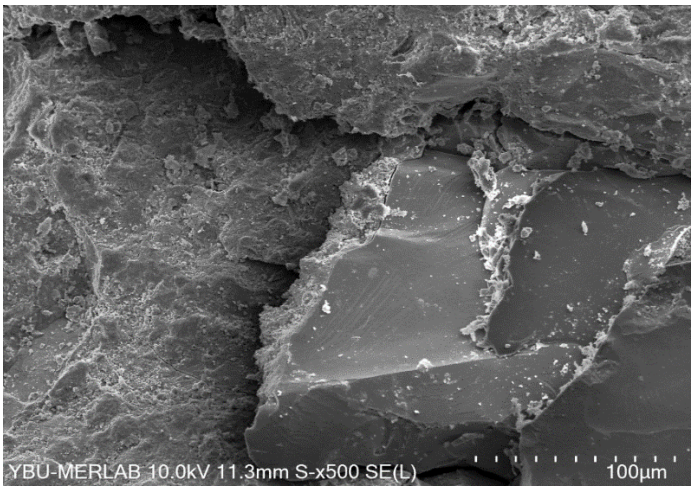

Figure 4.22 SEM image of aggregate (B) at w/c**:** 0.4 with curing temperature of 40°C.

Figure (4.22) illustrates the hydration of mortar paste, of the sample that made from aggregates (B), and 0.4 w/c with a curing temperature of 40°C. Where the image showed micro-cracks distributed on the mortar-paste, and between mortar-paste and aggregates. In addition to un-hydrated cement paste (white areas). Figure (4.23) belongs to the same sample that exist in Figure (4.22) but it had different resolution.

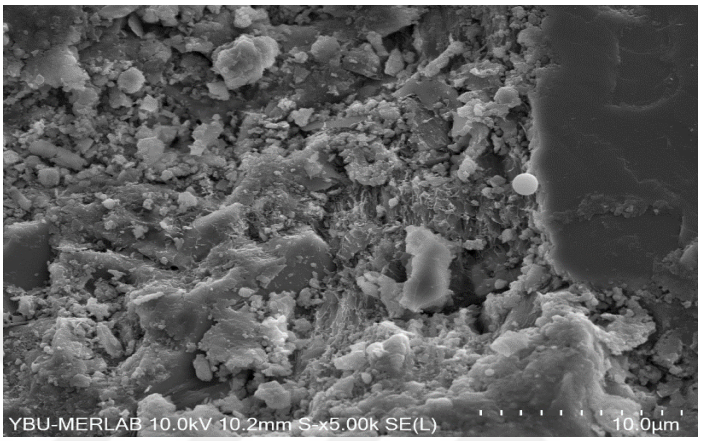

Figure 4.23 Hydration products of samples made from aggregate (B) at w/c: 0.4 and 40°C.

Figure (4.23) clarified close image of hydration products such as, friedel salt (FS), and monosulfo-aluminate. In addition to high formation of calcium hydroxide (CH).

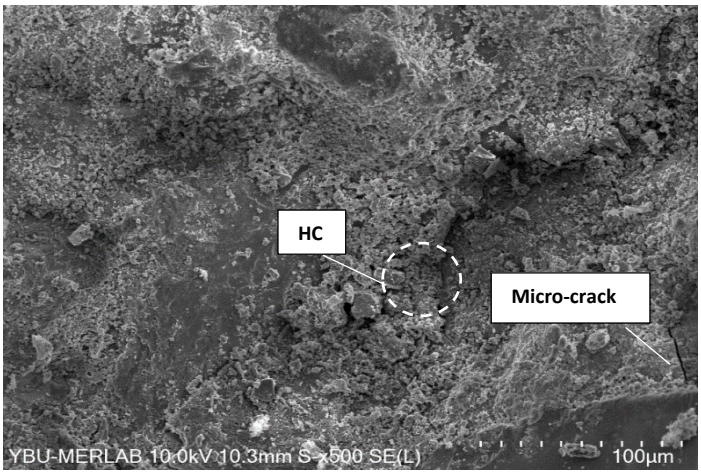

Figure 4.24 SEM image of aggregate (B) at w/c: 0.5 with a curing temperature of 40°C.

Figure (4.24) showed a foliated ASR gel covered the whole surface of mortar paste of the sample prepared from aggregate (B), and water/cement ratio of 0.5, with micro-cracks. Another product appears due to water absorption, which was hemi carbo-aluminate (HC).

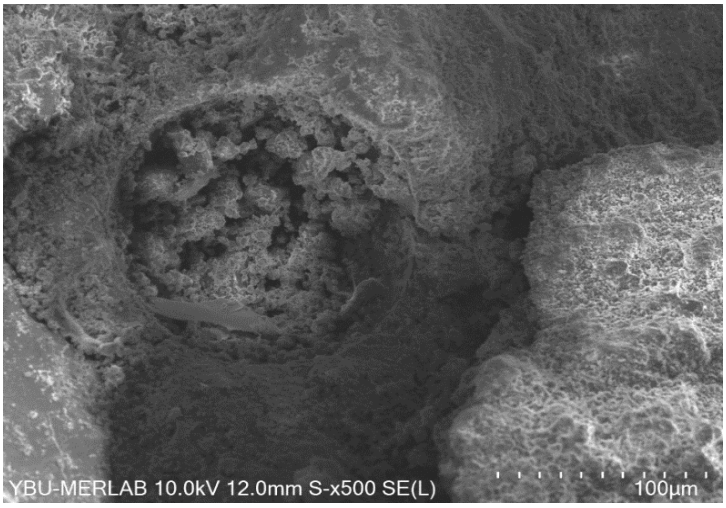

Figure 4.25 SEM image of aggregate (B) at w/c: 0.6 with curing temperature of 40°C.

Figure (4.25) illustrates microstructure of the specimen made from aggregate (B), where the amount of water/cement content in this sample raised to 0.6, and the image shows formation of secondary ettringite filled in the voids. The following SEM image (Figure 4.26) was belonged to the same sample in Figure 4.25, but it had different resolution.

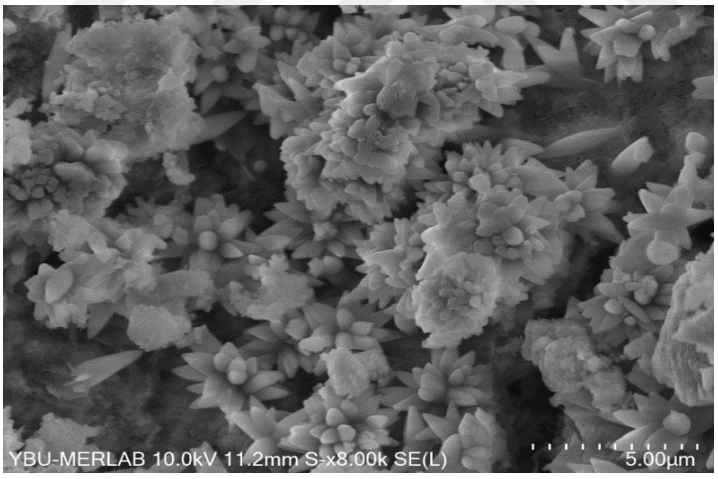

Figure 4.26 SEM images shows rosette crystals of ASR gel on aggregate (B) with at w/c: 0.6 and 40°C.

Figure 4.26 showed the influence of ASR on mortar paste at w/c: 0.6 with 40°C, where the image illustrates the crystallization of alkali gel in rosette lamellar shape. The outcomes of previous SEM images of aggregate (B) at different water/ cement ratios and 40°C, indicates that when the water/ cement ratio increased, the alkaline gel appears on the form of soft layer covering the specimen surface, as showed in Figure 4.26. Also, other products such as, hemi carbo-aluminate (HC) was formed in

abundance when the w/c was increased to 0.5 and 0.6. Furthermore, all of the cracks that shown in the previous SEM images was described as micro-cracks with no-deleterious effect. However, the following (EDX) results, provides the chemical elements that resulted from the ASR under the influence of 40°C, and different amounts of water cement ratios, respectively 0.4, 0.5, and 0.6, for samples prepared from aggregate (B).

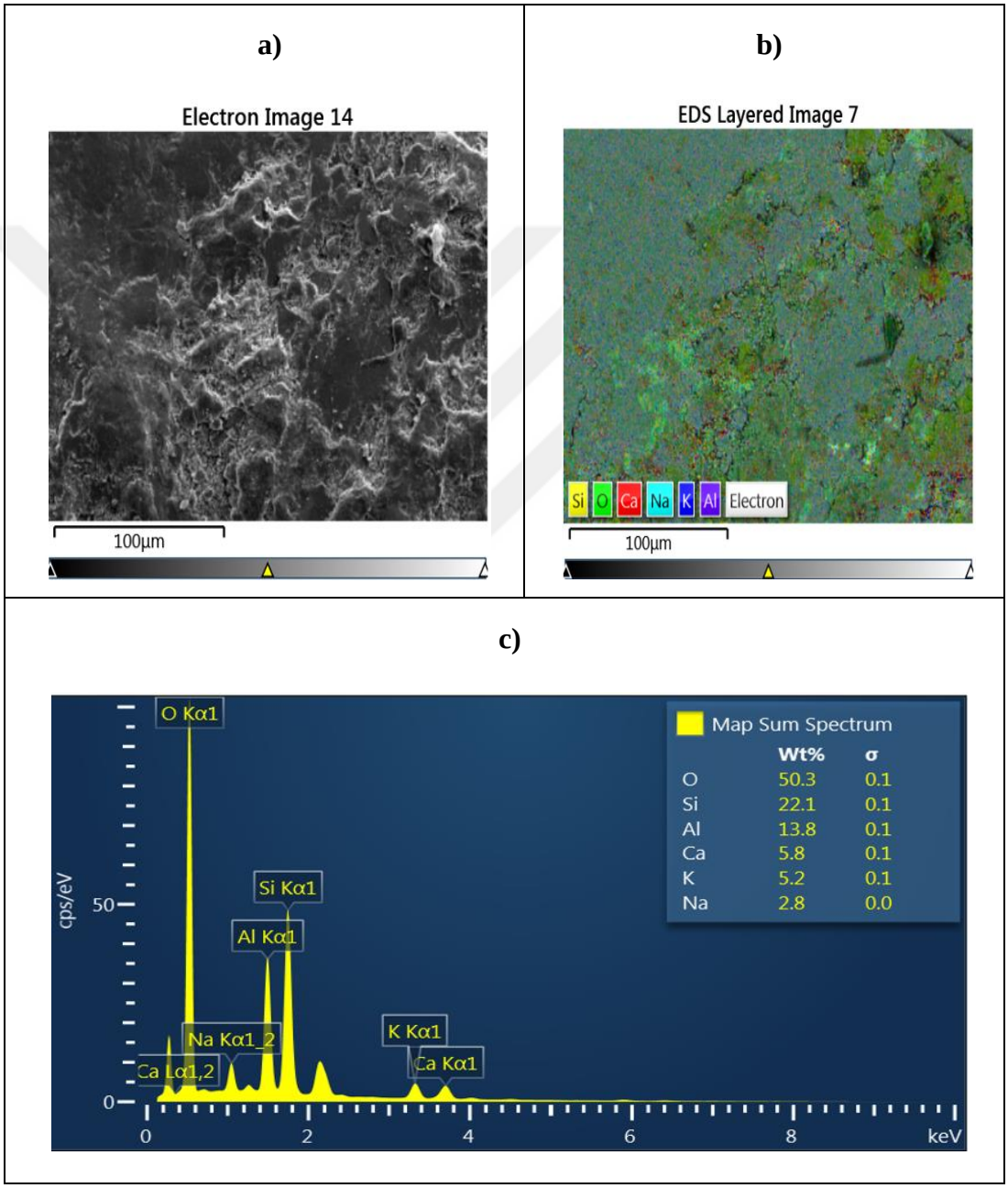

Figure 4.27 EDX results, **a)** electron image, **b)** EDS layered image, **c)** elemental ratios with Map sum spectrum of aggregate (B) at w/c: 0.4, and curing temperature of 40°C.

Figure (4.27) shows clear formation of silicate and aluminum throughout mortar paste and aggregates. In Figure 4.28, formation of calcium is higher than that of silicate, while the formation of aluminum and potassium is lowest. However, the formation of calcium is strongly distributed in the center of the mortar paste surface, because as shown in section (a) from this figure calcium hydroxide was produced intensively.

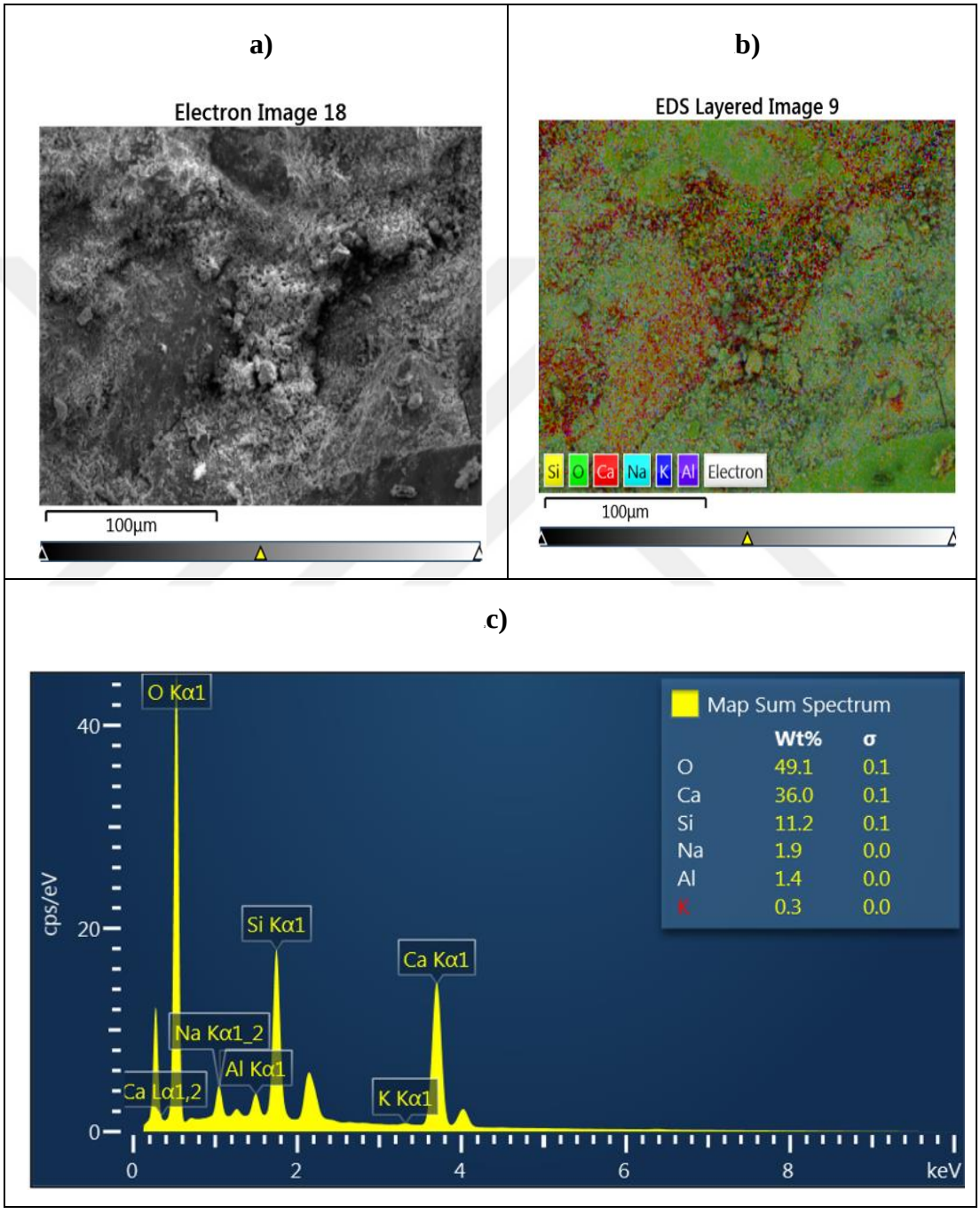

Figure 4.28 EDX results, **a)** electron image, **b)** EDS layered image, **c)** elemental ratios with Map sum spectrum of aggregate (B) at w/c:0.5 and curing temperature of 40°C.

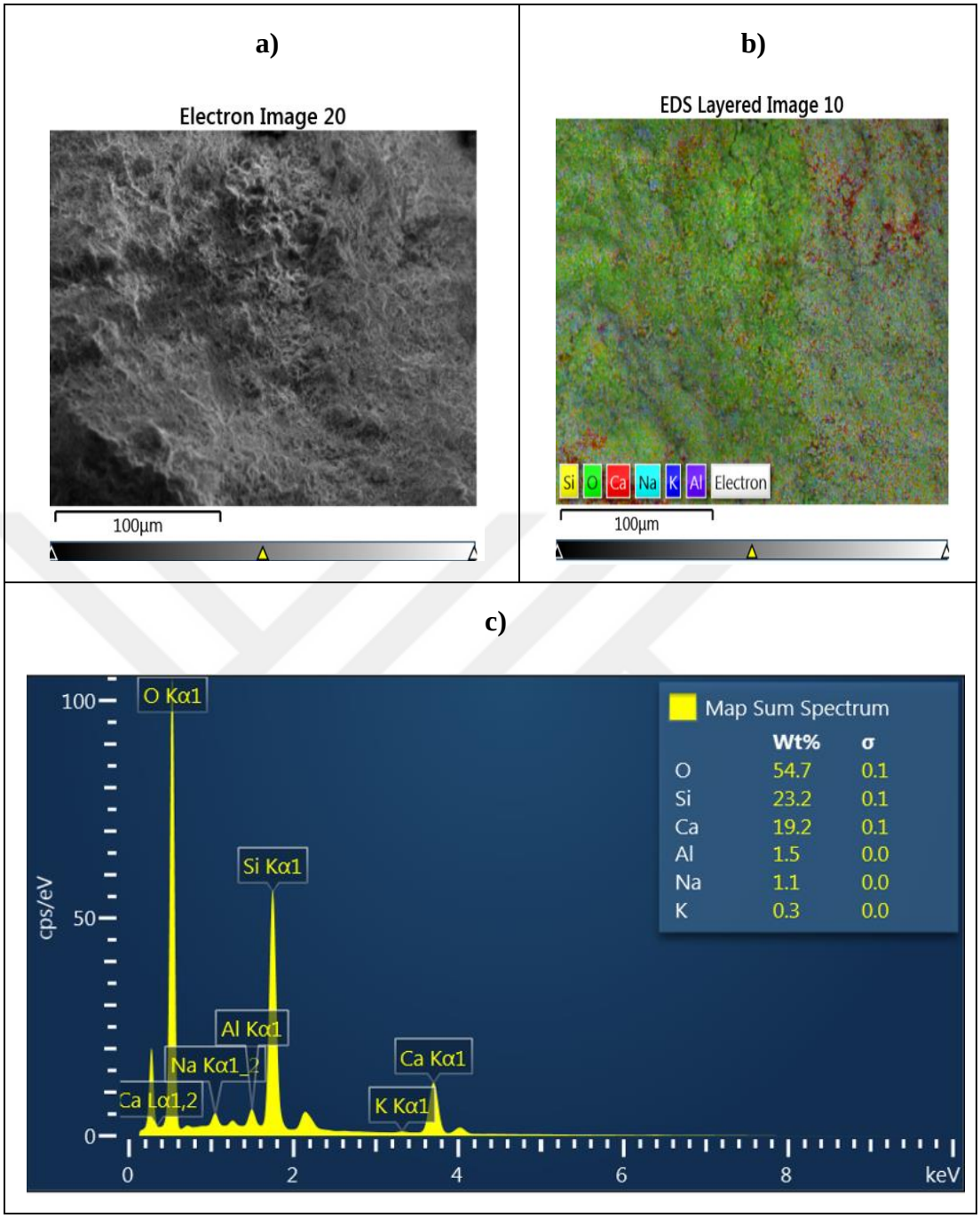

Figure 4.29 EDX-results, **a)** electron image, **b)** EDS layered image, **c)** elemental ratios with Map sum spectrum of aggregate (B) at w/c: 0.6 and curing temperature of 40°C.

When w/c ratio changed to 0.6, as shown in Figure 4.29, a high production of silicate was formed, and the concentration of silicate was higher than that of calcium, as shown in section (c) of this figure, and the concentration of additional alkalis such as sodium and potassium was negligible. However, Table (4.3) shows the elemental ratios due to

ASR of the samples made from aggregate (B), at different water/cement ratios of 0.4, 0.5, and 0.6, and under the effect of curing temperature of 40°C.

Table 4.3 Elemental ratios of aggregate (B) with various amounts of w/c contents at 40 ºC.

Water/cement	Ca/Si	(Na+K)/Si
0.4	0.26	0.37
0.5	3.21	0.19
0.6	0.83	0.06

According to Table 4.3, the elements that formed intensively at low water/cement content was potassium and sodium, but when water/cement contents increased to 0.5 and 0.6, calcium was formed intensively.

4.2.3 SEM/EDX-Results of Aggregates (A) at Different W/C Ratios and 60°C Curing temperature

The SEM images in this section were taken from samples of aggregate (A), and three ratios of water/cement contents (0.4, 0.5, and 0.6), the samples were placed at a temperature of 60°C within 28 days. Also, SEM images were taken with EDX map spectra. However, The SEM images in Figure 4.30, and Figure 4.31, showed the behavior of alkali silica reaction on the microstructure of sample made from aggregate (A), and water/cement content of 0.4, at curing temperature of 60°C. Figure 4.30 illustrate the hydrated cement paste in (light gray zones) covered by ettringite. In addition to micro-cracks and voids.

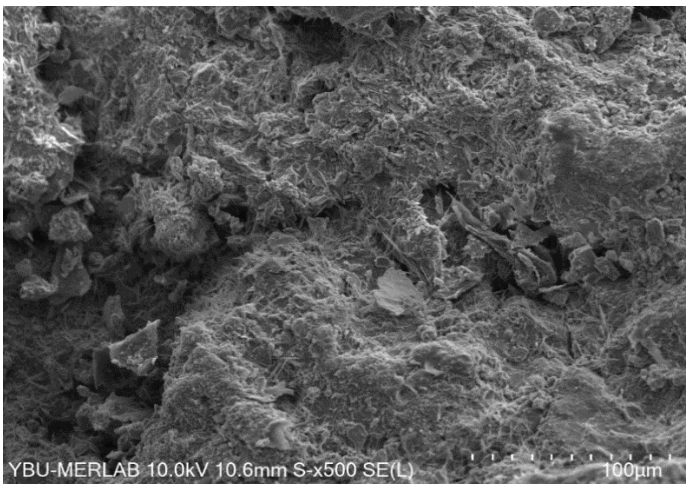

Figure 4.30 SEM image of aggregate (A) at w/c: 0.4 with curing temperature of 60°C.

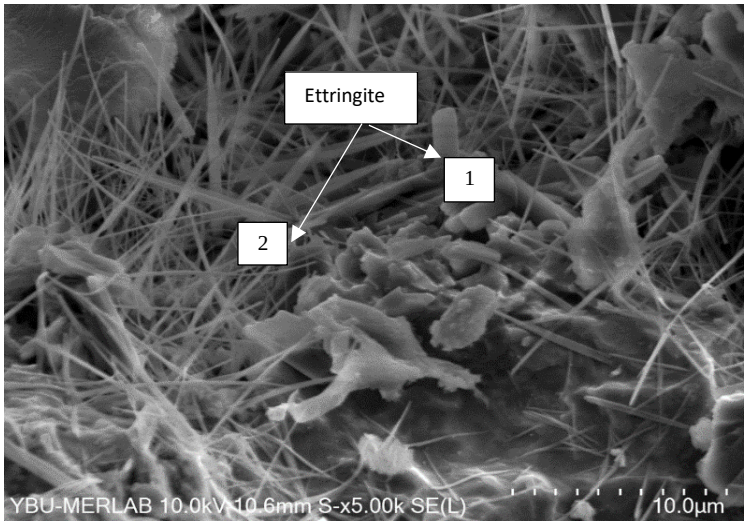

Figure 4.31 SEM image shows blade-crystal of ettringite of aggregate (A) at w/c: 0.4 and 60°C.

Figure 4.31 had a close resolution of (10.0 µm) to show the shape of ettringite, ettringite found as prismatic thick ettringite (1), and fine needles-ettringite (2).

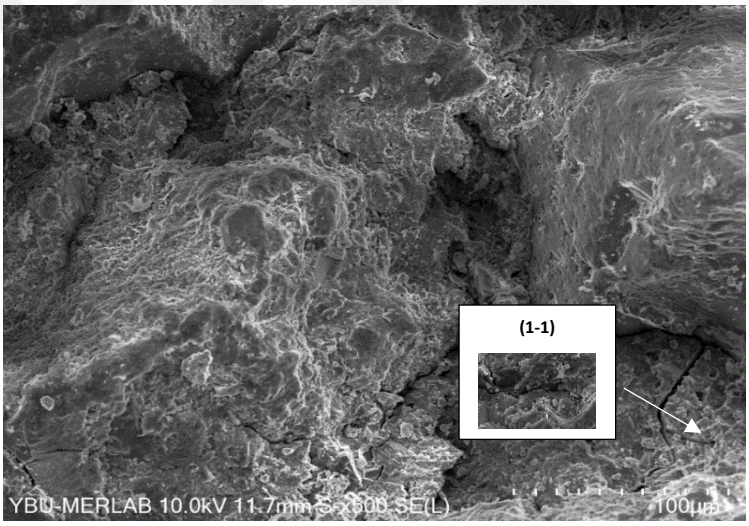

Figure 4.32 SEM image of aggregate (A) at w/c: 0.5 with curing temperature of 60°C.

When water/cement content increased to 0.5 the destructive behavior of ASR begins to appear on the head of mortar paste, as revealed in Figure 4.32, where width and length of these cracks increased, and most of the cracks were completely fill with ASR gel, where the alkali gel had a spongy texture.

Figure (4.33) illustrates section (1-1) to show some of the ASR products caused by high temperatures and 0.5 w/c, such as portlandite and silicon dioxide. While Figure (4.34) had a resolution of (40.0 µm) and shows the producing cracks that resulted from increasing the amount of water/cement contents up to 0.5.

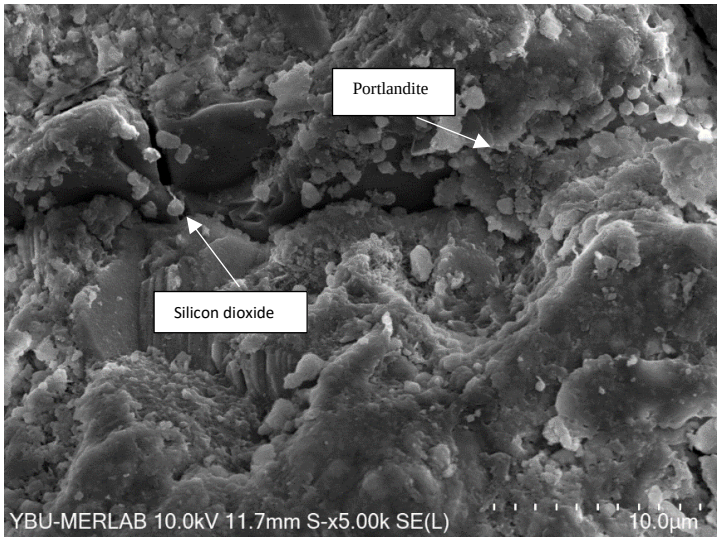

Figure 4.33 Section (1-1) shows portlandite and alkali gel of aggregate (A) at w/c: 0.5 and 60°C.

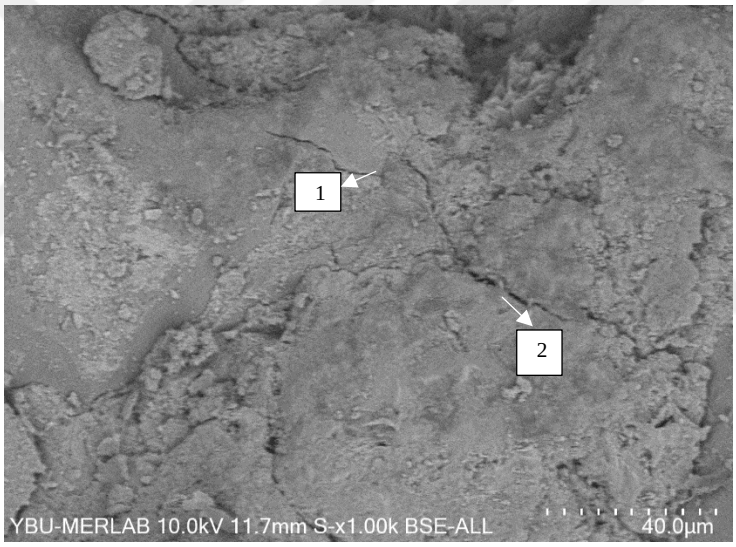

Figure 4.34 Cracks that appeared on the surface of mortar paste.

In Figure (4.34) two types of cracks were formed as a result of the deleterious effect of ASR, where the first crack (1) was micro-crack, and formed through cement mortar paste, and the second crack (2) is massive crack, and it was formed between cement paste and aggregate.

The following SEM images showed the influence of ASR on mortar pastes, at w/c: 0.6. As clarified in Figure (4.35) a massive crack with a large width has formed around the aggregate particles, with formation of ettringite in a shape of bands. Figure (4.36) shows section (1-2), which illustrating the ASR products.

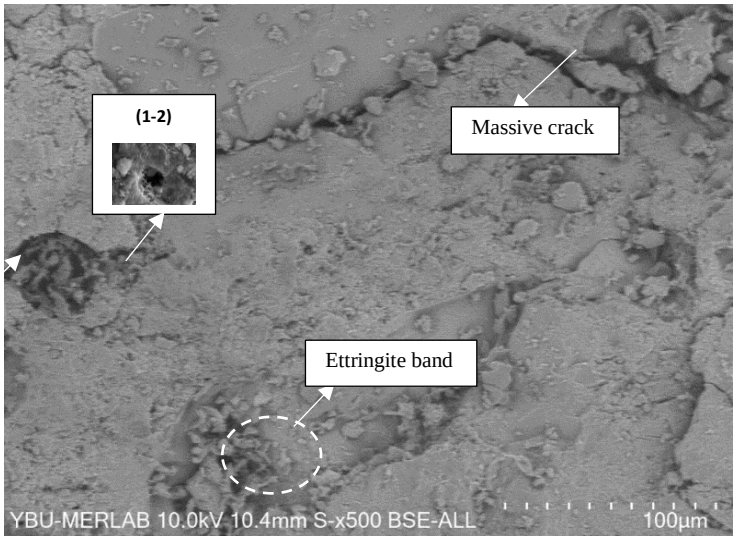

Figure 4.35 SEM image of aggregate (A) at w/c: 0.6 and curing temperature of 60°C.

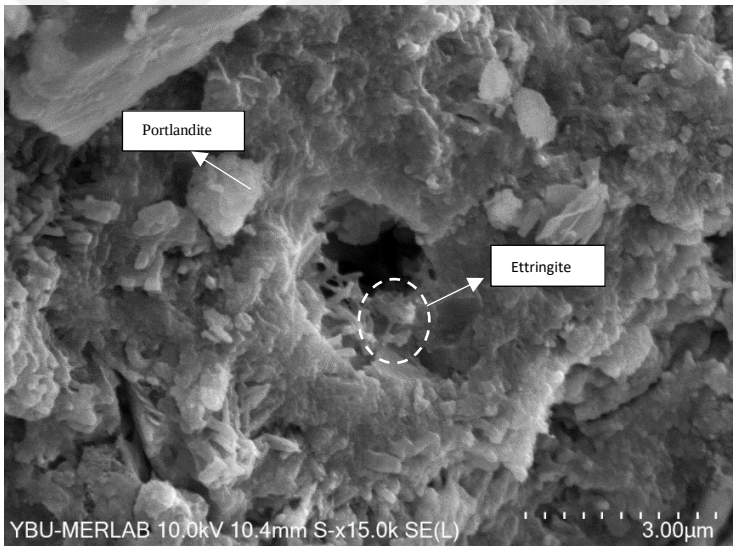

Figure 4.36 Section (1-2) shows ASR products of aggregate (A) at w/c of 0.6 and 60°C.

Figure (4.36) shows an excessive formation of portlandite, silicon dioxide, and ettringite. The ettringite forms in fibrous bundles at this stage, because of the existence of high water cement content in the mixture.

Comparing the preceding microscopic images, the reactivity of ASR was shown by develop of microscopic cracks at 0.4 w/c, to deleterious cracks around the aggregate particles at 0.5, and 0.6 w/c. Where the dimensions of these cracks increasing by enlarged the value of water/cement ratio. Portlandite and silicone dioxide also occur more frequently at 0.5 and 0.6 w/c. Moreover, the form of ettringite appears as fibrous bundles as the w/c content increases. In order to analyze the chemical elements that

appeared from the various amounts of water/cement contents, the following (EDX) results, shows the chemical elements that resulted from the ASR, under the influence of 60°C, for samples prepared from aggregate (A).

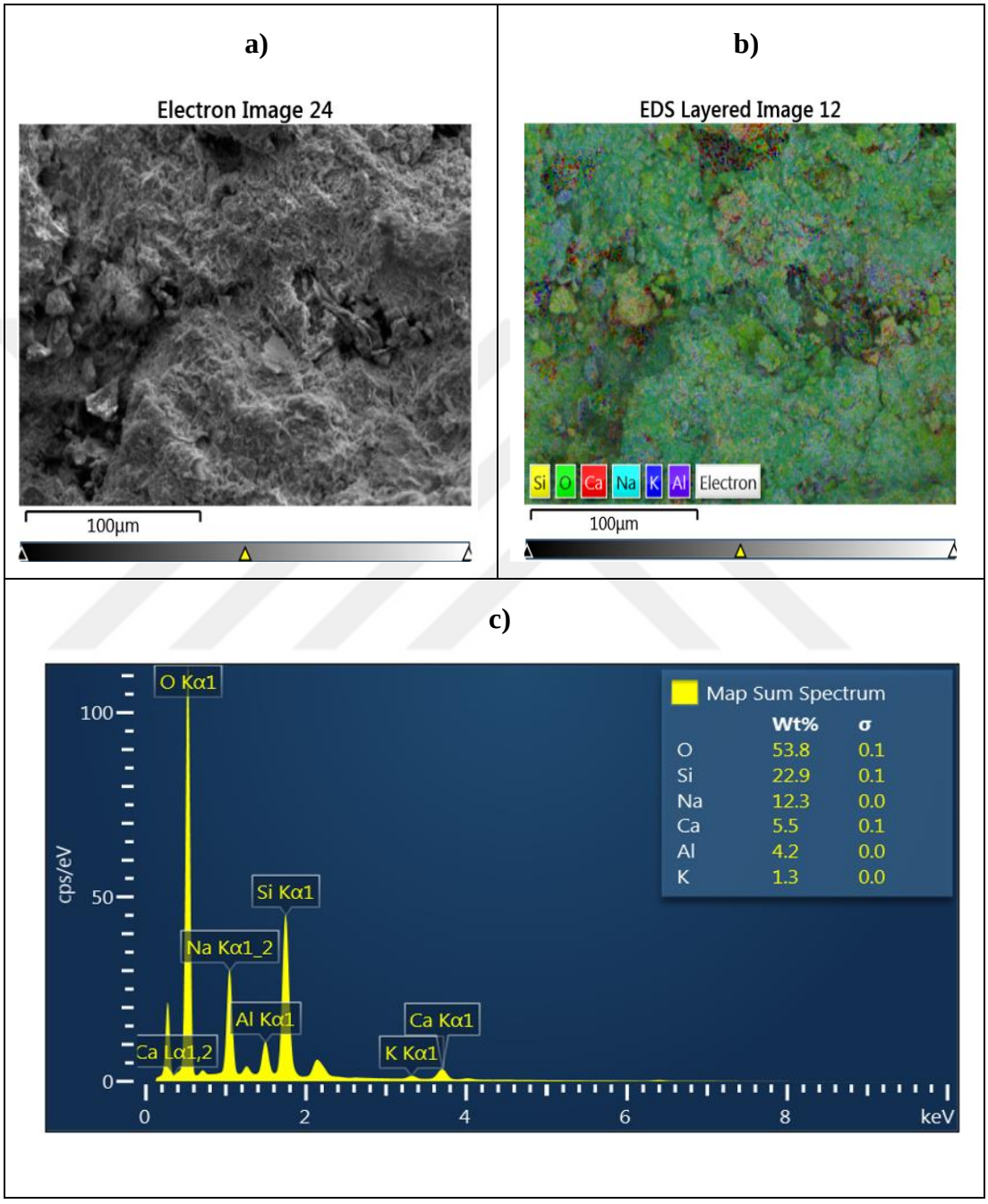

Figure 4.37 EDX results, **a)** electron image, **b)** EDS layered image, **c)** elemental ratios with Map sum spectrum of aggregate (A) at w/c: 0.4 and curing temperature of 60°C.

Figure (4.37) shows the distribution of chemical element ratios on the surface of mortar-paste, and as showed in section (c), the contraction of silicate was the highest, while calcium, aluminum, and potassium were lower than silicate and sodium.

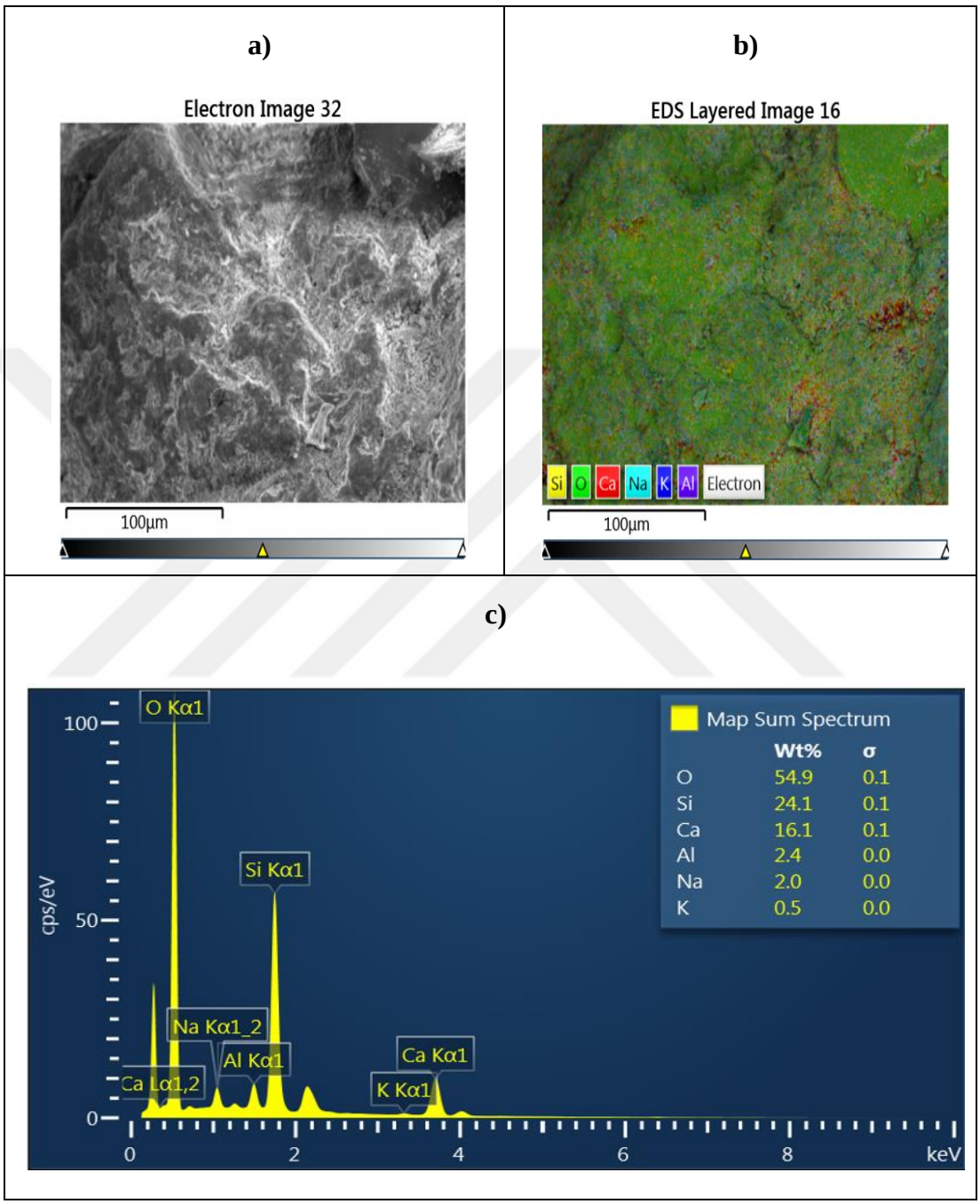

Figure 4.38 EDX results, **a)** electron image, **b)** EDS layered image, **c)** elemental ratios with Map sum spectrum of aggregate (A) at w/c: 0.5 and curing temperature of 60°C.

In Figure (4.38), as the water/cement content increased, two elements were intensively formed, silicate and calcium, and the concentration of silicate was higher than calcium.

As shown in section (b), calcium formed mainly in the areas where cracks formed, while silica was distributed over the entire specimen surface.

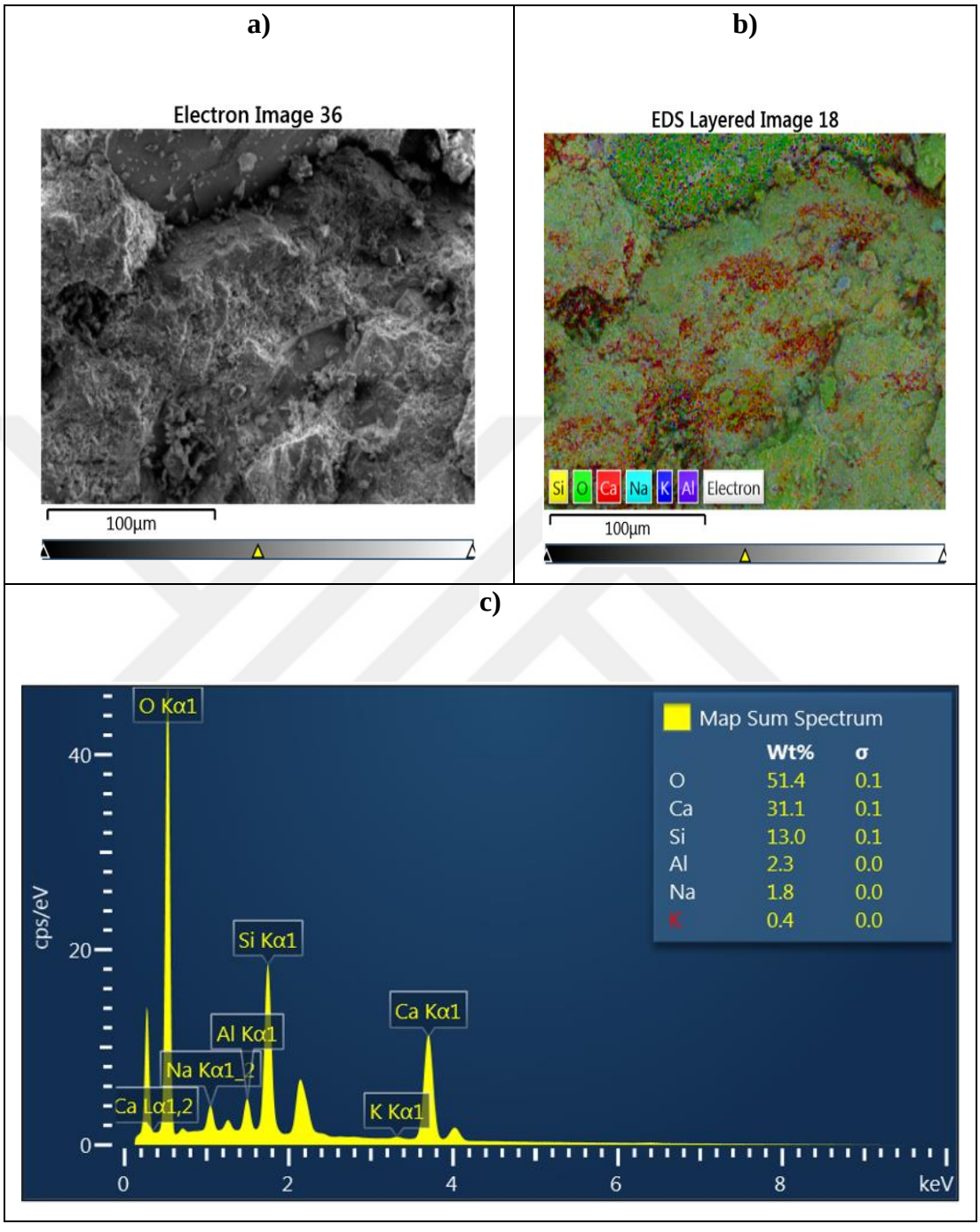

Figure 4.39 EDX results, **a)** electron image, **b)** EDS layered image, **c)** elemental ratios with Map sum spectrum of aggregate (A) at w/c: 0.6 and curing temperature of 60°C.

When the amount of water/cement content increased to 0.6, the concertation of calcium was increased and distributed all over the specimen surface as show in Figure 4.39, where the amount of calcium was higher than silicate. Furthermore, Table (4.4) shows the chemical elements ratios that formed from aggregate (A) at a curing temperature

of 60°C, with altered water/cement ratios. As shown, the (Ca/Si) ratios increases by increasing the quantity of water/cement content, the concertation of calcium was increased by water.

Table 4.4 Elemental ratios of aggregate (A) with various amounts of w/c contents at 60 ºC.

Water/cement	Ca/Si	(Na+K)/Si
0.4	0.24	0.59
0.5	0.67	0.1
0.6	2.39	0.17

4.2.4 SEM/EDX-Results of Aggregates (B) at Different W/C Ratios and 60°C Curing Temperature

The following SEM images shows the effect of ASR of sample made from aggregate (B), and changeable amounts of water/cement contents 0.4, 0.5, and 0.6. The samples were cured at a temperature of 60°C for 28 days, and soaked in NaOH solution. Also, SEM images were taken with EDX map spectra of the chemical elements, resulting from the presence of different water/cement ratios. The following image (Figure 4.40) illustrate the influence of ASR on the sample that made from water cement content of 0.4, where alkaline gel cover the surface of hydrated cement paste. Section (1-3) illustrates some of ASR products (See Figure 4.41).

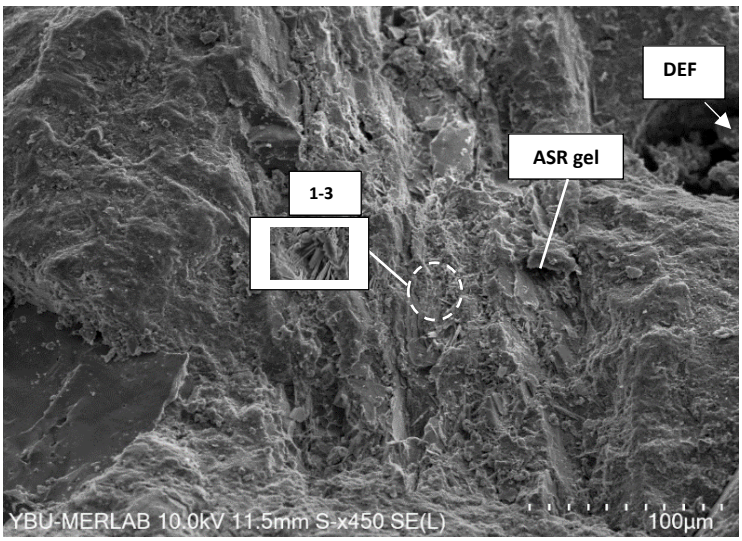

Figure 4.40 SEM image of aggregate (B) at w/c: 0.4 with curing temperature of 60°C.

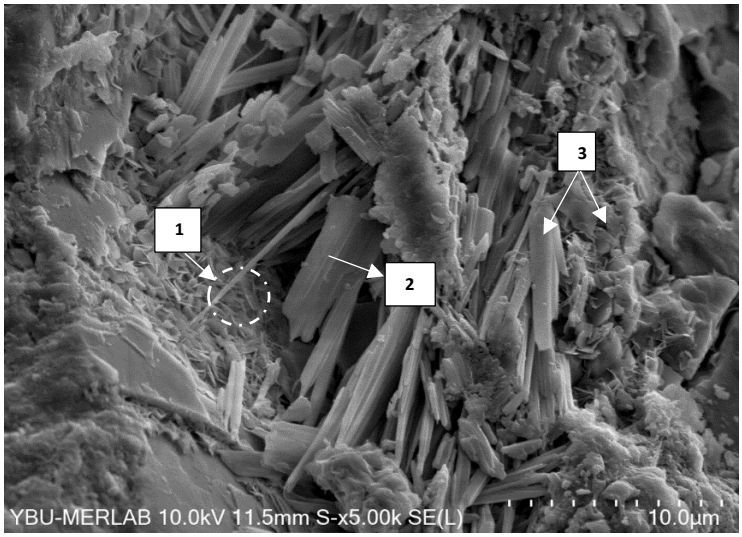

Figure 4.41 Section (1-3) shows tobermorite (1), columnar ettringite (2), and blade shape of ettringite (3).

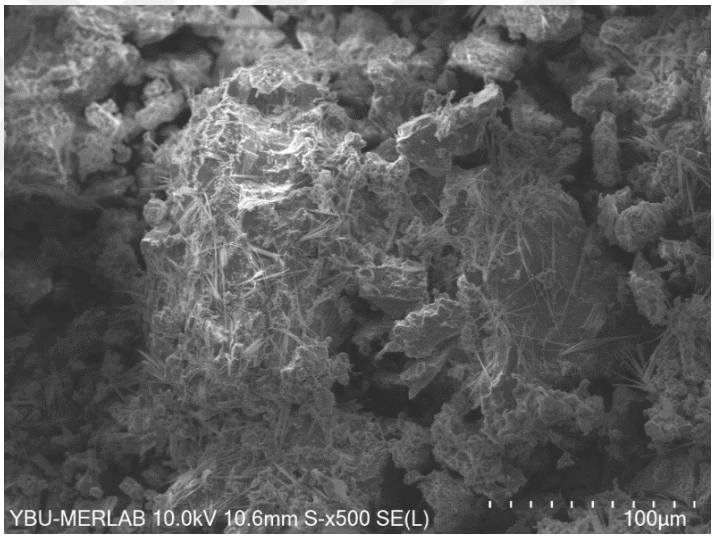

Figure 4.42 SEM image of aggregate (B) at w/c: 0.5 with a curing temperature of 60°C.

Figure (4.42) shows the surface of hydrated surface, when the water/cement content raised to 0.5, where an excessive amount of ettringite has formed. Also, the alkali-gel has a spongy texture, and cover the surface of the sample.

The following SEM images were made from aggregate (B), and 0.5 water/cement content, but they had different resolutions to show ASR products. Figure 4.43 and Figure 4.44, shows a high formation of columnar ettringite, portlandite, and bentonite on the surface. Also, to the appearance of cracks all over the sample. The cracks were classified as massive crack with deleterious effect.

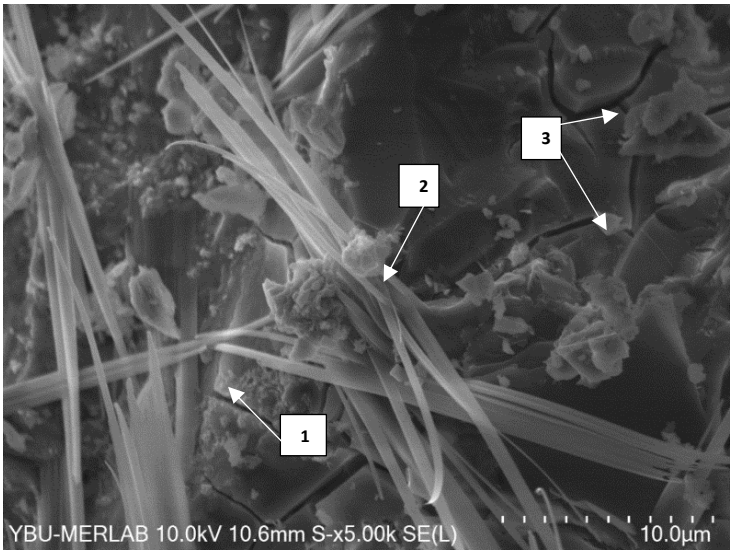

Figure 4.43 SEM image shows columnar shape of columnar ettringite (1), portlandites (2), cracks on cement filled with ASR gel (3).

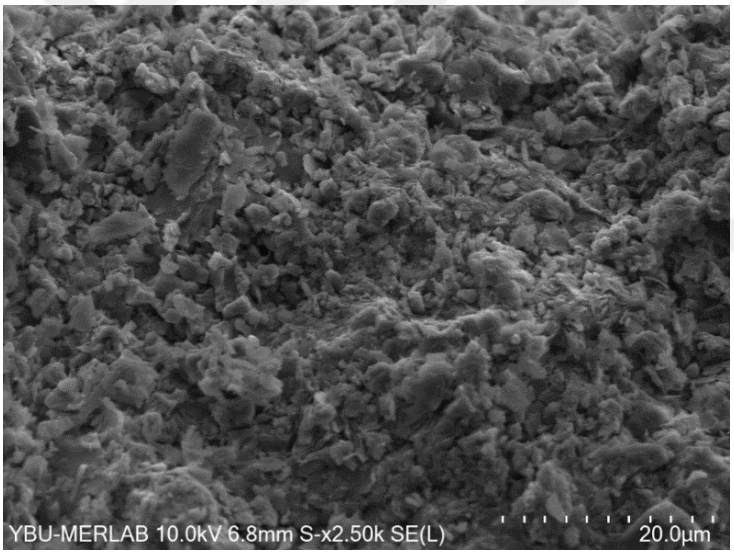

Figure 4.44 SEM images shows bentonite.

Figure 4.44 shows one of the most of ASR products that produced due to the deleterious effect of ASR, which was bentonite. However, the following SEM images Figure 4.45 and Figure 4.46 illustrated the effect of ASR when water/cement content was 0.6, for sample made from aggregate (B). However, the images were presented at different resolutions, with SEM images of 100 (µm) resolution to provide the main features of the internal structure of the sample surface, and SEM images of 10 (µm) resolution to show the hydration products due to ASR. In Figure 4.45, a massive gel was observed on the inner structure of the sample. While Figure 4.46 appears a non-

homogenous crystallization of ASR products covered the mortar paste. Most of the products includes ASR gel, portlandites, bentonite, silicon dioxide, and ettringite (needle –shape).

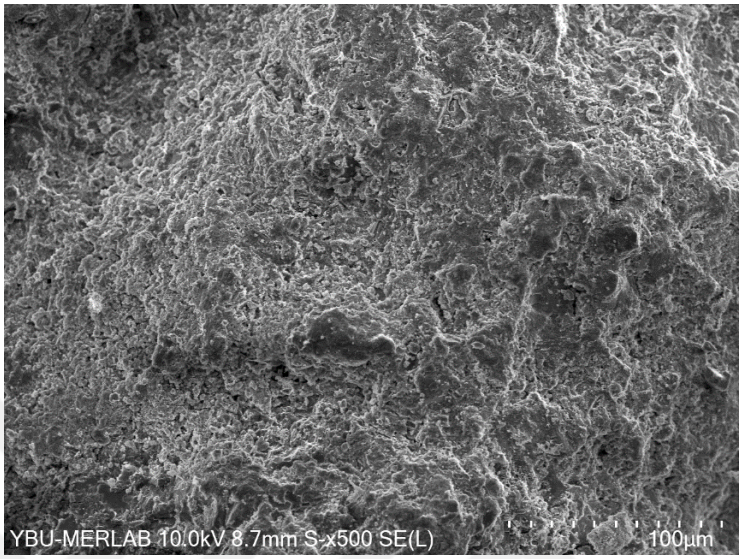

Figure 4.45 SEM image of aggregate (B) at w/c: 0.6 with a curing temperature of 60°C.

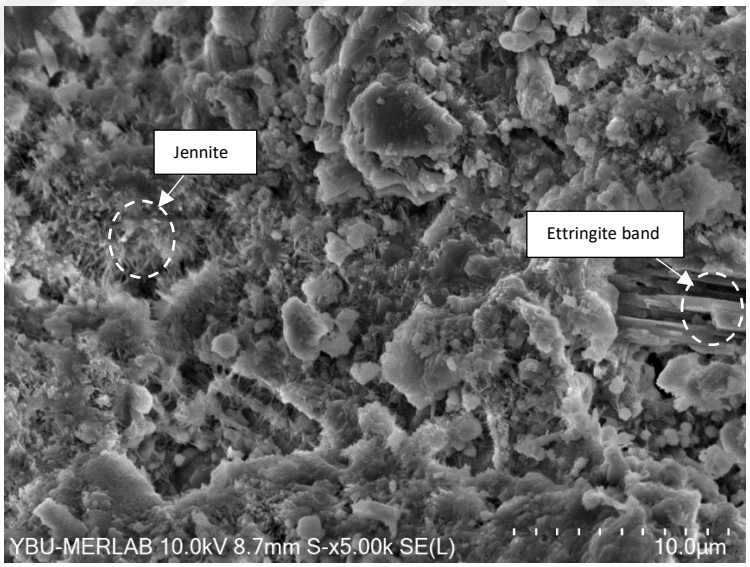

Figure 4.46 SEM image shows jennite.

Through comparing the preceding microscopic images at different water/cement content, the influence of alkali-silica reaction was shown by the different formation of ASR products and cracks appearance. However, when the amount of water cement content increased the length and width of the cracks increasing and distributed through cement paste and around aggregate particles. Also, by increasing the amount of water cement content the ASR products changed from tobermorite to jennite. The following

(EDX) results, provides the chemical elements that resulted from the ASR, under the effect of 60°C, and different amounts of water/cement contents (0.4, 0.5, and 0.6), for samples made from aggregate (B).

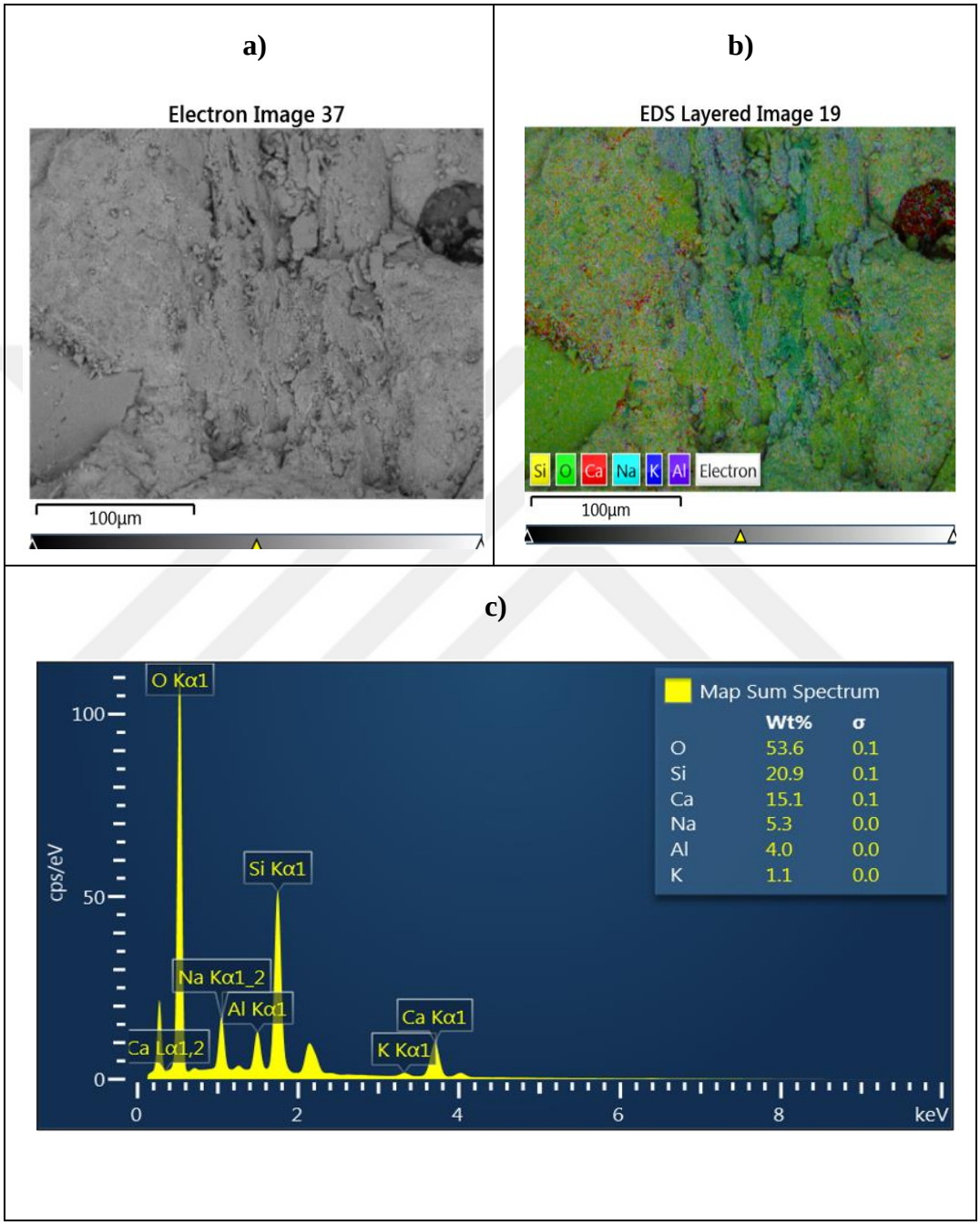

Figure 4.47 EDX results, **a)** electron image, b) EDS layered image, **c)** elemental ratios with Map sum spectrum for aggregate (B) at w/c: 0.4 and curing temperature of 60°C.

Figure 4.47 shows the concentration of elements of the sample prepared from aggregate (B) under the w/c of 0.4, where silicate formed intensively on the upper micro-surface of mortar paste. Also, section (b) in this figure displays a high

concentration of calcium in the air voids, while the formation of aluminum and potassium was the lowest.

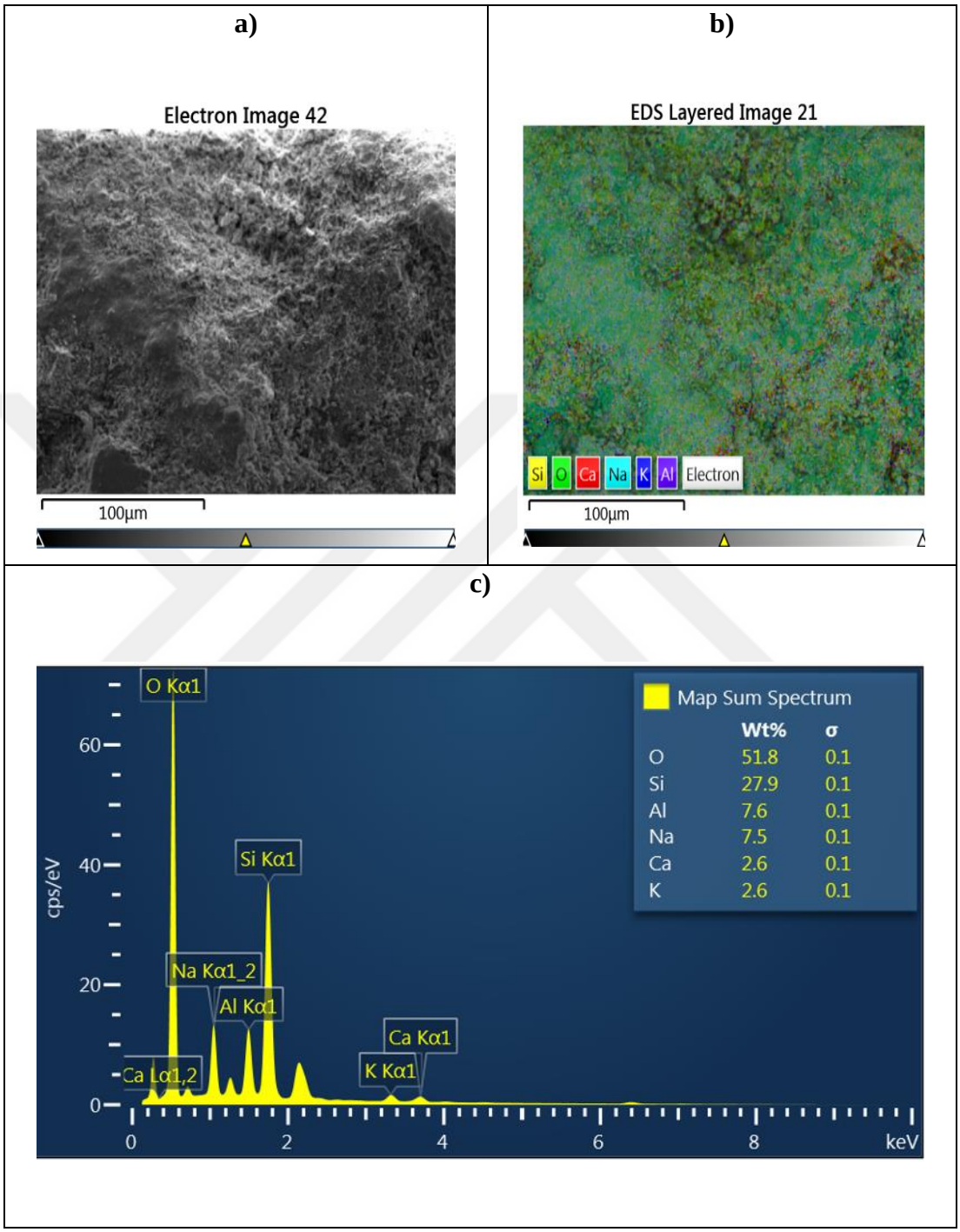

Figure 4.48 EDX results, **a)** electron image, **b)** EDS layered image, **c)** elemental ratios with Map sum spectrum for aggregate (B) at w/c: 0.5 and curing temperature of 60°C.

In Figure 4.48, when the w/c ratio increased to 0.5, the concertation of silicate was the highest, while the concertation of aluminum and sodium was equal. Also, the concertation of calcium and sodium was the lowest, as showed in section (c).

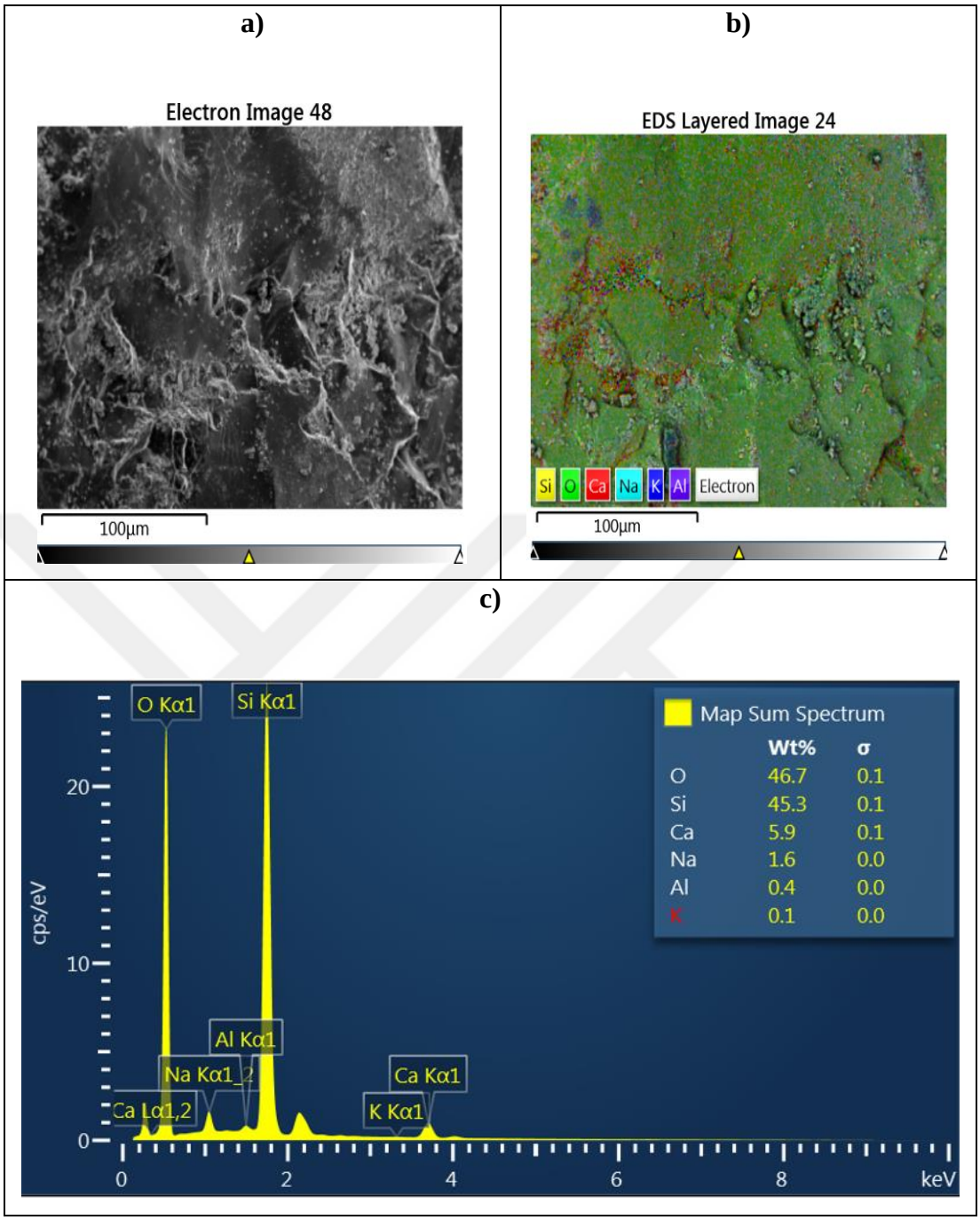

Figure 4.49 EDX-results, **a)** electron image**, b)** EDS layered image, **c)** elemental ratios with Map sum spectrum for aggregate (B) at w/c: 0.6 and curing temperature of 60°C.

The map spectra in Figure (4.49) observed a high concentration of silicate compared with other elements the concentration of silicate was 45.3 %, while the concentration of other chemicals did not exceed 6 %.

Table 4.5 shows the chemical elements ratios that formed from aggregate (B), at a curing temperature of 60°C, with different water/cement ratios.

Table 4.5 Elemental ratios of aggregate (B) with various amounts of w/c contents at 60 ºC.

Water/cement	Ca/Si	(Na+K)/Si
0.4	0.72	0.31
0.5	0.1	0.36
0.6	0.13	0.04

4.2.5 SEM/EDX-Results of Aggregate (A) at Different W/C Ratios and 80°C Curing Temperature

The following SEM images show the effect of ASR on specimens prepared from aggregate (A) and water/cement contents of 0.4, 0.5, and 0.6. The specimens were placed under a temperature of 80°C within 28 days, and completely immersed inside NaOH solution. By the end of the test period, SEM images were taken and EDX map spectra were used to plot the chemical elements. The following images (Figure 4.50 and Figure 4.51) shows the effects of ASR on the specimens with a water/cement content of 0.4 and aggregate (A).

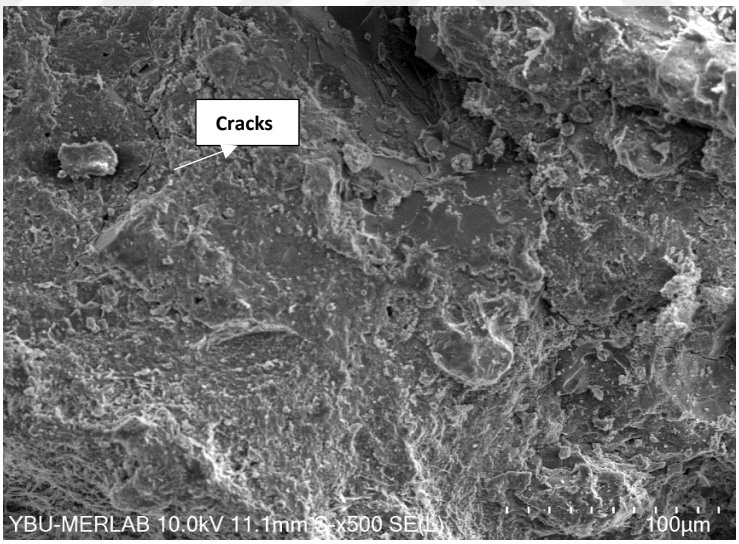

Figure 4.50 SEM image of aggregate (A) at w/c: 0.4 and curing temperature of 80°C.

In Figure 4.50, a massive gel formed on the surface of mortar paste, with cracks passed through mortar paste and near aggregate particles.

The figure below show SEM image with resolution of (10 µm) of the sample made from 0.4 w/c ratio, to clarify the hydration products.

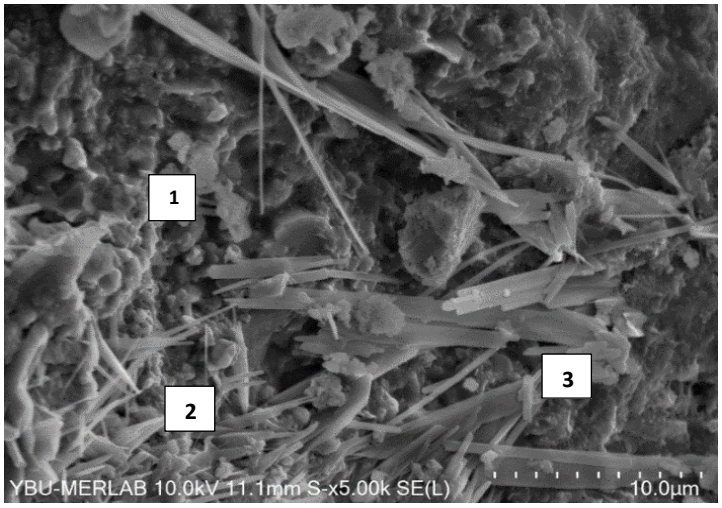

Figure 4.51 SEM image shows CaO (1), ettringite with short rods (2), bundles of ettringite (3).

When the amount of water cement/ content increases to 0.5, the surface shape of cement mortar paste appears as in Figure (4.52). The image shows two types of cracks, crack (1) is expansive cracks formed around aggregates particles, while the second crack (2) formed on cement paste and passed near aggregates. Section (1-4) in the figure shows the deterioration of ASR on mortar paste surface, but in different resolution (See Figure 4.53). Also, Figure (4.54) illustrate a close image of the crack (1), but in different resolution.

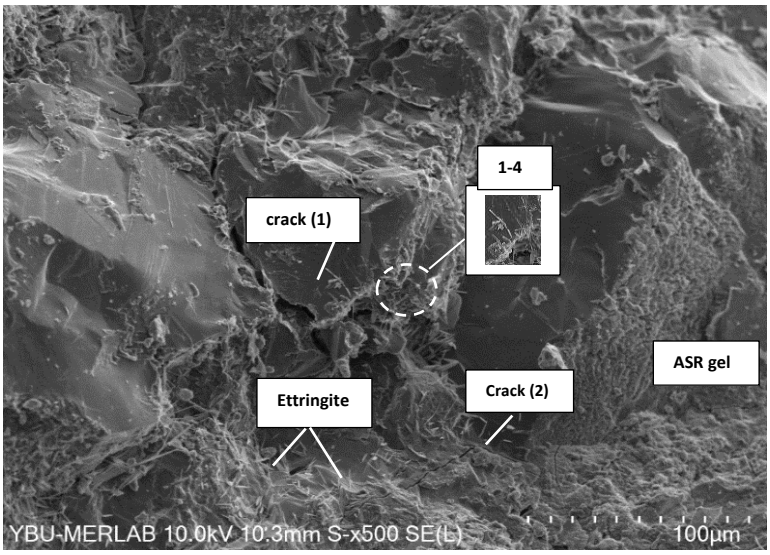

Figure 4.52 SEM image of aggregate (A) at w/c: 0.5 with a curing temperature of 80°C.

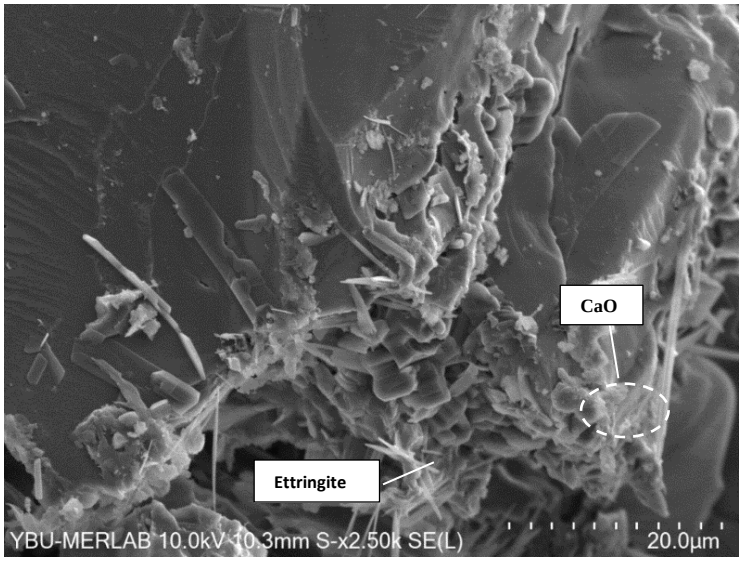

Figure 4.53 Section (1-4) shows deterioration of ASR on aggregate (A) sample at w/c: 0.5 and 80°C.

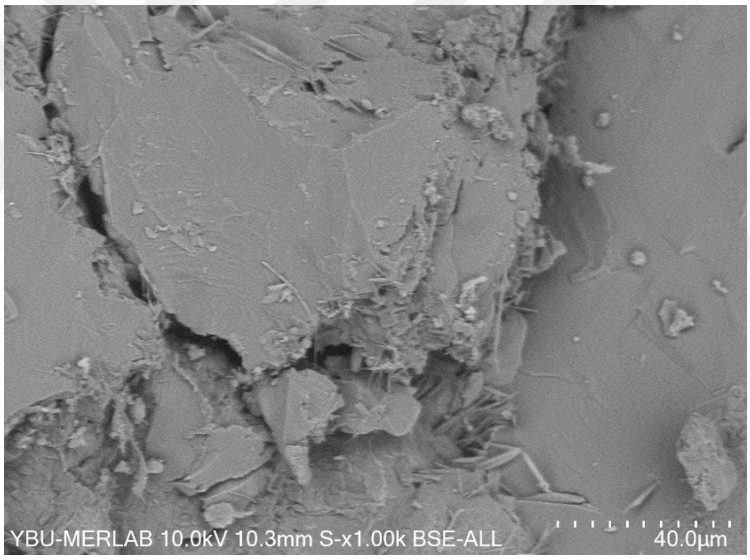

Figure 4.54 Close image of crack (1).

In Figure 4.54 the deterioration of ASR was showed by a massive crack formed through cement paste and aggregate. In addition to the formation of ettringite near the crack.

Figure 4.55, and Figure 4.56 clarified the destructive behavior of ASR at 0.6 water /cement content, where a massive gel covered the whole surface area of mortar paste. Moreover, there was a high distribution of ettringite, where the shape of ettringite appears as bundles with long needles. Also, excessive formation of calcium oxide (CaO) covered the surface, as shown in Figure 4.56 (resolution of 10 µm).

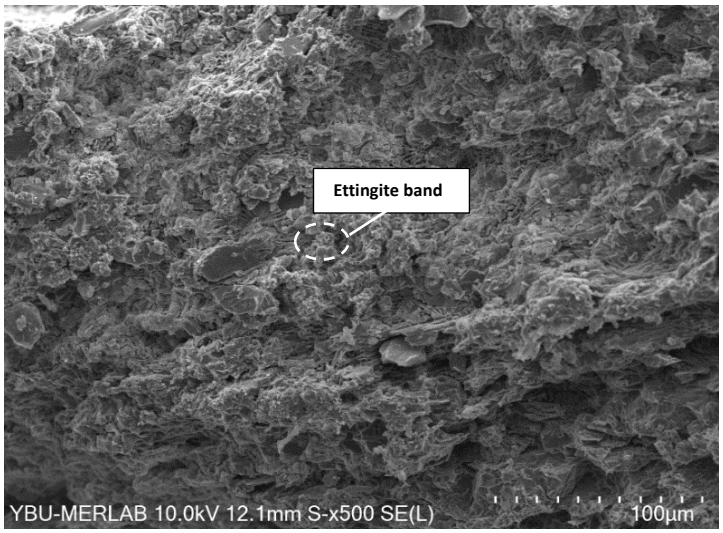

Figure 4.55 SEM image of aggregate (A) at w/c: 0.6 with a curing temperature of 80°C.

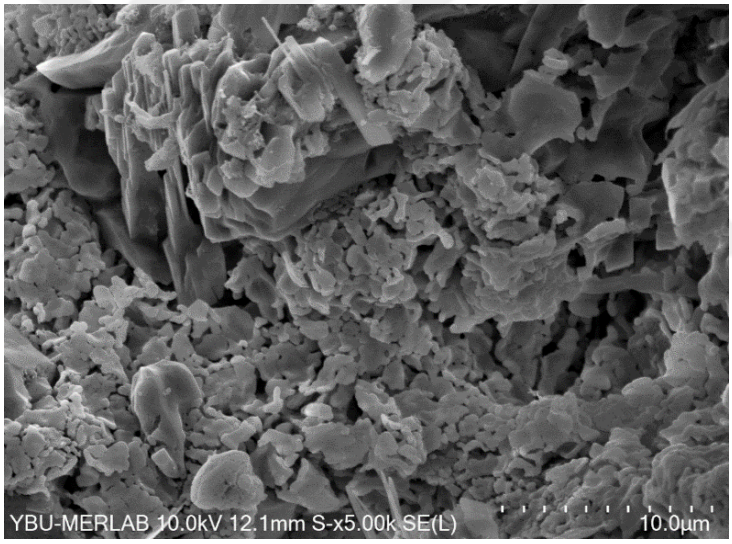

Figure 4.56 SEM image shows massive formation of calcium oxide.

By comparing the previous SEM images with different water cement contents, the images indicates to a high formation of massive gel, and calcium oxide, which were increasing by raising the amount of water/cement ratios, as shown when the water/cement contents were 0.4 , 0.5, and 0.6. Also, an expansive crack has formed around aggregate particles, as a result of the destructive behavior of ASR at 80°C. Furthermore, the width and length of the cracks increased by increasing the amount of water/cement ratios. The following Figures (4.57, 4.58, and 4.59) represent the EDX results of samples made from aggregate (A), and different amounts of water cement contents (0.4, 0.5, and 0.6), with 80°C.

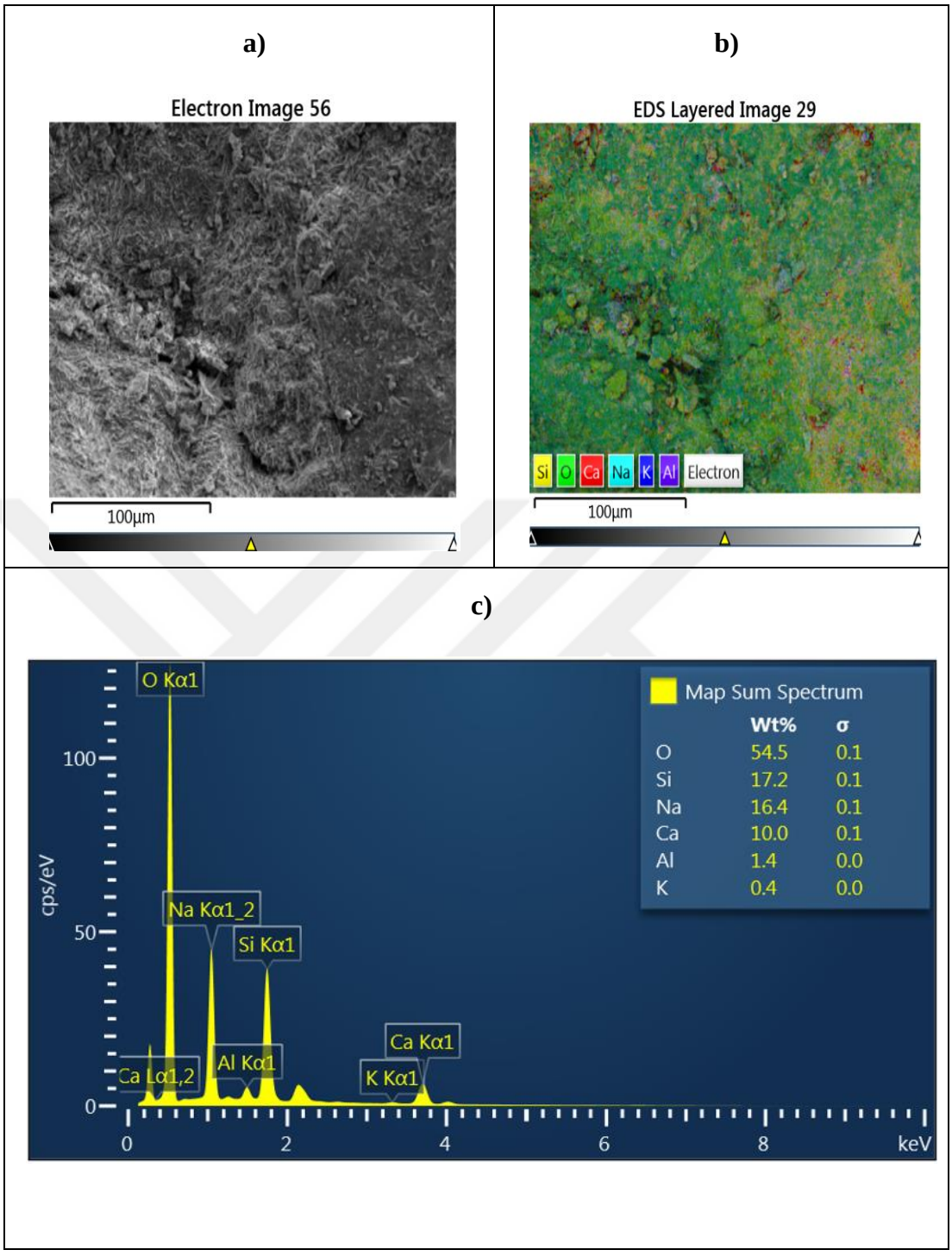

Figure 4.57 EDX results, **a)** electron image, **b)** EDS layered image, **c)** elemental ratios with Map sum spectrum of aggregate (A) at w/c: 0.4 and curing temperature of 80°C.

In Figure 4.57, the concentration sodium and silicate were similar, as shown in the map spectrum in section (c). Also, a strong variation between the concertation of aluminum and potassium with other elements, where the potassium had a concertation of 0.4%, and aluminum had a concertation of 1.4%

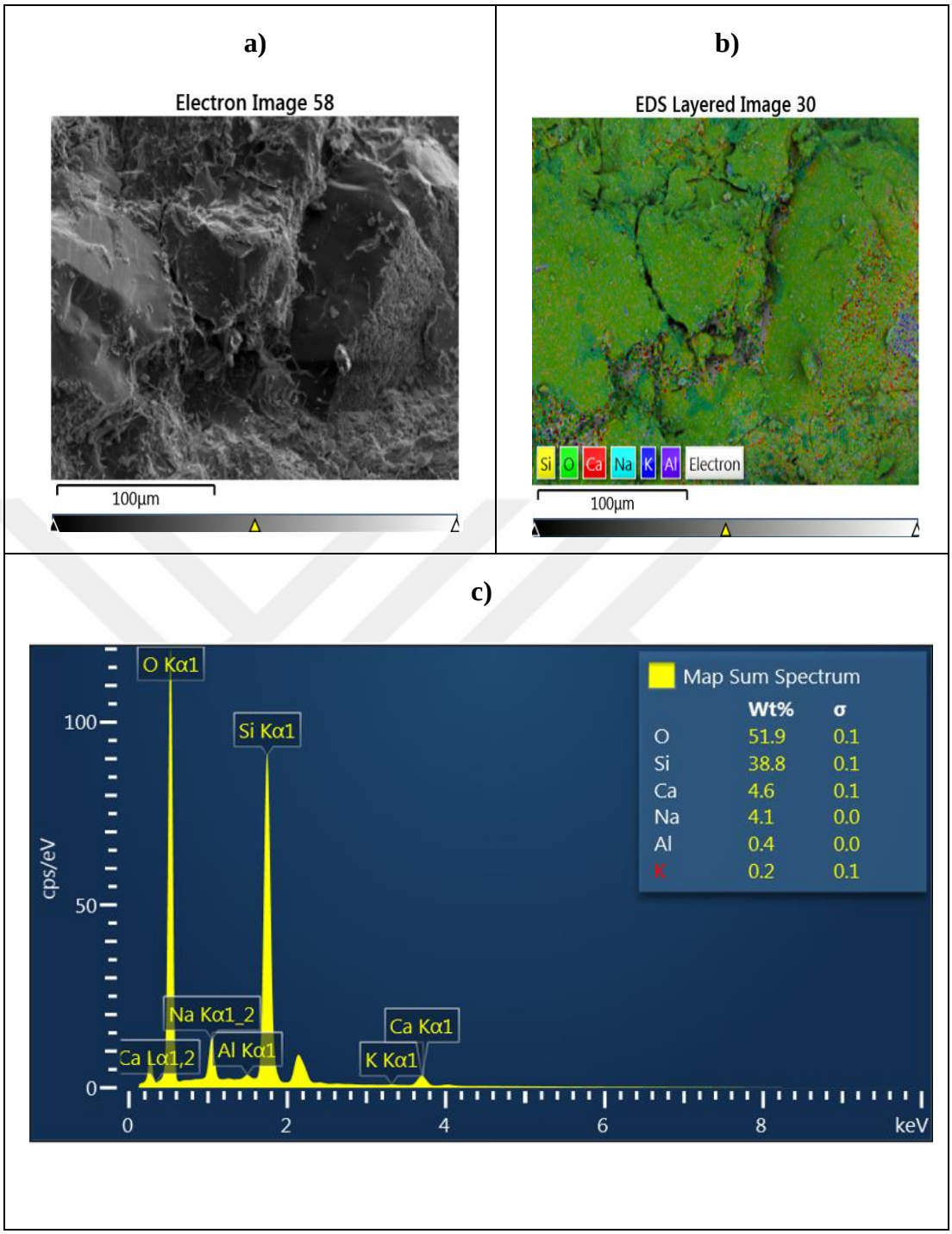

Figure 4.58 EDX results, **a)** electron image, **b)** EDS layered image, **c)** elemental ratios with Map sum spectrum of aggregate (A) at w/c: 0.5 and curing temperature of 80°C.

Figure 4.58 shows the concentration of the resulting elements at 0.5 w/c, where the silicate formed strongly and had a percent concentration of 38.8%, calcium with a percent concentration of 4.6%, and sodium with a percent concentration of 4.2%. While the percent concentration of the other elements such as, aluminum and potassium did not exceed 1%.

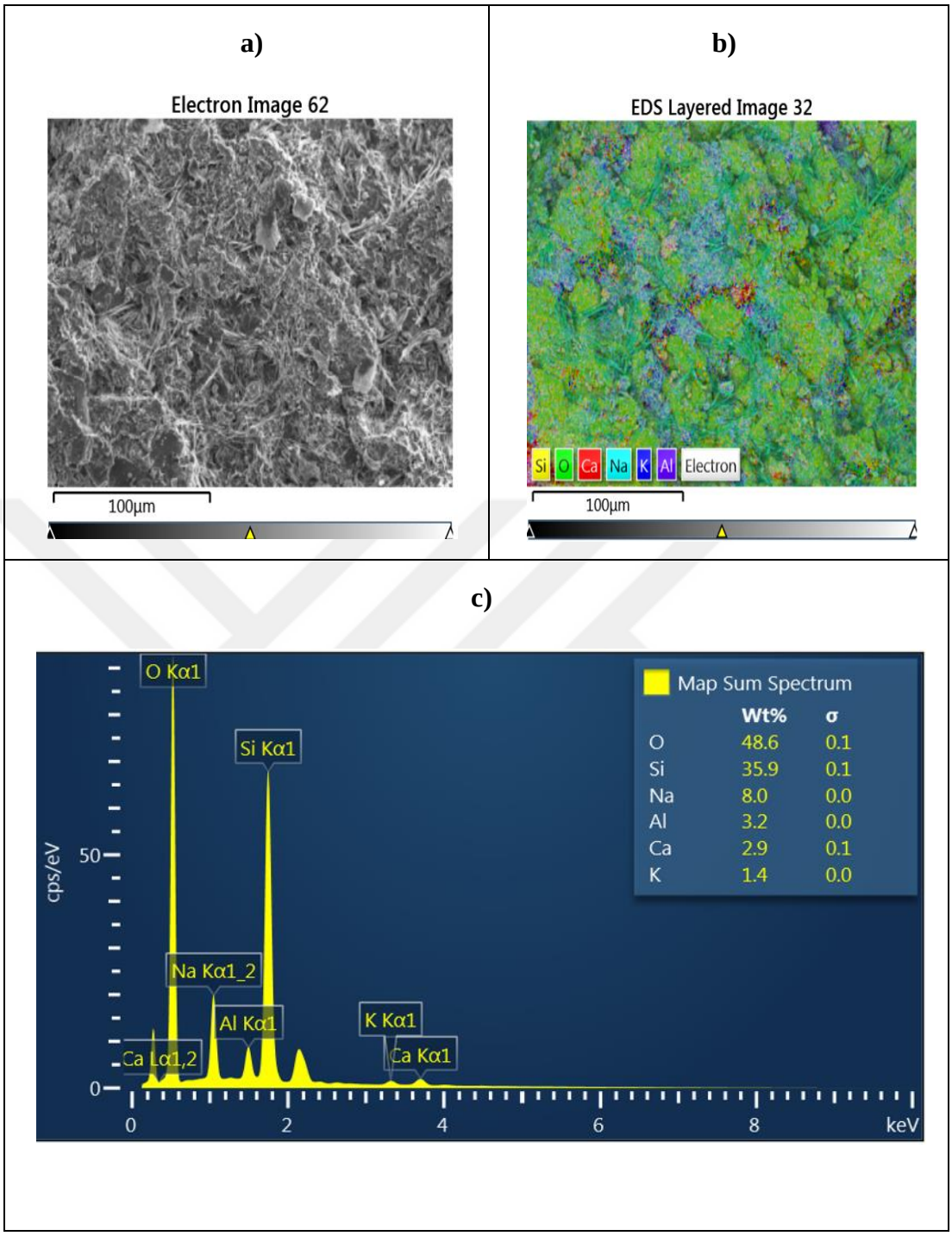

Figure 4.59 EDX- results, **a)** electron image, **b)** EDS layered image, **c)** elemental ratios with Map sum spectrum of aggregate (A) at w/c: 0.6 and curing temperature of 80°C.

In Figure 4.59, the concentration of the resulting elements at 0.6 w/c, was 35.9% for silicate, then a concentration gap was occurred between silicate and other elements. Also, the EDS layered image showed an obvious formation of aluminum and potassium on the edges, while the formation of calcium was centered near the crack.

Table 4.6 shows the chemical elements ratios that formed from aggregate (A), at a curing temperature of 80°C with different water/cement ratios.

Table 4.6 Elemental ratios of aggregate (A) with various amounts of w/c contents at 80 ºC.

Water/cement	Ca/Si	(Na+K)/Si
0.4	0.58	0.97
0.5	0.12	0.11
0.6	0.08	0.26

The elemental ratios indicates that when the amount of water /cement content increased, the amorphous gel contain higher silica and less amount of calcium and other alkalis (potassium and sodium).

4.2.6 SEM/EDX-Results of Aggregate (B) at Different W/C Ratios and 80°C Curing Temperature

The following SEM images show the effect of ASR of sample made from aggregate (B), and various water/cement contents (0.4, 0.5, and 0.6). Samples cured under a temperature of 80°C for 28 days and soaked in NaOH solution. At the end of the test duration, SEM images were taken, and EDX map spectra used to show the chemical elements that results from the presence of different water/cement ratios.

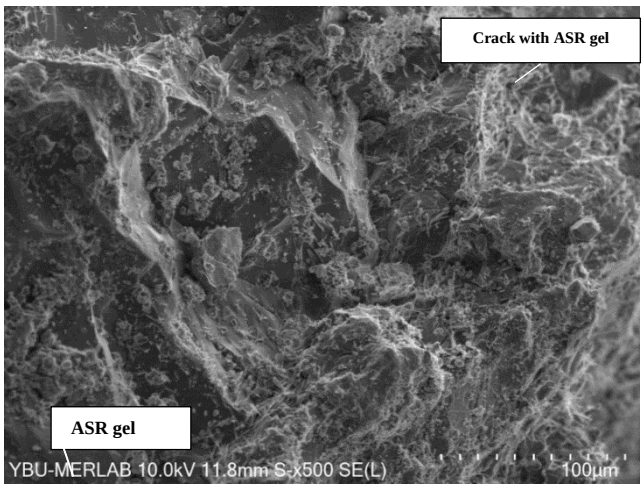

Figure 4.60 SEM image of aggregate (B) at w/c: 0.4 with a curing temperature of 80°C.

Figure (4.60) shows massive alkali gel formed on the surface of mortar paste, with high formation of ettringite and cracks near aggregates.

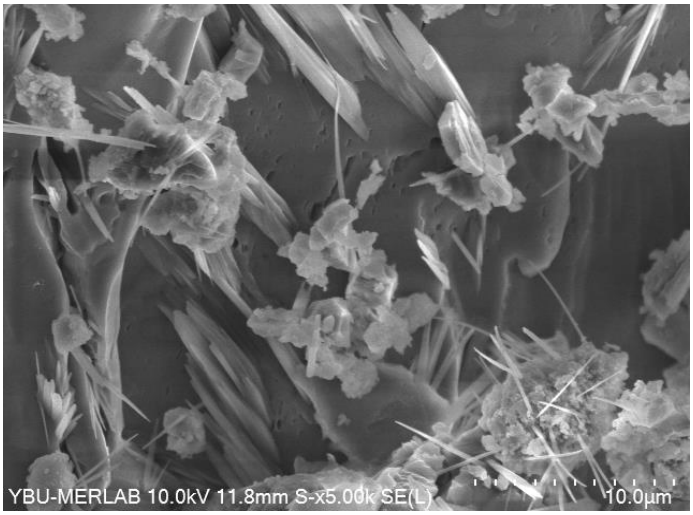

Figure 4.61 Close section of mortar paste surface of aggregate (B) at w/c: 0.4 and 80°C.

Figure 4.61 shows a close section from Figure 4.60 with different resolution. The image provides the surface of cement mortar paste covered with calcium hydroxide, and ettringite. Also, the surface to porous shape of the surface.

When the amount of water cement content increased to 0.5, the surface shape of cement mortar paste appears as figure below (Figure 4.62). Where a massive crack filled with ASR gel and formed near aggregate particles.

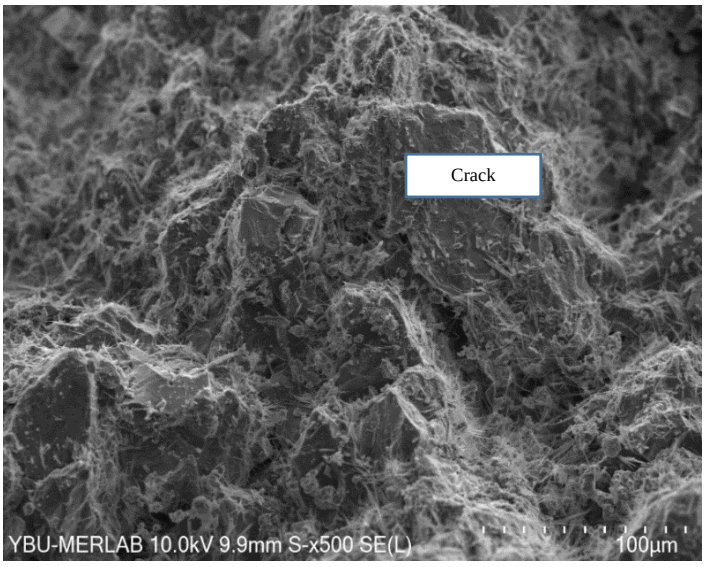

Figure 4.62 SEM image of aggregate (B) at w/c: 0.5 with a curing temperature of 80°C.

Figure (4.63) belongs to the same sample above, but it had different resolution. The figure shows a formation of ettringite on aggregate grains, with high amount of

calcium oxide. The ettringites has two shapes as shown either individual long needles (1), or bundles with long needles (2).

Figure 4.63 SEM image shows ettringite shape at w/c: 0.5 with a curing temperature of 80°C.

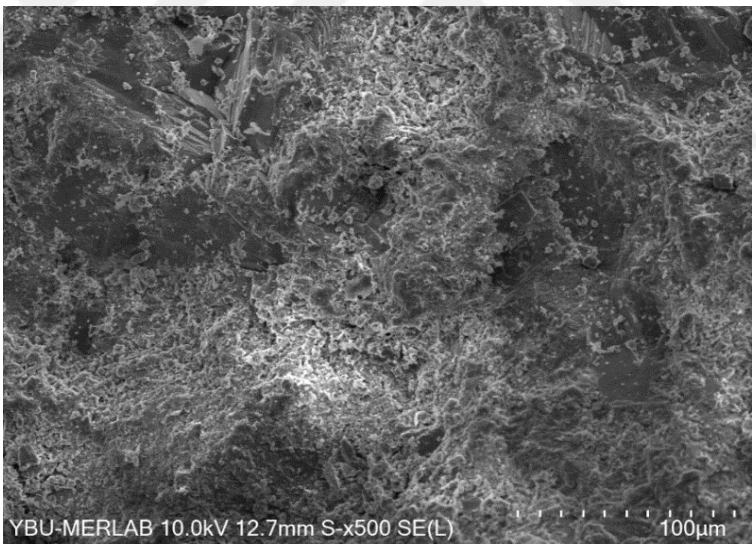

Figure 4.64 SEM image shows aggregate (B) surface at w/c: 0.6 with curing temperature of 80°C.

Figure 4.64 shows the performance of ASR at 0.6 water/cement content and 80°C, where a massive gel has covered the mortar paste. Also, most of ASR products covered the whole specimen surface.

Figure 4.65 had a close resolution of (10 µm), to illustrate the resulted ASR products, which were excessive formation of calcium oxide (CaO), with jennite. Other SEM

image was taken with different resolution to describe the manifestation of destruction on the outer surface of the specimen, as illustrated in Figure 4.66.

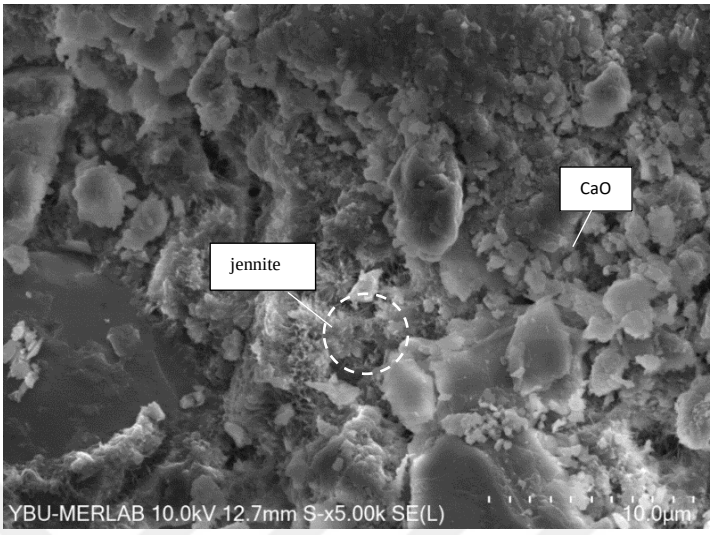

Figure 4.65 SEM image shows an excessive formation of jennite on aggregate (B) surface at w/c: 0.6 and 80°C.

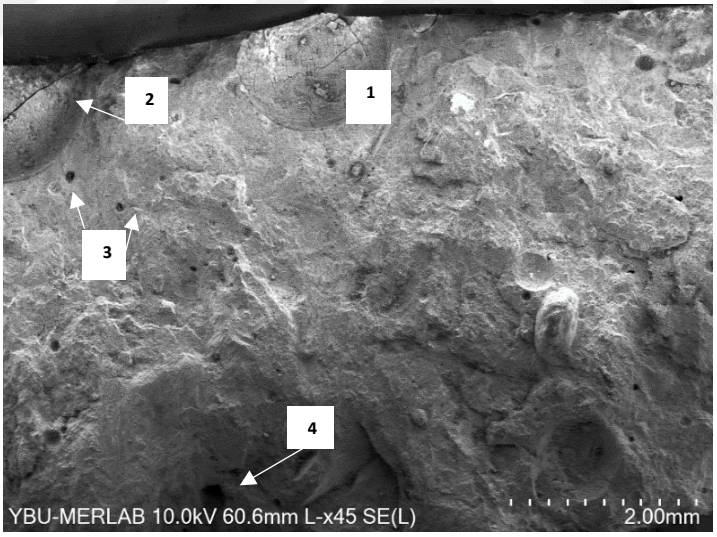

Figure 4.66 SEM image shows delayed ettringite formation (1), cracks with ASR gel (2), spherical air voids (3), voids filled with ASR gel (4).

Figure (4.66) illustrates the external surface of the specimen with a resolution of 2.00 (µm), the image shows a formation of delayed ettringite (DEF).

Through comparing the previous SEM images that contain of different water/cement ratios, the impact of alkali silica reaction was shown by high formation of calcium oxide, silicon dioxide, and jennite, these products were increased by increasing the amount of water cement contents. Also, most of the reaction products distributed over

the inner surface, and formed on aggregate particles. The following (EDX) results, provides the chemical elements that resulted from the ASR, under the effect of 80°C, and various amounts of water cement contents (0.4, 0.5, and 0.6), for samples prepared from aggregate (B).

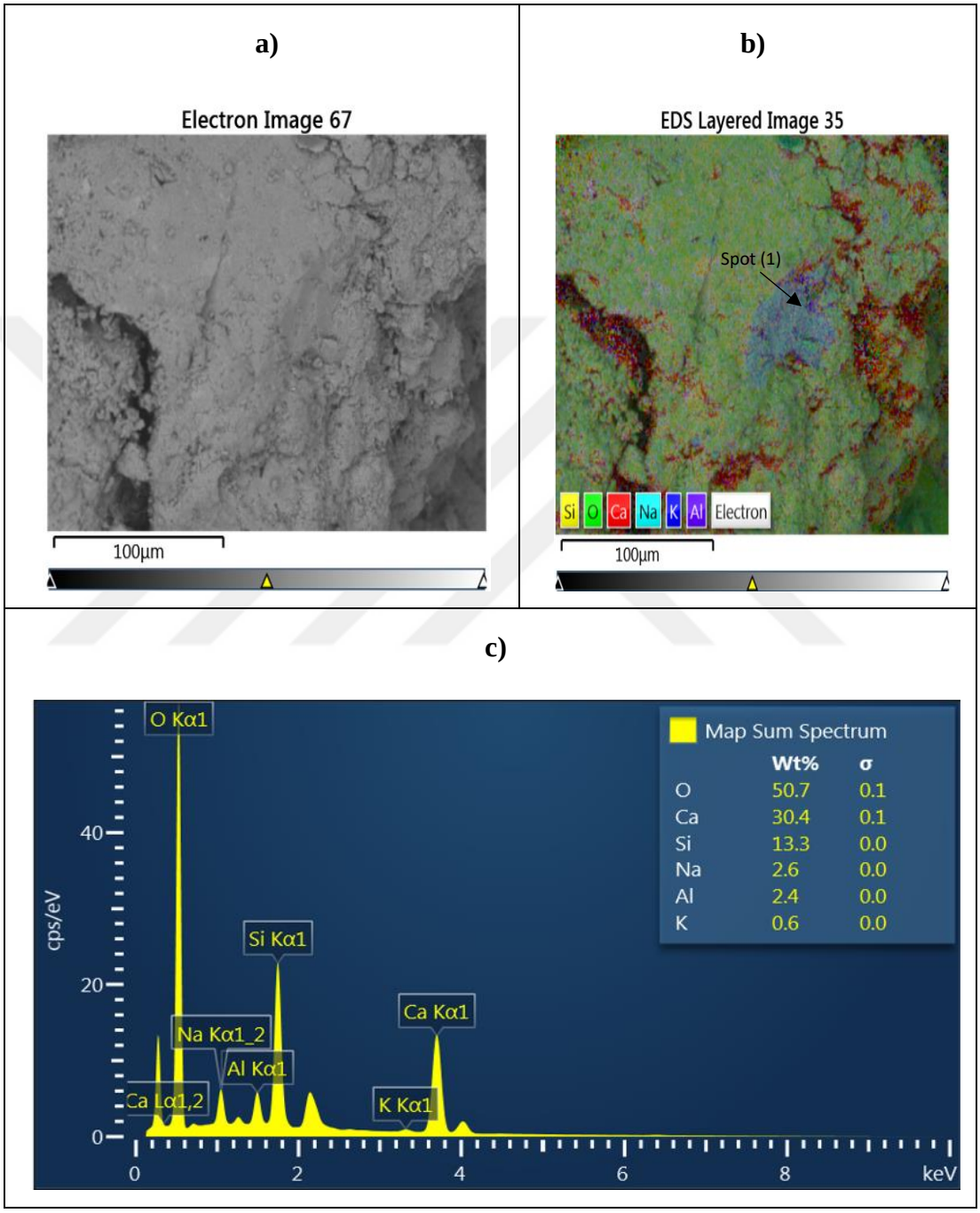

Figure 4.67 EDX results**, a)** electron image**, b)** EDS layered image, **c)** elemental ratios with map sum spectrum of aggregate (B) at w/c: 0.4 and 80°C

In Figure 4.67, the element ratios indicate extensive formation of calcium around the cracks, as seen in EDS layered image, while obvious formation of aluminum and

sodium was concentrate mainly at spot (1). Moreover, the concentrations of aluminum and sodium were similar, while potassium concertation was the lowest as shown in map spectra.

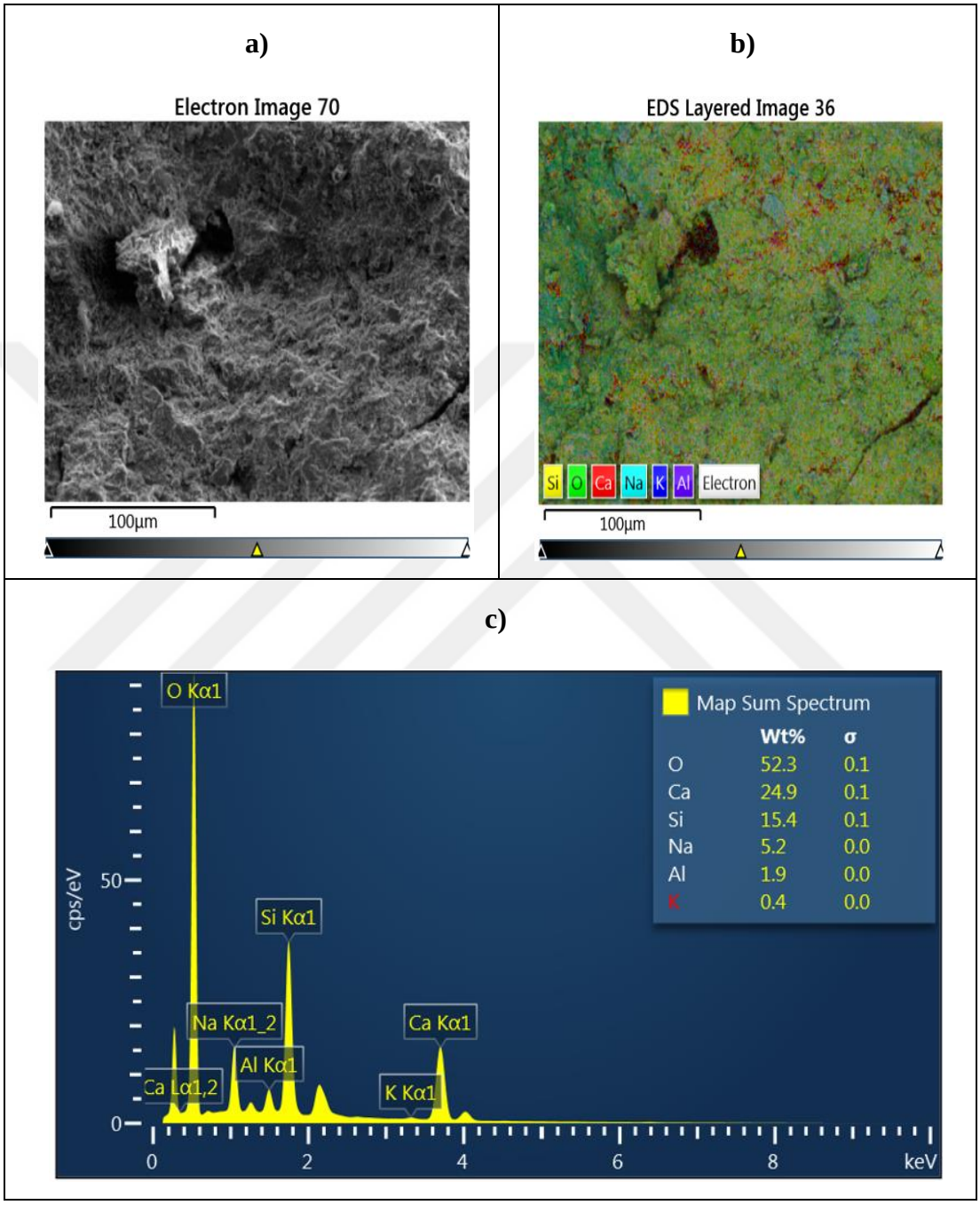

Figure 4.68 EDX results**, a)** electron image**, b)** EDS layered image, **c)** elemental ratios with map sum spectrum of aggregate (B) at w/c: 0.5 and of 80°C.

Figure 4.68 shows the distribution and concentration of the elements when the ratio of w/c is expand to 0.5. The results show a high concentration of calcium on the micro-

surface of mortar paste with a percent concentration of 24.9%, while the lowest formation is for potassium with a percent concentration of 0.4%.

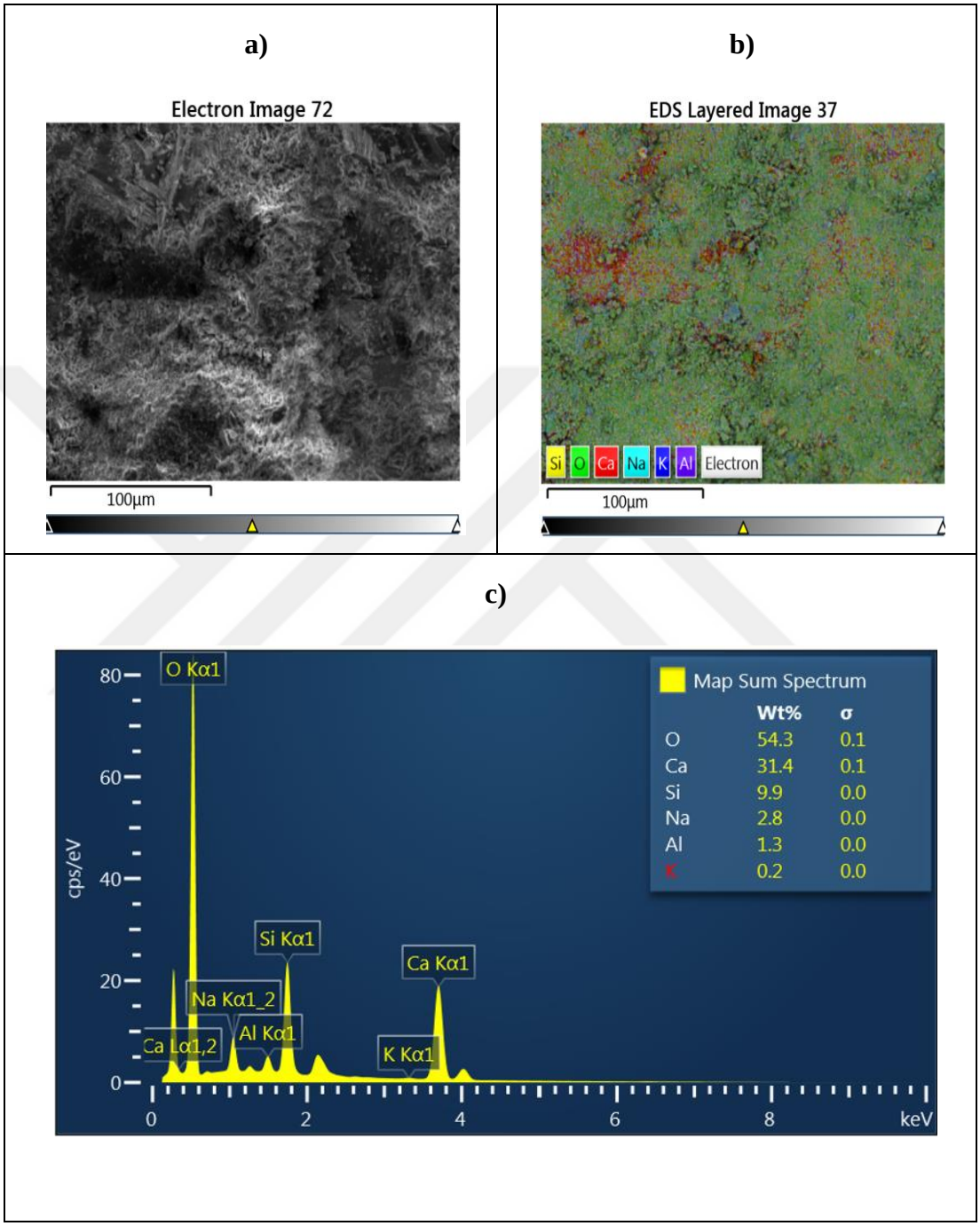

Figure 4.69 EDX results, **a)** electron image, **b)** EDS layered image, **c)** elemental ratios with map sum spectrum of aggregate (B) at w/c: 0.6 and 80°C.

In Figure 4.68, the concentration of the resulting elements at 0.6 w/c, was 31.4% for calcium, then a concentration gap was occurred between calcium and other elements such as, silicate, sodium, aluminum, and potassium. However, the concertation of other

elements did not exceed the percentage of 10%. Table 4.7 shows the chemical elements ratios that formed from aggregate (B) at a curing temperature of 80°C, with different water/cement ratios.

Table 4.7 Elemental ratios of aggregate (B) with various amounts of w/c ratios at 80ºC.

Water/cement	Ca/Si	(Na+K)/Si
0.4	2.28	0.24
0.5	1.61	0.36
0.6	3.17	0.3

According to the table above the Ca/Si ratio indicated to increasing of calcium element, with increasing the amount of w/c ratio to the mixture. Also, the ratio of alkalis raised by enlarged the amount of w/c ratio to the mixture, while the formation of silicate decreases.

4.3 Discussion

This section focuses on the results found by the accelerated mortar bar method (AMBT), and scanning electron microscopy with energy dispersive x-rays (SEM /EDX). In the first part of the discussion, the response of aggregates is studied in terms of expansion percentage under the effect of test conditions. The subsequent part analyzes how the test conditions affect the microstructure of the tested samples. In order to asses the potential reactivity aggregates tested, different curing temperatures and water/cement ratio were used in this investigation.

4.3.1 Accelerated Mortar Bar Method (AMBT)

In the first group, the effect of ASR of aggregates was tested at a curing temperature of 40ºC, and water/cement ratios of 0.4, 0.5, and 0.6. The results exhibited that the expansion values of aggregates at 0.4, 0.5 and 0.6 w/c, respectively, were 0.013%, 0.019%, and 0.024% for aggregate (A) and 0.018%, 0.015%, 0.019% for aggregate (B). Based on ASTM C 1260's deleterious expansion limit, 0.1%, the aggregate did not produce harmful expansion at 40ºC.

Previous study confirmed that the effect of alkali silica reaction at low temperatures is not harmful [85]. The reactivity of the tested aggregates in Figure (4.4) confirms this statement. Also, the different water/cement ratios at 40ºC had a minor effect on

increasing the expansion values. The reason for the lack of reactivity at this stage of the test is due to the limitation of the alkali gel, where the gel hinders seepage from the pore structure because the viscosity of the gel is high [79].

At a temperature of 60ºC, the expansion of samples begins to increase gradually with the amount of water/cement ratio increases. At first, when the w/c content was 0.4, the expansion percentage of aggregate (A) was 0.043%, and 0.078%, according to ASTM C 1260's the reactivity of tested aggregate was harmless. Then when the amount of water/cement contents raised to 0.5, the expansion values increased to be 0.1% for aggregate (A), and 0.137% of aggregate (B), based on the standard, the tested aggregates had deleterious effect. In Figure (4.7), the expansion values at 0.6 w/c were higher than 0.1% and were considered harmful.

Comparing the expansion results at w/c of 0.4 and 0.5, the reactivity of aggregate (B) was higher than aggregate (A), but when the water/cement ratio enlarged to 0.6, the opposite has occurred, especially for the final expansion values (See Figure 4.8). Previous study indicate that there is no relationship between the final expansion and temperature [78]. While other study state that high temperatures causes to leach the alkalis in quick form, and that leads to consume the amount of alkalis from pore solutions, and that explains the lower final expansions by time [77].

On a temperature of 80ºC, the expansion values of tested aggregates exceeds the limit of 0.2%, and relied on the standard the aggregates were highly deleterious. Some explanations detect that reactive aggregates have the ability to absorb water, and the absorption rate depends on the amount of water they contain [75]. Which explains the increasing in expansion rate of the samples as water/cement content increases at 80ºC. The expansion values at 0.4, 0.5, and 0.6 water/cement content were 0.178%, 0.180%, and 0.22% for aggregate (A), and 0.219%, 0.223%, and 0.226% for aggregate (B). The reactivity of aggregate (B) was higher than aggregates (A).

4.3.2 Scanning Electron Microscopy with Energy Dispersive and X-Ray (SEM/EDX)

First, the SEM /EDX analysis was performed to observe the effects of different water/cement contents on the cement mortar at different curing temperatures of 40ºC, 60ºC and 80ºC. This investigation was carried out for both types of aggregates, and

the results were recorded and analyzed. At a curing temperature of 40ºC, the SEM images of aggregate (A and B) at w/c: 0.4 showed hydration products such as: calcium hydrate (CH), friedel's salt, and primary ettringite, in addition to the formation of monosulfo-aluminate on the specimen made from aggregate (B). Moreover, the distribution of hydration products was homogenous, as showed in Figure (4.16). The reason of homogenous distribution related to the development of dense layer of C-S-H, when the amount of water/cement content is low, which causes a well-organization of hydration products [73]. When the amount of water/cement ratio increased to 0.5, the formation of ettringite in the specimens prepared from aggregate (A and B) increased, and the ettringite has formed in short rods, but in the specimen prepared form aggregate (B), hemi carbo-aluminate (HC) was also formed (See Figure 4.24). When the water/cement content was 0.6, a poor features of ASR appeared in the form of excessive ettringite formation on the interior surface of the specimens made from aggregate (A and B). In addition, secondary ettringite was formed on the specimen made from aggregate (B), as showed in Figure 4.25. It was found that the formation of secondary ettringite (SE) has no harmful effect and does not contribute in the expansion [41].

At curing temperature of 60ºC, the effect of ASR start to appear clearly on mortar paste. The results showed significant amount of ettringite with needle shape formed on the mortar paste, and increased by increases the amount of water/cement ratio. Previous study confirmed that the fast crystallizing of hydration products in short time leads to form fibers with long needles [30].

For aggregate (A) at 0.4 w/c, the ettringite was shaped in a bundles. The formation of ettringite in bundles, related to the growth of ASR. [40]. At 0.5 w/c, portlandite and silicon dioxide has appeared intensively (See Figure 4.33), and when the amount of w/c increased to 0.6, a massive crack was observed. For aggregate (B) at w/c of 0.4, blade shape of ettringite was formed in addition to the formation of columnar ettringite.

Also, high formation of ettringite, portlandite, and bentonite on the surface of mortar cement paste were observed at 0.5 w/c. It's important to mention that the formation of bentonite caused from high alkali region. However, at w/c: 0.6 massive gel was formed on mortar-paste surface, as showed in Figure 4.45.

At a temperature of 80ºC, the reactivity of ASR showed in spherical voids, and irregular massive cracks formed close to aggregate particles, which increase by water/cement ratios. The appearance of theses massive cracks, refers to the pressure that causes by water evaporation due to the high temperature, which leads to the destructive in pore walls collapse [84]. Where a previous study showed that the cracks that pass through cement paste and around aggregate contain higher amount of calcium compared with silica, and these cracks formed by the swelling of alkali gel [101]. The SEM images of the specimens made from aggregate (A) at 0.4 w/c showed two types of ettringite formation, first type was ettringite with short rods, and the second type was bands of ettringite with needle-shape. Also, there was a clear formation of calcium oxide when the w/c increased to 0.5, in addition to the formation of massive crack, as showed in Figure 4.54. When the value of water/cement content increased to 0.6, massive gel with excessive formation of calcium oxide were formed, as illustrated in Figure 4.55 and Figure 4.56. For aggregate (B) at 0.4 w/c, the surface of mortar paste has a porous shape, and covered with calcium hydroxide $Ca(OH)_2$, and ettringite with long needle shape (See Figure 4.61), but when w/c was 0.5 a deleterious massive crack was formed, and filled with ASR gel. The excessive formation of calcium oxide and massive cracks were detected when the w/c raised 0.6, the formation of calcium oxide increases with increasing water/cement ratio. A previous study explained that the formation of calcium oxide is formed through the disbanding of portlandite under the effect of high temperatures [84]. Additionally to the appearance of delayed ettringite (See Figure 4.66). The fast growth of ettringite under high curing temperature, leads to initial deterioration of sample microstructure, and this case is called delayed ettringite formation (DEF) [70].

Previous study confirmed that the ratio of (Ca/Si) determine some minerals, such as tobermorite and jennite. When the ratio range between (0.83 - 1.5) tobermorite appears, and when the ratio exceed 1.5, jennite appears [37]. Also, the amount of calcium silica ratio gives an indication of alkaline gel texture. For example, when the amount of (Ca/Si) is 0.4, the texture displays in rosette crystal gel, and its caused after 84 hour of test duration [43]. Other study mention that when the amount of (Ca/Si) range from 0.82 to 1.2, spongy gel formed, and when the ratio range from 0.55 to 0.61, a massive gel formed [43]. In this study the ratio of (Ca/Si) at 40ºC, of the specimens

prepared of aggregate (A) were 0.14, 2.91, and 1.35, and for aggregates (B) were 0.26, 3.21, and 0.83. A rosette shape of alkali gel appeared on aggregates (B), at 0.5 w/c (See Figure 4.26). The reason for these variations in Ca/Si ratios, related that these samples were taken from different locations. For clarification, the concentricity of chemical elements in the middle of the sample is different from its edges. However, the ratios of Ca/Si increased by increasing the amount of water cement ratios.

At 60ºC, when water/cement ratios were 0.4, 0.5, and 0.6, respectively, the ratios of Ca/Si were 0.24, 0.67 and 2.39 of aggregates (A), and for aggregates (B) were 0.72, 0.1 and 0.13. The results found that when the amount of water /cement content increased, the ratio of Ca/Si increased. Also, the higher ratio of Ca/Si indicates to high formation of calcium, while low ratios of Ca/Si shows high formation of silica. The variation of these ratios was related to SEM images were taken from different locations, as explained before. The exudation of alkali gel continued when the w/c increased, caused to form a spongy gel, and massive gel, as shown in SEM images (Figure 4.32, Figure 4.42, and Figure 4.45). Spongy gel leads to deterioration to the inner structure of the sample, the deterioration demonstrated by SEM images, as cracks partially filled of ASR gel, and the width of the cracks increased by increases the amount of water/cement ratio, while the orientation of cracks were intensively distributed on the surface of mortar-paste and near the aggregate particles. It was revealed that the cracks that appeared near the aggregate particles, reflected a high level of amorphous gel with a small amount of calcium ions inside. This case occurred only when the expansion caused by ASR was harmful [97]. Moreover, in the samples that prepared from aggregates (B), when water cement/ratio was 0.4w/c, tobermorite has appeared as showed in Figure 4.41, and when the water/cement content raised to 0.6w/c, jennite has formed (See Figure 4.46). At 80ºC, the ratios of Ca/Si of aggregate (A) were 0.58, 0.12, and 0.08 (when water/cement contents were 0.4, 0.5, and 0.6, respectively). For aggregate (B), the ratios of Ca/Si were 2.88, 1.61, and 3.17. The variation of these values was explained before. However, these results indicate to high formation of jennite minerals as showed in Figure 4.65.

The following table (Table 4.8) describes the influence of ASR on mortar-paste samples, under the effect of numerous ratios of water/cement contents and curing temperatures.

Table 4.8 Description of ASR products at (0.4, 0.5 and 0.6) w/c with 40ºC, 60ºC, and 80ºC.

Curing temperature	Fiber's description	Hydration products	Alkali gel morphology	Crack statement
40 °C	Short fibers	1-Calcium hydrate (CH) 2-Friedel's salt (FS) 3- Hemi carbo aluminate (HC) 4- primary ettringite	Foliated gel	Micro-cracks distributed through cement paste.
60 °C	Long needles	1- Silicon dioxide	Spongy gel	Micro-cracks throughout cement paste, expansive cracks around aggregate grain.
	Columnar ettringite	3- Portlandite 4- Bentonite 5- Tobermorite		
80 °C	Very long needles	1-Calcium oxide (CaO) 2- Jennite 3- Excessive formation of ettringite covering the cement paste surface (DEF)	Massive gel	Expansive cracks inside cement paste and near aggregate particles.

CHAPTER 5

CONCLUSION

The main goal of this experimental study was to exposing the two types of aggregates (A and B) to altered curing temperatures of 40°C, 60°C, and 80°C, and various amounts of water/cement ratios (0.4, 0.5, and 0.6), for investigate the effect of ASR on tested aggregates under these conditions. In addition to performing SEM /EDX analysis to detect the reaction products. Where the study yielded on the following results.

- The ASR expansion at temperature 40°C was negligible and the expansion of mortar bars was insignificant. Also, the water/cement ratios had minor effect on ASR expansion at 40°C.
- The temperature effect on ASR expansion was seen at 60°C, and the deleterious effects of ASR occurred with an increase in water/cement ratio on the expansion curves at this temperature.
- The findings demonstrated a positive relationship between the increase in curing temperature with water/cement ratios, and expansion of the specimens.
- At 40 ºC the distributions of hydration products in SEM images were homogenous.
- Ettringite with needle-shape has formed in intensive form when the curing temperature were 60 ºC and 80 ºC. Where the length of ettringite (needle-shape) and the diameter depends on the water absorption. If the amount of absorbed water increases at high temperatures, the needle becomes longer, and the diameter becomes smaller.
- Most of ASR products changed from foils to fibrils with heterogeneous distribution, especially at 60 ºC and 80 ºC.
- New minerals were formed at 60ºC and 80 ºC, which were tobermorite, and jennite.

- When the temperature exceeds 60ºC, high formation of calcium oxide produced as a result of portlandite dissolution, in addition to delayed ettringite formation.
- The alkali gel texture and type depends mainly on curing temperature. The SEM images showed a foliated gel at 40ºC, spongy gel at 60ºC, and when the curing temperature raised to 80ºC massive gel has formed.
- The amount of initial products such as, calcium hydrate, friedel salt, primary ettringite, and C-S-H, was higher than that of external products (alkali gel) at low temperature, and the reverse was true at high temperature. This explains the uniform distribution of the initial products at low temperature, and the heterogeneous distribution of the outer products at high temperature.

RECOMMENDATION

ASTM C 1260 utilizes 0.47w/c and curing temperature of 80ºC. Based on the results of this limited study, it is recommended to modify the water to cement ratio as 0.5, and the curing temperature to 60 ºC.

REFERENCES

[1] S. I. Ahmad, “Coarse and Fine Aggregates Presented by Md . Shahrior Alam Bangladesh University of Engineering,” no. August, 2020.

[2] M. Thomas, “The effect of supplementary cementing materials on alkali-silica reaction: A review,” Cem. Concr. Res., vol. 41, no. 12, pp. 1224–1231, 2011.

[3] J. Lahdensivu, A. Köliö, and D. Husaini, “Alkali-silica reaction in Southern-Finland’s bridges,” Case Stud. Constr. Mater., vol. 8, no. March, pp. 469–475, 2018.

[4] U. Ramasamy, “Alkali-Silica Reaction Resistant Concrete Using Pumice Blended Cement,” no. August, 2014.

[5] Š. Šachlová, R. Přikryl, and Z. Pertold, “Alkali-silica reaction products: Comparison between samples from concrete structures and laboratory test specimens,” Mater. Charact., vol. 61, no. 12, pp. 1379–1393, 2010.

[6] M. D. A. Thomas, B. Fournier, and K. J. Folliard, “Alkali-Aggregate Reactivity (AAR) Facts Book,” Book, p. 224, 2013.

[7] Q. Nie, C. Zhou, X. Shu, Q. He, and B. Huang, “Chemical, mechanical, and durability properties of concrete with local mineral admixtures under sulfate environment in Northwest China,” Materials (Basel)., vol. 7, no. 5, pp. 3772–3785, 2014.

[8] M. H. Shehata and M. D. A. Thomas, “Effect of fly ash composition on the expansion of concrete due to alkali-silica reaction,” Cem. Concr. Res., vol. 30, no. 7, pp. 1063–1072, 2000.

[9] R. K. Dhir, T. D. Dyer, and M. C. Tang, “Alkali-silica reaction in concrete containing glass,” Mater. Struct. Constr., vol. 42, no. 10, pp. 1451–1462, 2009.

[10] J. M. Ponce and O. R. Batic, “Different manifestations of the alkali-silica reaction in concrete according to the reaction kinetics of the reactive aggregate,” Cem. Concr. Res., vol. 36, no. 6, pp. 1148–1156, 2006.

[11] I. Fernandes and M. A. T. M. Broekmans, “Alkali-Silica Reactions: An Overview. Part I,” Metallogr. Microstruct. Anal., vol. 2, no. 4, pp. 257–267, 2013.

[12] A. Damilare, “Influence of Moisture on Alkali Silica Reaction,” no. December, 2016.

[13] S. Diamond and S. Diamond, “Printed in the United States . (Communicated by G . M . Idorn) (Received Feb . 9 , 1976 ; in final form April 20 , 1976).

[14] J. A. Farny and B. Kerkhoff, “Diagnosis and Control of Alkali-Aggregate Reactions in Concrete,” Concr. Technol., pp. 1–23, 1997.

[15] S. Thokchom, P. Ghosh, and S. Ghosh, “Effect of water absorption, porosity and sorptivity on durability of geopolymer mortars,” J. Eng. Appl. Sci., vol. 4, no. 7, pp. 28–32, 2009.

[16] G. Geng et al., “An in-situ 3D micro-XRD investigation of water uptake by alkali-silica-reaction (ASR) product,” Cem. Concr. Res., vol. 141, no. December 2020, 2021.

[17] J. Lindgård et al., “Alkali-silica reaction (ASR) - Performance testing: Influence of specimen pre-treatment, exposure conditions and prism size on alkali leaching and prism expansion,” Cem. Concr. Res., vol. 53, pp. 68–90, 2013.

[18] Y. Kawabata, C. Dunant, K. Yamada, and K. Scrivener, “Impact of temperature on expansive behavior of concrete with a highly reactive andesite due to the alkali–silica reaction,” Cem. Concr. Res., vol. 125, no. April, p. 105888, 2019.

[19] S. Chatterji, “Chemistry of alkali-silica reaction and testing of aggregates,” Cem. Concr. Compos., vol. 27, no. 7–8, pp. 788–795, 2005.

[20] M. Cabinets, M. Rooms, B. Statements, and T. Method, “Standard Test Method for Potential Alkali Reactivity of Aggregates (Mortar-Bar,” pp. 12–16, 2008.

[21] M. M. Mohsen, “Al-Hussein Bin Talal University Faculty of Engineering Department Of Mining Engineering. Cement Manufacturing Relationship between Mining and Cement Manufactaring,” vol. 10, no. 4, pp. 3–26, 2015.

[22] P. Chindaprasirt, S. Hatanaka, T. Chareerat, N. Mishima, and Y. Yuasa, “Cement paste characteristics and porous concrete properties,” Constr. Build. Mater., vol. 22, no. 5, pp. 894–901, 2008.

[23] S. W. Tang, Y. Yao, C. Andrade, and Z. J. Li, “Recent durability studies on concrete structure,” Cem. Concr. Res., vol. 78, pp. 143–154.

[24] J. Olek et al., “Alkali-silica reaction (ASR) mechanisms and detection: An advanced understanding,” p. 243, 2013.

[25] M. Thomas, B. Fournier, K. Folliard, J. Ideker, and M. Shehata, “Test methods for evaluating preventive measures for controlling expansion due to alkali-silica reaction in concrete,” Cem. Concr. Res., vol. 36, no. 10, pp. 1842–1856, 2006.

[26] C. A. Rogers, “Multi-laboratory study of the accelerated mortar bar test (ASTM C 1260) for alkali-silica reaction,” Cem. Concr. Aggregates, vol. 21, no. 2, pp. 185–194, 1999.

[27] C. Shi, Z. Shi, X. Hu, R. Zhao, and L. Chong, “A review on alkali-aggregate reactions in alkali-activated mortars/concretes made with alkali-reactive aggregates,” Mater. Struct. Constr., vol. 48, no. 3, pp. 621–628, 2015.

[28] I. Matteini, P. Noyce, and G. Crevello, “ASR: Practical investigative techniques and field monitoring systems used to assess ASR for service life modeling,” MATEC Web Conf., vol. 289, 2019.

[29] M. B. Santos, J. De Brito, and A. S. Silva, “A review on alkali-silica reaction evolution in recycled aggregate concrete,” Materials (Basel)., vol. 13, no. 11, 2020.

[30] A. Santos Silva, D. Soares, L. Matos, I. Fernandes, and M. Salta, “Alkali-aggregate reactions in concrete: Methodologies applied in the evaluation of alkali reactivity of aggregates for concrete,” Mater. Sci. Forum, vol. 730–732, no. November, pp. 409–414, 2013.

[31] J. M. Neves, “the Alkali-Silica Reaction in Alkali-Activated Fly Ash Concrete,” no. May, 2016.

[32] K. Scrivener, A. Ouzia, P. Juilland, and A. K. Mohamed, “Cement and Concrete Research Advances in understanding cement hydration mechanisms,” Cem. Concr. Res., vol. 124, no. August, p. 105823, 2019.

[33] S. Rahimi-aghdam, “Cement Hydration from Hours to a Century Controlled by Diffusion through Barrier Shells of C-S-H.”

[34] J. W. Bullard et al., “Mechanisms of cement hydration,” Cem. Concr. Res., vol. 41, no. 12, pp. 1208–1223, 2011.

[35] S. Poyet et al., “Influence of Water on Alkali-Silica Reaction: Experimental Study and Numerical Simulations,” J. Mater. Civ. Eng., vol. 18, no. 4, pp. 588–596, 2006.

[36] John E. R., “Composition and morphology of C-A-S-H in pastes of alite and cement blended with supplementary cementitious materials,” Lab. Constr. Mater., vol. 6294, 2014.

[37] P. Kazemi, M. R. Nikudel, M. Khamehchiyan, and P. Giri, “Assessment of Alkali – Silica Reaction Potential in Aggregates,” Materials (Basel)., 2022.

[38] C. Karakurt and I. B. Topçu, “Effect of blended cements produced with natural zeolite and industrial by-products on alkali-silica reaction and sulfate resistance of concrete,” Constr. Build. Mater., vol. 25, no. 4, pp. 1789–1795, 2011.

[39] Z. Zhang, G. W. Scherer, and A. Bauer, “Morphology of cementitious material during early hydration,” Cem. Concr. Res., vol. 107, no. May 2018, pp. 85–100, 2018.

[40] W. Kunther, B. Lothenbach, and J. Skibsted, “Influence of the Ca/Si ratio of the C-S-H phase on the interaction with sulfate ions and its impact on the ettringite crystallization pressure,” Cem. Concr. Res., vol. 69, pp. 37–49, 2015.

[41] T. Katayama, “The so-called alkali-carbonate reaction (ACR) - Its mineralogical and geochemical details, with special reference to ASR,” Cem. Concr. Res., vol. 40, no. 4, pp. 643–675, 2010.

[42] G. Davies and R. E. Oberholster, “Alkali-silica reaction products and their development,” Cem. Concr. Res., vol. 18, no. 4, pp. 621–635, 1988.

[43] X. F. Wang, Z. J. Yang, J. R. Yates, A. P. Jivkov, and C. Zhang, “Monte Carlo simulations of mesoscale fracture modelling of concrete with random aggregates and pores,” Constr. Build. Mater., vol. 75, pp. 35–45, 2015.

[44] N. Kabir, S. Aliyu, M. A. Nasara, A. U. Chinade, and A. Shehu, “Characteristics of Different Type of Coarse Aggregate on Properties of High Performance Concrete,” Sustain. Struct. Mater., vol. 2, no. 1, pp. 88–96, 2019.

[45] M. Y. Akbulut and H. Şahbaz, “Characterization of Crushed Natural Stone Aggregates,” J. Innov. Civ. Eng. Technol., vol. 2021, no. 2, pp. 55–77, 2021.

[46] Feininger, T. (2002). Igneous Rocks: A Classification and Glossary of Terms (Recommendations of the IUGS Subcommission on the Systematics of Igneous Rocks). Edited by RW LeMaitre. Cambridge University Press, New York, NY, 2002.

[47] Anon, "Guide To Durable Concrete.," J Am Concr Inst, vol. 74, no. 12, pp. 573–609, 1977.

[48] M. Ahmad, M. K. Ansari, R. Singh, L. K. Sharma, T. N. Singh, and S. Pires, "Assessment of Potential Alkali Aggregate Reactivity for Siliceous and Carbonate Aggregates: A Case Study," J. Geol. Soc. India, vol. 91, no. 4, pp. 467–474, 2018.

[49] J. Žvironaite and J. Pranckevičiene, "The Investigation of Alkali-Silica Reactivity (ASR) of Lithuanian Aggregates," Procedia Eng., vol. 172, pp. 1305–1310, 2017.

[50] P. Czapik, "Microstructure and degradation of mortar containing waste glass aggregate as evaluated by various microscopic techniques," Materials (Basel)., vol. 13, no. 9, pp. 25–30, 2020.

[51] A. K. Saha and P. K. Sarker, "Expansion due to alkali-silica reaction of ferronickel slag fine aggregate in OPC and blended cement mortars," Constr. Build. Mater., vol. 123, pp. 135–142, 2016.

[52] M. Moranville-Regourd, "Products of reaction and petrographic examination," 8th Int. Conf. Alkali-aggregate React. Concr. Kyoto, Jpn., pp. 445–456, 1989.

[53] F. A. Rodrigues, P. J. M. Monteiro, and G. Sposito, The alkali-silica reaction, vol. 29, no. 4. 1999.

[54] E. R. Gallyamov, A. Leemann, B. Lothenbach, and J. F. Molinari, "Predicting damage in aggregates due to the volume increase of the alkali-silica reaction products," Cem. Concr. Res., vol. 154, p. 106744, 2022.

[55] A. Gholizadeh Vayghan, F. Rajabipour, and J. L. Rosenberger, "Composition-rheology relationships in alkali-silica reaction gels and the impact on the Gel's deleterious behavior," Cem. Concr. Res., vol. 83, pp. 45–56, 2016.

[56] M. D. A. Thomas, B. Fournier, and K. J. Folliard, "Alkali-Aggregate Reactivity (AAR) Facts Book," Book, p. 224, 2013.

[57] N. B. Singh, S. Chaturvedi, and S. Rai, “Chemistry of portland cement,” J. Indian Chem. Soc., vol. 80, no. 4, pp. 319–325, 2003.

[58] G. Kakali, S. Tsivilis, E. Aggeli, and M. Bati, “Hydration products of C3A, C3S and Portland cement in the presence of CaCO3,” Cem. Concr. Res., vol. 30, no. 7, pp. 1073–1077, 2000.

[59] J. Ingham, “Delayed ettringite formation in concrete structures,” Proc. Inst. Civ. Eng. Forensic Eng., vol. 165, no. 2, pp. 59–62, 2012.

[60] A. Leemann, Z. Shi, and J. Lindgård, “Characterization of amorphous and crystalline ASR products formed in concrete aggregates,” Cem. Concr. Res., vol. 137, no. June, p. 106190, 2020.

[61] T. Kim, S. Sanyal, J. Bin Koo, J. A. Son, I. H. Choi, and J. Yi, “Analysis of cement deterioration in outdoor high-voltage insulator,” Materials (Basel)., vol. 12, no. 24, pp. 1–13, 2019.

[62] N. Smaoui, M. A. Bérubé, B. Fournier, B. Bissonnette, and B. Durand, “Effects of alkali addition on the mechanical properties and durability of concrete,” Cem. Concr. Res., vol. 35, no. 2, pp. 203–212, 2005, doi: 10.1016/j.cemconres.2004.05.007.

[63] P. Feng, C. Miao, and J. W. Bullard, “Factors Influencing the Stability of AFm and AFt in the Ca-Al-S-O-H System at 25°C,” J. Am. Ceram. Soc., vol. 99, no. 3, pp. 1031–1041, 2016.

[64] J. J. Thomas, S. A. FitzGerald, D. A. Neumann, and R. A. Livingston, “State of Water in Hydrating Tricalcium Silicate and Portland Cement Pastes as Measured by Quasi-Elastic Neutron Scattering,” J. Am. Ceram. Soc., vol. 84, no. 8, pp. 1811–1816, 2001

[65] A. Olugbenga, “Civil and Environmental Research,” Civ. Environ. Res., vol. 6, no. 3, pp. 39–43, 2011.

[66] D. P. Bentz, “Influence of water-to-cement ratio on hydration kinetics: Simple models based on spatial considerations,” Cem. Concr. Res., vol. 36, no. 2, pp. 238–244, 2006.

[67] R. A. Deschenes, E. R. Giannini, T. Drimalas, B. Fournier, and W. M. Hale, “Effects of moisture, temperature, and freezing and thawing on Alkali-Silica reaction,” ACI Mater. J., vol. 115, no. 4, pp. 575–584, 2018.

[68] S. Rasiah, “Evaluation of self-curing admixture in a flowing fly ash concrete EVALUATION OF A SELF-CURING ADMIXTURE IN A,” no. September, 2015.

[69] E. Knapen and D. Van Gemert, “Cement hydration and microstructure formation in the presence of water-soluble polymers,” Cem. Concr. Res., vol. 39, no. 1, pp. 6–13, 2009.

[70] N. Samson, A. Aondowase, and J. Shiwua, “Effect of Water-Cement Ratio on the Compressive Strength of gravel - crushed over burnt bricks concrete .,” vol. 3, no. 4, pp. 74–82, 2013.

[71] V. Živica, “Effects of the very low water/cement ratio,” Constr. Build. Mater., vol. 23, no. 12, pp. 3579–3582, 2009.

[72] V. Jensen, “Reclassification of Alkali Aggregate Reaction,” 14th Int. Conf. Alkali-Aggregate React. Concr., vol. 1, pp. 10–28, 2012.

[73] M. J. Munir, S. Abbas, A. U. Qazi, M. L. Nehdi, and S. M. S. Kazmi, “Role of test method in detection of alkali-silica reactivity of concrete aggregates,” Proc. Inst. Civ. Eng. Constr. Mater., vol. 171, no. 5, pp. 203–221, 2018.

[74] B. Li, L. Baingam, K. Kurumisawa, T. Nawa, and L. XiaoZhou, “Micro-mechanical modelling for the prediction of alkali-silica reaction (ASR) expansion: Influence of curing temperature conditions,” Constr. Build. Mater., vol. 164, pp. 554–569, 2018, doi: 10.1016/j.conbuildmat.2018.01.007.

[75] Y. Kawabata, C. Dunant, K. Yamada, and K. Scrivener, “Impact of temperature on expansive behavior of concrete with a highly reactive andesite due to the alkali–silica reaction,” Cem. Concr. Res., vol. 125, no. July, p. 105888, 2019.

[76] V. Saouma and L. Perotti, “Constitutive model for alkali-aggregate reactions,” ACI Mater. J., vol. 103, no. 3, pp. 194–202, 2006.

[77] L. Yang, M. Pathirage, H. Su, M. Alnaggar, G. Di Luzio, and G. Cusatis, “Computational modeling of temperature and relative humidity effects on concrete expansion due to alkali–silica reaction,” Cem. Concr. Compos., vol. 124, no. August, 2021.

[78] Y. Kawabata, C. Dunant, S. Nakamura, K. Yamada, and T. Kawakami, “Effects of temperature on expansion of concrete due to the alkali-silica

reaction: A simplified numerical approach," Mater. Construcción, vol. 72, no. 346, p. e282, 2022.

[79] M. C. Crovace et al., "Understanding the mixed alkali effect on the sinterability and in vitro performance of bioactive glasses," J. Eur. Ceram. Soc., vol. 41, no. 7, pp. 4391–4405, 2021.

[80] J. Bizzozero, C. Gosselin, and K. L. Scrivener, "Expansion mechanisms in ettringite systems," Calcium Aluminates Proc. Int. Conf., no. March 2018, 2014.

[81] K. Ma, G. Long, and Y. Xie, "A real case of steam-cured concrete track slab premature deterioration due to ASR and DEF," Case Stud. Constr. Mater., vol. 6, pp. 63–71, 2017.

[82] A. Fernández-Jiménez, J. Y. Pastor, A. Martín, and A. Palomo, "High-temperature resistance in alkali-activated cement," J. Am. Ceram. Soc., vol. 93, no. 10, pp. 3411–3417, 2010.

[83] N. Sinno and M. H. Shehata, "Role of temperature on Alkali-Silica reaction and the efficacy of supplementary cementitious materials," Constr. Build. Mater., vol. 313, no. June, p. 125427, 2021.

[84] I. Comby-Peyrot, F. Bernard, P. O. Bouchard, F. Bay, and E. Garcia-Diaz, "Development and validation of a 3D computational tool to describe concrete behaviour at mesoscale. Application to the alkali-silica reaction," Comput. Mater. Sci., vol. 46, no. 4, pp. 1163–1177, 2009.

[85] S. Beauchemin, B. Fournier, and J. Duchesne, "Evaluation of the Concrete Prism and the Accelerated Mortar Bar Tests for Assessing the Potential Alkali-Silica Reactivity of Recycled Concrete Aggregates," Proc. 15th Int. Conf. Alkali-Aggregate React. Concr., no. Series 1, p. 10, 2016.

[86] Z. Owsiak, "Testing alkali-reactivity of selected concrete aggregates," J. Civ. Eng. Manag., vol. 13, no. 3, pp. 201–207, 2007, doi: 10.1080/13923730.2007.9636438.

[87] R. D. Hooton and C. A. Rogers, "Development of the NBRI rapid mortar bar test leading to its use in North America," Constr. Build. Mater., vol. 7, no. 3, pp. 145–148, 1993.

[88] W. H. Tam and M. Division, “KK LIU and W.H. TAMThe use of accelertaed mortar bar test methods for assessment of alkali aggregate reactivity of aggregate in Hong Kong,” no. December, 2002.

[89] P. I. Sims and P. Nixon, “RILEM Recommended Test Method AAR-0 : Detection of Alkali-Reactivity Potential in Concrete – Outline guide to the use of RILEM methods in assessments of aggregates for potential alkali-reactivity,” vol. 36, no. September 2003, pp. 472–479, 2004.

[90] B. Ribeiro, S. Silva, and E. Civil, “ALKALI-AGGREGATE REACTION , AAR – DEALING WITH AAR,” pp. 1–10.

[91] C. Trottier, R. Ziapour, A. Zahedi, L. Sanchez, and F. Locati, “Microscopic characterization of alkali-silica reaction (ASR) affected recycled concrete mixtures induced by reactive coarse and fine aggregates,” Cem. Concr. Res., vol. 144, no. December 2020, p. 106426, 2021.

[92] D. L. Gress, R. L. Kozikowski, and T. T. Eighmy, “Accelerated ASR testing of recycled concrete,” Waste Manag. Ser., vol. 1, no. C, pp. 221–233, 2000.

[93] M. Barreto Santos, J. de Brito, A. Santos Silva, and A. Hawreen, “Evaluation of alkali-silica reaction in recycled aggregates: The applicability of the mortar bar test,” Constr. Build. Mater., vol. 299, no. June, 2021.

[94] P. E. Walker, H. N.; Lane, S. D.; Stutzman, “Petrographic Methods of Examining Hardened Concrete : A Petrographic Manual,” Fhwa-Hrt-04-150, no. July, p. 353, 2006.

[95] K. Pospíšil, A. Frýbort, A. Kratochvíl, and J. Macháčková, “Scanning Electron Microscopy Method as a Tool for the Evaluation of Selected Materials Microstructure,” Trans. Transp. Sci., vol. 1, no. 1, pp. 13–20, 2008.

[96] J. H. Shin, L. J. Struble, and R. J. Kirkpatrick, “Microstructural changes due to alkali-silica reaction during standard mortar test,” Materials (Basel)., vol. 8, no. 12, pp. 8292–8303, 2015.

[97] M. Voltolini, N. Marinoni, and L. Mancini, “Synchrotron X-ray computed microtomography investigation of a mortar affected by alkali-silica reaction: A quantitative characterization of its microstructural features,” J. Mater. Sci., vol. 46, no. 20, pp. 6633–6641, 2011.

[98] N. Thaulow, U. H. Jakobsen, and B. Clark, “Composition of alkali silica gel and ettringite in concrete railroad ties: Sem-edx and x-ray diffraction analyses,” Cem. Concr. Res., vol. 26, no. 2, pp. 309–318, 1996.

[99] I. Fernandes, “Composition of alkali-silica reaction products at different locations within concrete structures,” Mater. Charact., vol. 60, no. 7, pp. 655–668, 2009.

[100] A. Mladenovič, J. S. Šuput, V. Ducman, and A. S. Škapin, “Alkali-silica reactivity of some frequently used lightweight aggregates,” Cem. Concr. Res., vol. 34, no. 10, pp. 1809–1816, 2004.

[101] P. Alaejos, V. Lanza, M. A. Bermúdez, and A. Velasco, “Effectiveness of the accelerated mortar bar test to detect rapid reactive aggregates (including their pessimum content) and slowly reactive aggregates,” Cem. Concr. Res., vol. 58, pp. 13–19, 2014.

[102] D. Stokes, F. M. C. Corporation, D. Johnston, S. Dakota, R. Surdahl, and F. H. Administration, “the 2-Year Concrete Prism Test for Asr – Is It Worth the Wait ?,” vol. 1.

[103] J. H. Ideker, B. L. East, K. J. Folliard, M. D. A. Thomas, and B. Fournier, “The current state of the accelerated concrete prism test,” Cem. Concr. Res., vol. 40, no. 4, pp. 550–555, 2010.

[104] “Application of the Nbri Accelerated Mortar Bar Test To Siliceous,” vol. 21, no. c, pp. 1069–1082, 1991.

[105] J. Cao, N. Gowripalan, V. Sirivivatnanon, and W. South, “Assessment of ASR expansions using an ultra-accelerated test,” no. 2, pp. 1–7, 2019.

[106] E. R. Giannini and K. J. Folliard, “A Rapid Test to Determine Alkali-Silica Reactivity of Aggregates Using Autoclaved Concrete Prisms,” no. January, p. 21, 2013.

[107] Z. C. Lu et al., “Characterization data of reference cement CEM I 42.5 R used for priority program DFG SPP 2005 ‘Opus Fluidum Futurum – Rheology of reactive, multiscale, multiphase construction materials,’” Data Br., vol. 27, 2019.

[108] I. Petre and I. Mohanu, “DE ALCALII DIN CLINCHER INFLUENCE OF BYPASS DEGREE ON THE ALKALIS CONTENT,” no. October, 2019.

CURRICULUM VITAE

PERSONAL INFORMATION

Name Surname: Lina Mohmmad Abed Aljawad

Date of Birth :

Phone :

E-mail :

EDUCATION

High School **:** Al-Jubbiha seconday school, Jordan

Bachelor : Alhliyya Amman University, Jordan

Master Degree : Yıldırım Beyazıt University, Turkey

Experience:

February 2015 –August 2015 Sinohydro Corporation – Building and Construction, Qatar as Structural Design Coordinator

Key Project Handled:

Title: **Hamad Port**

Description: Shop Drawing.

The project includes a cargo terminal with a capacity of 107 million tons / year, a receiving station with a capacity of up to 500 thousand cars / year, a support station, a marine station, a cattle station and a coastal reception station. It also includes a customs inspection area and a 110-meter observation tower, the port was divided into zones the development was on zone 3.

Key Result Areas:

- Inspection of civil works according to approved specification and shop drawings, materials and method statements.

- Inspection of architectural works internal, external: layout, plaster painting, aluminum, marble, and other finishing elements according to specification and the project manager's recommendation.

September 2015 – January 2019	Raslan Architectural Services, Jordan as Structural Design Engineer

Key Project Handled:

Title: **KELIOPETRA HOUSING PROJECT**

Description: Site engineer, 3108.3 $m^{2,}$ 8 floors, 7 months.

Title: **NAJEH AL-SAQQA HOUSING PROJECT**

Description: Site engineer, 1248 m^2, 5 floors, 3 months.

Key Result Areas:

- Carry out our building as required.
- Compiling data for Structural plans, specifications, cost estimates, reports etc.
- Providing clear and unambiguous direction to members of the project team.
- Writing Reports and small-scale Project Management.
- Preparing as built drawings.
- Ability to balance, co-ordinate and translate the needs of multiple stakeholders.
- Possess a thorough knowledge of building regulations.
- Able to lead a project with multiple technical resources involved.
- Good knowledge in the use of AutoCAD for the preparation of feasibility plans, sketch designs and planning application drawings.
- Coordinate missions between site, office and contractors.
- Prepare time schedule to execute the project as given time line.

Title: **HAMAD ABDELFATTAH HOUSING PROJECT**

Description: Design engineer, 1248 m^2, 5 floors.

Title: **AL WALEED KHRAIM HOUSING PROJECT**

Description: Design engineer, 1745 m^2, 4 floors.

Title: **MOHAMMAD AL-MASRI HOUSING PROJECT**

Description: Design engineer, 361 m^2, 2 floors.

Title: **TAMKEEN GROUP**

Description: Design engineer, 744 m^2, 3 floors.

Title: **ZAHRET AL ARBAEEN HOUSING PROJECT**

Description: Design engineer, 1960 m^2, 5 floors.

Title: **MHAMMAD JOMAA HOUSING PROJECT**

Description: Design engineer, 2019 m^2, 5 floors.

Title: **KHALEED FAAEQ HOUSING PROJECT**

Description: Design engineer, 745 m^2, 2 floors.

Key Result Areas:

- Design our plans related to the Jordanian code.
- Analysis and design building structure using prokon.
- Making design drawings using Auto-cad.
- Checking of quantity estimation.


ANKARA YILDIRIM BEYAZIT ÜNİVERSİTESİ